Probabilistic Estimation and Prediction of Groundwater Recharge in a Semi-Arid Environment

by
Gene-Hua Crystal Ng

A.B. Applied Mathematics, Harvard University, 2003

Submitted to the Department of Civil and Environmental Engineering in partial fulfillment of the requirements for the degree of

Doctor of Philosophy in the field of Environmental Engineering
at the
MASSACHUSETTS INSTITUTE OF TECHNOLOGY

February 2009

Author ……...
Department of Civil and Environmental Engineering
September 5, 2008

Certified by ……..……..
Dennis McLaughlin
H.M. King Bhumibol Professor of Civil and Environmental Engineering
Thesis Supervisor

Certified by ……..……..
Dara Entekhabi
Bacardi and Stockholm Water Foundations Professor of Civil and Environmental Engineering
Thesis Supervisor

Accepted by ……..
Daniele Veneziano
Chairman, Departmental Committee for Graduate Students

Probabilistic Estimation and Prediction of Groundwater Recharge in a Semi-Arid Environment

by Gene-Hua Crystal Ng

Submitted to the Department of Civil and Environmental Engineering on September 5, 2008, in partial fulfillment of the requirements for the degree of Doctor of Philosophy in the field of Environmental Engineering

ABSTRACT

Quantifying and characterizing groundwater recharge are critical for water resources management. Unfortunately, low recharge rates are difficult to resolve in dry environments, where groundwater is often most important. Motivated by such concerns, this thesis presents a new probabilistic approach for analyzing diffuse recharge in semi-arid environments and demonstrates it for the Southern High Plains (SHP) in Texas. Diffuse recharge in semi-arid and arid regions is likely to be episodic, which could have important implications for groundwater. Our approach makes it possible to assess how episodic recharge can occur and to investigate the control mechanisms behind it.

Of the common recharge analysis methods, numerical modeling is best suited for considering control mechanisms and is the only option for predicting future recharge. However, it is overly sensitive to model errors in dry environments. Natural chloride tracer measurements provide more robust indicators of low flux rates, yet traditional chloride-based estimation methods only produce recharge at coarse time scales that mask most control mechanisms. We present a data assimilation approach based on importance sampling that combines modeling and data-based estimation methods in a consistent probabilistic manner.

Our estimates of historical recharge time series indicate that at the SHP data sites, deep percolation (potential recharge) is indeed highly episodic and shows significant interannual variability. Conditions that allow major percolation events are high intensity rains, moist antecedent soil conditions, and below-maximum root density. El Niño events can contribute to interannual variability of percolation by bringing wetter winters, which produce modest percolation events and provide wet antecedent conditions that trigger spring episodic recharge.

Our data assimilation approach also generates conditional parameter distributions, which are used to examine sensitivity of recharge to potential climate changes. A range of global circulation model predictions are considered, including wetter and drier futures. Relative changes in recharge are generally more pronounced than relative changes in rainfall, demonstrating high susceptibility to climate change impacts. The temporal distribution of rainfall changes is critical for recharge. Our results suggest that increased total precipitation or higher rain intensity during key months could make strong percolation peaks more common.

Thesis Supervisors:

Dennis McLaughlin	Dara Entekhabi
H.M. King Bhumibol Professor of Civil and Environmental Engineering	Bacardi and Stockholm Water Foundations Professor of Civil and Environmental Engineering

Acknowledgements

I would like to express deep gratitude to my advisors, Dennis McLaughin and Dara Entekhabi. I greatly appreciated having the opportunity to learn through their direct mentorship and from their example to address challenging and fascinating questions in hydrology and data assimilation. They devoted much time and effort in not only making sure my work came through, but also to make sure I developed the skills and insights to become a better researcher. Their advice and encouragement will certainly continue to guide me through my professional future.

I am also indebted to my other thesis committee members. Bridget Scanlon not only provided me with the unsaturated zone data that made this work possible, but contributed invaluable insights over innumerable phone meetings. I am also very grateful to Charlie Harvey for asking the probing questions that helped shape and improve this thesis.

I am thankful for having wonderful past and present research group-mates, from whom I learned a great deal. Many other members of Parsons Lab also helped make my time here a truly enjoyable experience. Special thanks to Piyatida Hoisungwan, Behnam Jafarpour, Adel Ahanin, and David González Rodríguez for sharing my struggles and celebrations over the past years. I also very much appreciate all the constant encouragement from friends outside of Parsons.

I am especially grateful for the boundless love and support of my family. My parents always manage to strike that seemingly impossible balance of motivating me to aim high while also being completely supportive though all my decisions. My big sister Dawn has always looked out for me, and she inspires me to live life to the fullest. Thanks to my husband Tzung-bor, for, quite simply, always being there for me.

Finally, I dedicate this thesis to my little nieces Naila and Isis, whose beautiful new smiles carried me through the home stretch.

Contents

List of Figures

List of Tables

Chapter 1

Introduction

Groundwater resources are critical for meeting the growing water demands throughout the world, especially in semi-arid to arid regions. This has made groundwater recharge, the water flux across the water table that replenishes aquifers, a very important component of the water cycle to estimate and characterize. Groundwater is estimated to make up at least 50% of potable water, 40% of industrial water, and 20% of irrigation water in the world [*Foster and Chilton*, 2003], and increasing reliance on groundwater has led to over-exploitation of many aquifers. Salinization and man-made and agricultural pollutants are a threat to much of the remaining groundwater supply. Recharge quantification can supply an upper bound on sustainable groundwater pumping and provide information on aquifer susceptibility to contamination. Understanding the conditions that give rise to recharge can help land-use and agricultural managers make decisions that could avoid or mitigate adverse effects on valuable subsurface water supplies.

In addition to characterizing current recharge conditions, future recharge predictions are important, considering the increased water scarcity expected with future population growth [*Vörösmarty et al.*, 2000]. Because recharge originates from precipitation that escapes evaporation, transpiration, and runoff at the surface, climate change is likely to impact future recharge rates; precipitation changes would directly affect the moisture supply for recharge, and increased temperatures could lead to higher evaporative demands that could limit recharge amounts. As documented in the Intergovernmental Panel on Climate Change's Fourth Annual Report [2007], much progress has been made in predicting future climate change using global climate models. The assessment of possible impacts on recharge by these climate predictions has been initiated for a number of watersheds [*Herrera-Pantoja,* 2008; *Green et al.,* 2007*; Jyrkama and Sykes* 2007; *Serrat-Capdevila et al.,* 2007; *Scibek and Allen,* 2006*; Brouyere et al.,* 2004*; Croley and Luukkonen,* 2003*; Eckhardt and Ulbrich,* 2003*; Loaiciga,* 2003*; Kirshen,* 2002*; and Rosenberg et al.,* 1999]. Predicting potential changes in recharge could be critical for preparing for future water resource problems.

Unfortunately, however, due to difficulties in direct subsurface observation, groundwater recharge is one of the most difficult fluxes of the hydrological cycle to resolve. Its estimation is particularly difficult in dry climates, where groundwater resources are especially vital. In these settings, the common approach of subtracting bulk evapotranspiration and runoff from precipitation averages fails because typically small and variable recharge rates are lost in the error of the surface flux measurements [*Gee and Hillel,* 1988]. Resolving these small values using more sophisticated models is still unreliable due to sensitivities to parameter errors. This is particularly problematic for

making future recharge predictions, which must rely on model simulations. These difficulties motivate the need for quantifying and minimizing uncertainty in recharge estimates and predictions.

The methods generally used for estimating recharge depend on the process by which recharge occurs in the location of interest. Recharge is categorized as "diffuse" (or "direct") when it originates from precipitation that infiltrates the soil directly and percolates vertically to the water table. Non-diffuse recharge, which includes focused or indirect, occurs when moisture travels laterally at or near the land surface and then collects in streams or topographic depressions before infiltrating. The latter process becomes more dominant in drier environments, where high potential evapotranspiration often prevents any appreciable diffuse recharge. Recharge also often occurs via preferential pathways, though these dynamics are difficult to characterize. Although diffuse recharge is believed to play a diminishing role with aridity, *Kearns and Hendrickx* [1998] point out that small diffuse recharge rates over large areas yield significant volumetric contributions to groundwater. In areas of land-use change where deep-rooted natural vegetation has been removed, diffuse recharge has become significant in semi-arid settings [*Scanlon et al.*, 2007; *Cook et al.*, 1989], which have caused significant salinization problems in Australia [*Cook et al.*, 1989]. Motivated by such concerns, this study examines diffuse recharge in semi-arid settings, where subsurface water supplies are often critical.

While numerical modeling of diffuse recharge provides the most comprehensive method for estimating recharge because it can simulate recharge at any time scale under varying conditions, many studies caution against using numerical modeling in dry

environments due to its significant sensitivity to model errors, as mentioned earlier. Tracer-based recharge estimation methods are instead endorsed by *Gee and Hillel* [1988] and *Allison et al.* [1994] over water balance modeling. Due to its ubiquitous availability, meteoric chloride is popularly employed using variants of the chloride mass balance method [*Scanlon et al.*, 2002]. By assuming that over the long term, the average rate of chloride deposition at the surface equals the rate of chloride flushing out of the unsaturated zone via recharge, subsurface chloride measurements can provide long term average diffuse recharge estimates.

However, the drawbacks of traditional chloride-based recharge estimation approaches include their inapplicability for future prediction studies and their inability to resolve fine time scale dynamics. Fine scale recharge estimates can be important for contaminant concerns, and they can help reveal control mechanisms that allow recharge to occur. Numerical modeling of recharge provides flexible yet inaccurate estimates, and chloride-based recharge estimation methods produce robust but time-integrated results, yet few studies have combined the two complementary approaches. Some studies (e.g. *Cook et al.* [1992], *Flint et al.* [2002], and *Scanlon et al.* [2003]) use chloride measurements to validate numerical models, but they fall short of quantitatively integrating the two sources of information. Most other recharge estimation studies use either tracers or numerical modeling alone. Similarly, many climate change impact and recharge studies rely on uncalibrated numerical models, which entirely overlook model errors that can significantly affect results. Some other studies calibrated and/or validated their recharge models using groundwater level or stream flow data [*Rosenberg et al.,* 1999*; Krishen,* 2002*; Eckhardt and Ulbrich,* 2003*; Croley and Luukkonen,* 2003*;*

Brouyere et al., 2004*; Herrera-Pantoja,* 2008]. However, their use of single parameter sets fails to properly represent uncertainty due to the typical non-uniqueness of the calibration problem. Even if the calibration procedure successfully captures the single most likely parameter set, the non-linear nature of unsaturated zone dynamics may result in misleading recharge simulations.

This thesis presents a novel probabilistic approach to recharge estimation and prediction that integrates modeling and unsaturated zone data while properly accounting for sources of uncertainty using data assimilation. Data assimilation, the practice of statistically combining observations with models, has been applied to a number of other hydrological applications [e.g. *Dunne and Entekhabi*, 2006; *Margulis et al.*, 2002; *Reichle et al.*, 2002; *Vrugt et al.*, 2005; *Kitanidis and Bras*, 1980; *McLaughlin et al.*, 1993], and its capacity to spatially downscale coarse resolution observations has been demonstrated by *Reichle et al.* [2001]. In this work, we use data assimilation to *temporally* downscale unsaturated zone chloride and soil moisture profile data using the transient information of a numerical model. Estimation results include distributions of historical recharge time series and distributions of model parameters. While fine time scale estimates of recharge can help characterize recharge under current conditions, constrained distributions of model parameters provide the opportunity to explore potential climate change impacts on recharge.

This probabilistic approach to recharge analysis is introduced using a test region in the semi-arid Southern High Plains region of Texas, where replacement of natural grassland with rain-fed cotton crops over the last century has led to observed flushing of unsaturated zone chloride, indicating increased diffuse recharge. Chapter 2 describes the

data assimilation method chosen for this work and details its application to the recharge problem. Recharge and parameter estimates are then presented, and main recharge mechanisms under current conditions are identified for the test sites. Chapter 3 applies the data-constrained model parameters found in Chapter 2 to produce probabilistic recharge predictions under various future climate scenarios for the region projected by different climate models. The incorporation of climate model outcomes for recharge simulations is discussed, and the range of potential future recharge changes is considered. Using this recharge analysis approach, improved understanding of how recharge occurs in this (or other) test sites today and how it could be affected in the future can facilitate better groundwater resources management.

Chapter 2

Assimilation of Chemical and Physical Data for Parameter and Recharge Estimation

2.1. Introduction and Background

Quantifying and characterizing groundwater recharge are critical for management of water resources, land-use, subsurface contaminants, and geochemical reservoirs. In particular, understanding the conditions which allow for or restrict recharge is paramount for such applications. The controls of recharge are well-known to be meteorology, soil properties, vegetation, and topography. However, how these controls interact to affect subsurface fluxes can be complex and difficult to predict.

The methods used for estimating recharge depend on the process by which recharge occurs in the location of interest; a discussion of recharge processes is provided by *de Vries and Simmers* [2002]. Generally, recharge is categorized as "diffuse" (or "direct") when it originates from precipitation that infiltrates the soil directly and

percolates vertically to the water table. Non-diffuse recharge occurs when moisture travels laterally at (or near) the land surface and then collects in streams or topographic depressions before infiltrating. The latter process becomes more dominant in drier environments, where high potential evapotranspiration often prevents any appreciable diffuse recharge. Recharge also often occurs via preferential pathways (instead of matrix flow), but these dynamics are difficult to characterize.

Although diffuse recharge is believed to play a diminishing role with aridity, it can still have significant impacts in drier climates. *Kearns and Hendrickx* [1998] point out that small diffuse recharge amounts over large areas yield significant volumetric contributions to groundwater. In areas of land-use change where deep-rooted vegetation has been removed, diffuse recharge rates have become significant in semi-arid settings [e.g. *Scanlon et al.*, 2007; *Cook et al.*, 1989]. This has sparked a major environmental problem in Australia, where natural unsaturated zone reservoirs of salt have been flushed into valuable ground and surface water reservoirs [*Leaney et al.*, 2003; *Cook et al.*, 1989]. Motivated by such concerns, this study examines diffuse recharge controls in semi-arid settings, where subsurface water supplies are often critical. It is known that unlike humid environments, where recharge occurs often, recharge is likely to happen episodically in dry regions [Gee and Hillel; 1987], and this has been found to be the case in a number of settings (e.g. *Lewis and Walker* [2002], *Zhang et al.* [1999a, b]). Because this type of recharge dynamics can have important implications on water management practices, it is important to find whether episodic recharge occurs in a particular site, to quantify how episodic it is, and to investigate what constellation of meteorological, soil, and vegetation conditions allows for it.

A comprehensive review of common recharge estimation methods can be found in *Scanlon et al.* [2002]. Of the approaches typically used, numerical modeling of diffuse recharge lends itself best to investigating its control mechanisms, because of its ability to resolve fine scale effects in time and space and produce sensitivity tests. Accordingly, Richards solvers of unsaturated zone moisture flow have been used in a number of such studies. In a modeling study of the semiarid southwestern United States, *Small* [2005] found diffuse recharge to be sensitive to rainfall seasonality and storm size distribution, although to different degrees depending on soil type. *Keese et al.* [2005] modeled diffuse recharge across Texas and quantified effects of vegetation inputs and soil layering. *Zhang et al.* [1999a, b] modeled diffuse recharge in an agricultural region of Australia and showed it occurs episodically and is affected by agricultural practices.

While modeling can be the best way to reveal how recharge is affected by different control conditions, many studies (e.g. *Gee and Hillel* [1988] and *Allison et al.* [1994]) caution against estimating recharge with numerical models in dry environments. Even when diffuse recharge is appreciable in such settings, their magnitudes are small, and are thus very sensitive to uncertain parameterizations and model inputs. For this reason, the common approach of assigning recharge to the residual of precipitation and evaporation should be avoided in dry conditions, where flux magnitudes are of the order of evaporation and precipitation estimation errors. Tracer-based recharge methods are therefore endorsed by *Gee and Hillel* [1988] and *Allison et al.* [1994] over water balance modeling schemes in semi-arid and arid environments. Historical isotope tracers and applied tracers (e.g. dyes) are useful for shorter time scales [*Scanlon et al.,* 2002], but natural tracers such as meteoric chloride are popular due to their ubiquitous availability.

Chloride concentrations in the unsaturated and/or saturated zone are most often employed for recharge estimation using a simple chloride mass balance (CMB), which assumes that over the long term, the average rate of chloride deposition at the surface equals the rate of chloride flushing out of the unsaturated zone via recharge [*Scanlon et al.*, 2002]:

$$R * C_{soil} = P * C_{precip}, \quad \textbf{(2-1)}$$

where R is long term recharge, P is average precipitation rate, and C_{soil} and C_{precip} are chloride concentrations in the soil and precipitation. The drawback of using CMB to investigate recharge controls is that it cannot resolve fine time-scale dynamics that link diffuse recharge to surface transient controls (weather and vegetation). To address this issue, there are some quasi-transient chloride methods that associate portions of the unsaturated profile to times in the past. The quasi-steady state and generalized CMB applies mass balance to different portions of an unsaturated zone chloride profile [*Cook et al.*, 1992; *Ginn and Murphy*, 1997; *Murphy et al.*, 1996], and the chloride front displacement method tracks the velocity at which a high concentration profile section (reflecting low flux rates) is flushed by recent high flux rates (reflected in low concentrations) [*Allison and Hughes*, 1983; *Walker et al.*, 1991].

However, these semi-transient recharge estimation schemes using chloride data are limited by the dispersion time of solutes in the unsaturated zone. *Cook et al.* [1992] found that climatic events of 4-5 years length that yielded greater than about 20 mm/yr recharge rates may be preserved in the unsaturated zone for more than 50 years, but shorter and weaker signals can be lost quickly. Thus, chloride data cannot reveal

recharge sensitivity to seasonal effects, past annual events or other short duration transient dynamics.

Numerical modeling of recharge provides detailed yet inaccurate estimates, while chloride-based recharge estimation methods produce robust but aggregated results, yet few studies combine the two complementary approaches. Some studies (e.g. *Cook et al.* [1992], *Flint et al.* [2002], and *Scanlon et al.* [2003]) use chloride measurements to validate numerical models, but they fall short of quantitatively integrating the two sources of information. This study introduces an approach of assimilating unsaturated zone measurements with numerical simulations to exploit advantages of both.

Data assimilation, the practice of integrating observations with models, is commonly used in other hydrological applications [e.g. *Dunne and Entekhabi*, 2006; *Margulis et al.*, 2002; *Reichle et al.*, 2002; *Vrugt et al.*, 2005; *Kitanidis and Bras*, 1980; *McLaughlin et al.*, 1993]. *Reichle et al.* [2001] used data assimilation to spatially downscale satellite data with grid-scale information provided by a distributed watershed model to estimate soil moisture. Similarly, we seek to use data assimilation to *temporally* downscale unsaturated zone chloride and soil moisture profile data using the fine scale and transient information of a numerical model. Recognizing the errors of observations and models, we employ a probabilistic scheme known as importance sampling to produce likely distributions of transient subsurface fluxes and model parameters. While *Scanlon* [2000] explored uncertainties in recharge estimates from the CMB method, its application does not generally provide probabilistic information.

This probabilistic data and model integration approach is introduced using a test region in the semi-arid Southern High Plains region of Texas, where the replacement of

natural grassland with rain-fed cotton crops over the last century has led to observed flushing of unsaturated zone chloride, indicating increased diffuse recharge. Data collected in the region was presented in *Scanlon et al.* [2007] and analyzed using CMB and chloride front displacement methods. The data-constrained flux simulations and parameter estimates produced in this work allows for recharge control investigations not allowed by the traditional estimation methods considered previously. By understanding how recharge occurred in this (or other) test sites and by constraining model parameters, we can better predict how recharge, and consequently groundwater systems, may be affected.

2.2. Estimation Method: Importance Sampling

The two main components of data assimilation problems are the system model and observation model, which can be expressed, respectively, as:

$$x_{1:T} = f(x_0, p, b_{1:T}, \varepsilon_{1:T}) \quad \textbf{(2-2)}$$

$$y_{1:T} = h(x_{1:T}, \eta_{1:T}), \quad \textbf{(2-3)}$$

where $x_{1:T}$ is the vector of system states over a time range of length T, x_0 is the initial state vector, p is the parameter vector, $b_{1:T}$ is the boundary condition vector over time, $\varepsilon_{1:T}$ is the state model error vector not included in other inputs, $y_{1:T}$ is the observation vector, and $\eta_{1:T}$ is the observation error vector. For this recharge problem, f is a soil moisture and solute transport model; x includes soil moisture, chloride concentrations, and moisture fluxes at different depths; p includes soil and vegetation parameters; b includes

meteorological and solute deposition forcing; and y includes soil moisture and chloride concentration measurements. For this particular data assimilation study, measurements are taken only once at time T, which simplifies equation (2-3) to:

$$y_T = h(x_T, \eta_T) \tag{2-4}$$

Many model calibration methods use observations to estimate a single parameter set that provides a "best fit" according to some arbitrary objective measurement. However, models and observations are uncertain, making probabilistic estimates desirable, especially for nonlinear systems. The optimal probabilistic estimate is the posterior distribution $p(X|y)$, which gives the uncertainty measure of X (values to be estimated, such as $x_{1:T}$, p, and/or $b_{1:T}$) conditioned on y (measurements). Bayes' theorem provides the way to calculate this posterior distribution ($p(X|y)$) from prior probabilistic knowledge of the system ($p(X)$) and the likelihood of the measured values ($p(y|X)$):

$$p(X \mid y) = \frac{p(y \mid X)\, p(X)}{p(y)}. \tag{2-5}$$

When the distributions of equation (2-5) are Gaussian, it suffices to calculate the moments of X (mean and covariance). This coincides with the well-known Kalman filter [*Kalman and Bucy*, 1961; described in linear estimation textbooks, e.g. *Gelb*, 1974; *Kailath et al.*, 2000], in which the posterior mean is a linear weighting of the prior mean and observations. However, closed forms for the distributions of (2-5) generally do not exist, especially when X contains parameters and states over time for a nonlinear system, as is the case for the recharge problem; sub-optimal Bayesian estimators must then be used. One suite of such approaches comprises of Kalman-based ensemble methods [*Evensen,* 2003], which employs the linear Kalman estimator, but represents distributions

discretely. These can produce favorable approximations of the posterior distribution in certain applications (e.g. *Zhou et al.* [2006]), yet the estimator relies on a strong Gaussian assumption. Because system states and parameters are strongly non-Gaussian in the recharge problem, we elect to use importance sampling, a concept commonly used in particle filters, which is an alternative sub-optimal estimator that also uses discrete representations of distributions, yet avoids distributional assumptions in its theory. Widely used in tracking and signal processing [*Djurić et al.*, 2003], the particle filter has also been implemented in hydrological applications [*Moradkhani et al.*, 2005; *Zhou et al.*, 2006; *Pan et al.*, 2007; *Weerts and El Serafy*, 2006; *Smith et al.*, 2008]

Arulampalam et al. [2002] provides a good tutorial on the different varieties of particle filters; components of the Sequential Importance Resampling (SIR) type of particle filter are used in this recharge problem. The full filter sequentially assimilates observations (usually over time), but since only one observation time is used in the recharge problem, mainly only the importance sampling element of the SIR is needed. A non-sequential version is adapted for this work and is described here.

In particle filters, the posterior distribution is represented discretely using a set of $i=1, \ldots, N$ state and/or parameter points (X^i) and associated weights (w^i):

$$p(X \mid y) \approx \sum_{i=1}^{N} w^i \delta(X - X^i) \tag{2-6}$$

$$\sum_{i=1}^{N} w^i = 1 \tag{2-7}$$

where δ(.) is the Dirac delta function. Note that (2-7) must apply in order to have a valid probability distribution function. Importance sampling is the process by which the set of system points (X^i) and associated weights (w^i) are assigned. It assumes there is an

importance density $q(X|y)$ that provides a first estimate of $p(X|z)$ and can be easily sampled. Then, if X^i are random samples of $q(X|y)$, the weights can be found from:

$$w^i \propto \frac{p(X^i \mid y)}{q(X^i \mid y)} \tag{2-8}$$

along with (2-7). By applying Bayes' theorem, equation (2-8) may be expanded to

$$w^i \propto \frac{p(y \mid X^i)p(X^i)}{p(y)q(X^i \mid y)} \tag{2-9}$$

$$w^i \propto \frac{p(y \mid X^i)p(X^i)}{q(X^i \mid y)} \tag{2-10}$$

(since $p(y)$ is independent of X, and is thus a scaling term, it may be dropped in (2-10)). Thus, provided prior system knowledge and the likelihood of the observations, only a choice for $q(X|y)$ is needed for approximating the posterior distribution.

Because posterior state values are drawn from $q(X|y)$, finding an importance density with significant overlap with the target posterior density distribution is critical. The SIR filter assigns the prior distribution $p(X)$ as the importance density. Note that when X includes state values, Monte Carlo simulations of the system model (2-2) provide random prior samples. With this choice of importance density, equation (2-10) reduces to

$$w^i \propto p(z \mid X^i), \tag{2-11}$$

which is especially convenient when only a discrete representation of the prior distribution exists. To determine the likelihood function in equation (2-11), the measurement operator in (2-4) is used.

In summary, importance sampling is carried out by first drawing a random sample of system points $\{X^i; i=1, \ldots N\}$ according to our prior knowledge before considering the

data; the prior weight of each sample is *1/N*. The posterior probabilistic weight for each system point is calculated in (2-11) as proportional to the likelihood of the observed values given that particular point. It can thus be seen that higher weights are appropriately assigned to model sets that match well with observations. The posterior weights should also sum to unity to provide a valid probability distribution in equation (2-6).

A cartoon example of importance sampling is shown in Figure 2-1 for a univariate problem. The set of points X^i is drawn at random from the importance density, which in this approach is the prior distribution, and are indicated by the asterisks. Because they come from a random draw, the prior weight for each point is the same (*1/N*). It can then be seen that the posterior distribution (conditioned on observations) is shifted and peakier than the prior, yet it is also represented by the same set of X^i. However, the posterior weights (represented by particle size in cartoon) are now different than the prior, with higher values assigned to points with higher likelihood function results.

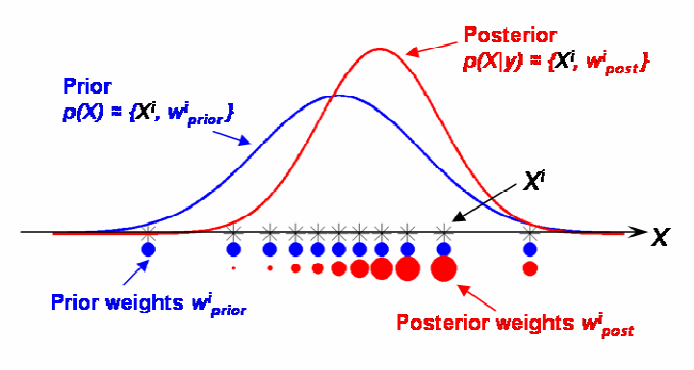

Figure 2-1: Importance sampling cartoon. Prior and posterior particle weights are represented by circle sizes.

Note that this SIR approach suffers when the prior distribution is not a good estimate of the posterior distribution, because high posterior probability states have low prior probability. In such cases, a very large set of points (large N) becomes necessary to ensure the sampling of these low prior probability states for the set $\{X^i\}$. This problem is exacerbated when X is high-dimensional, because of the large sample size required for adequately covering the state and/or parameter space. If X^i are generated using a computationally expensive model for equation (2-2), which is often the case when X is high-dimensional, using a large N may prove infeasible; this is known as "the curse of dimensionality" [*Daum*, 2002]. However, because this recharge problem considers only a single vertical profile, thus keeping the problem dimension manageable, importance sampling is a tractable approach. *Arulampalam et al.* [2002] offers insights for finding importance densities that may perform better than the prior, but the SIR algorithm is chosen here for its ease of implementation.

2.3. Application of Importance Sampling to the Recharge Problem

A schematic diagram of the estimation approach is outlined in Figure 2-2; the components are described here.

2.3.1. Data and Study Site

The Southern High Plains (SHP) region of the United States is a 75,000 km^2 region spanning parts of northern Texas and eastern New Mexico, and is characterized by flat topography and about 16,000 draining playas or ephemeral lakes (see Figure 2-3). It overlies part of the High Plains (or Ogallala) aquifer, which provides about 30% of the

U.S.'s irrigation water and is thus of great economic significance [USGS Factsheet, http://co.water.usgs.gov/nawqa/hpgw/factsheets/DENNEHYFS1.html]. With mean annual precipitation spanning about 375-500 mm, SHP is considered to have a semi-arid climate. In areas with natural grassland and shrubland, recharge occurs almost exclusively through playas [*Wood and Sanford,* 1995*; Scanlon and Goldsmith,* 1997].

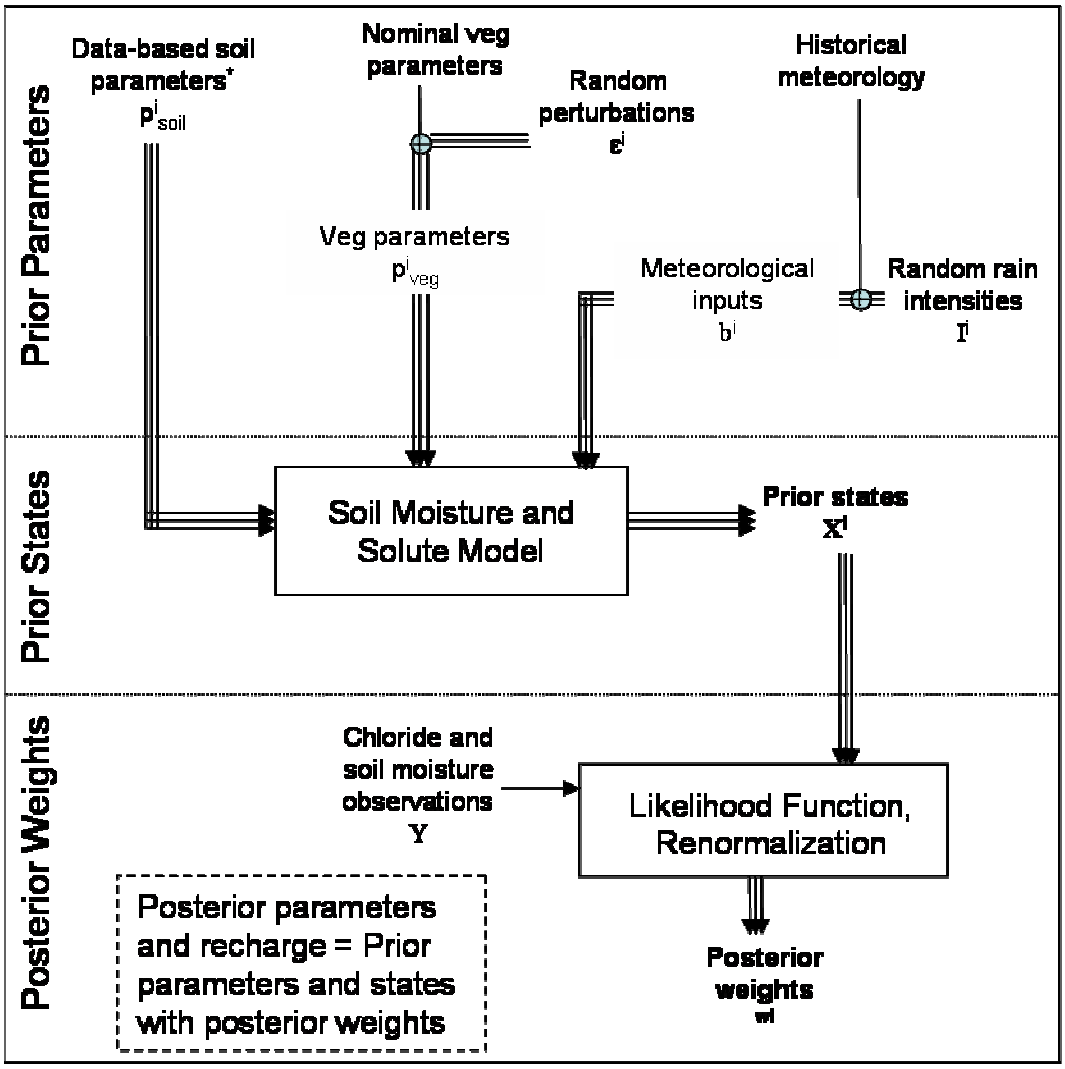

Figure 2-2: Schematic diagram of estimation approach. *Details of soil parameter uncertainty model included in Figure 2-6.

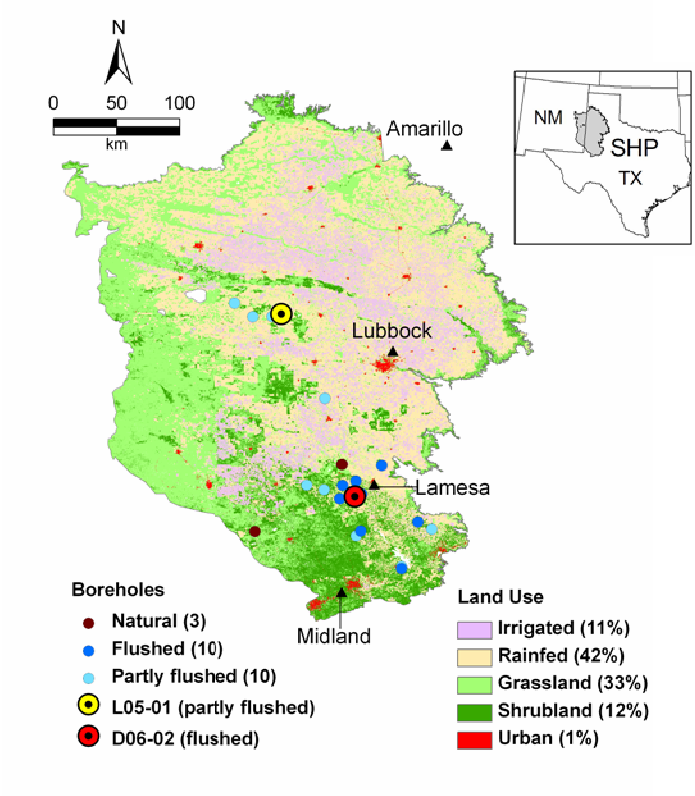

Figure 2-3: Southern High Plains map (adapted from *Scanlon et al.* [2007], Figure 1). Inset shows location of SHP in Texas and New Mexico. Data sites used in this study are fully-flushed D06-02 and partly-flushed L05-01.

However, clearance of natural vegetation for shallow-rooted cropland (much of it rain-fed cotton) in the early 1900's led to suspected increases in diffuse recharge. *Scanlon et al.* [2007] collected and analyzed 20 unsaturated zone boreholes in rain-fed cotton areas of SHP (indicated in Figure 2-3) to investigate the effect of the land-use change on recharge in the region, where cotton is mostly grown without irrigation in continuous monoculture. Similar to studies in Australia that found low chloride concentrations in the unsaturated zone following the clearing of eucalyptus trees [*Cook et al.*, 1989; *Kennet-Smith et al.*, 1994], *Scanlon et al.* [2007] found widespread occurrence of flushed chloride concentrations in their profiles. In great contrast to the slightly upward fluxes prominent before land-use change in interplaya settings [*Scanlon et al.*,

2003], their CMB calculations ranged from 4.8 to 70 mm/yr average diffuse recharge under cropland. Such changes in recharge could cause water table levels to rise, which could compromise water quality with water-logging and salinization problems. By re-examining the data collected by *Scanlon et al.* [2007] using a data and model integration approach, this work elucidates the control mechanisms behind the increased diffuse recharge. Understanding how the recharge occurs can influence better land-use and groundwater management.

Half of the rain-fed profiles in *Scanlon et al.* [2007] were fully flushed with low chloride concentrations brought by post-development high fluxes, while the remainder showed high concentration bulges at depth remnant of pre-development conditions. The positions of chloride bulges in the partially flushed profiles convey information about the flux history; accordingly, they were used by *Scanlon et al.* [2007] in chloride front displacement calculations to corroborate CMB results. For this recharge study, a representative profile from each group was selected for analysis: the fully-flushed profile D06-02, and the partially-flushed profile L05-01. Their locations are included in Figure 2-3.

Unsaturated zone profile measurements taken by *Scanlon et al.* [2007] include soil moisture, chloride concentration, bromide concentration, matric potential, and soil texture (percent clay, silt, and sand). Chemical concentrations were found by first drying samples, adding water and shaking, and then using ion chromatography to measure concentrations in the supernatant. Soil moisture was measured gravimetrically, matric potential was measured using chilled-mirror pyschrometers and tensiometers, and soil texture was measured using sieve and hydrometer methods. Further details on

measurement methods are provided in *Scanlon et al.* [2007]. The ratio of chloride to bromide concentrations confirmed that chloride in the soil moisture should be of atmospheric origin instead of geologic. Data from the National Atmospheric Deposition program [http://nadp.sws.uiuc.edu/] provided the basis for the atmospheric chloride deposition rates. To establish matrix flow as the dominant transport mechanism as opposed to preferential flow, total chloride integrated over the flushed depths were checked against total chloride deposition calculations since the time of land-use change. Identifying flow mechanisms is important for the choice of numerical model in the data assimilation approach.

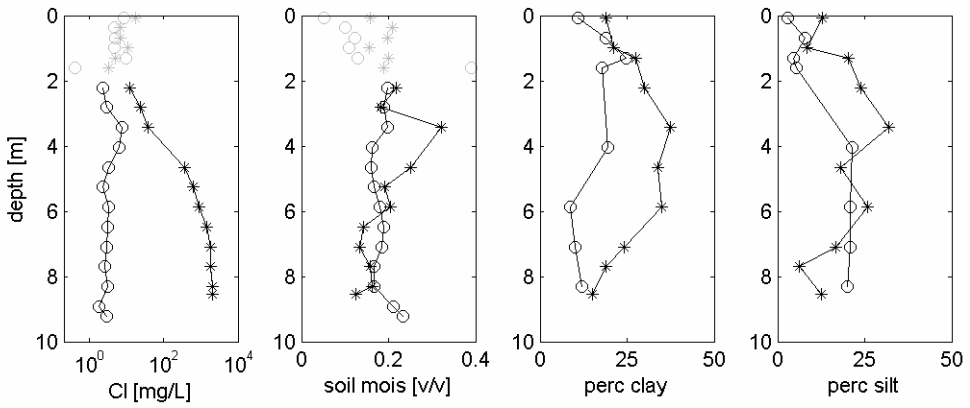

Figure 2-4: Observation profiles for D06-02 (circles) and L05-01 (asterisks). State observations within root zone area, indicated in gray, are not included in assimilation.

The data assimilated in our work include soil moisture and chloride concentrations. Matric potential measurements were not assimilated, due to the occurrence at some sites of very negative readings at depth that were not reproducible by our numerical model. Because chloride provides the more robust indicator of fluxes on the time scales of interest here, their omission was not considered important. Also omitted are chloride and

soil moisture measurements taken above 2 m, because the numerical 1-D Richards model (described below) is not expected to simulate well the transient state of the root zone, which is often affected by non-piston flow and mixing [Cook et al., 1992; Tyler and Walker, 1994]. The measurements used in this work are shown in Figure 2-4, and main results for profiles D06-02 and L05-01 found by Scanlon et al. [2007] are summarized in Table 2-1.

Table 2-1: Site data from *Scanlon et al.* [2007]

	D06-02	**L05-01**
Latitude / Longitude	32.63°N / 102.09°W	33.93°N / 102.61°W
Water table depth	10 m	36 m
$[Cl^-]$ in precipitation	0.34 mg/L	0.28 mg/L
Elapsed time since land-use change (Time used in this work)	67-75 yrs (71 yrs)	70-85 yrs (76 yrs)
CMB recharge estimate from *Scanlon et al.* [2007]	70 mm/yr	14 mm/yr

2.3.2. Unsaturated Zone Moisture and Solute Transport Model

In this recharge estimation approach, unsaturated zone profile data of soil moisture and chloride concentrations are assimilated with numerical model simulations. The numerical model used here for (2-2) is the Soil-Water-Atmosphere-Plant (SWAP) model version 3.0.3, which is described in *Kroes and van Dam* [2003]. SWAP has been used in a wide range of hydrological and agricultural studies in various climate conditions over the last 15 years [*van Dam et al. 2008*]. It is a one-dimensional vertical vadose zone model of soil moisture transport, solute transport, heat transport, and

vegetation. The heat transport component of SWAP was not used here, and, due to the evident dominance of matrix flow in the test sites, the macropore flow module is also not used. Soil moisture is simulated in SWAP using a finite difference numerical solver for the well-known Richards equation

$$\frac{\partial \theta}{\partial t} = \frac{\partial}{\partial z}\left[K(h)\left(\frac{\partial h}{\partial z} + 1 \right) \right] - T_a(t,z), \qquad \textbf{(2-12)}$$

and solute transport is simulated using a finite difference numerical solver for the advection-dispersion equation (for non-sorbing solutes and assuming no uptake by roots)

$$\frac{\partial \theta C}{\partial t} = \frac{\partial}{\partial z}\left[\theta (D_{dif} + D_{disp}) \frac{\partial C}{\partial z} - qC \right], \qquad \textbf{(2-13)}$$

where θ is volumetric soil moisture, h is matric potential, K is unsaturated conductivity, T_a is water uptake by roots, C is solute concentration in the pore water, D_{dif} and D_{disp} are molecular diffusion and dispersion coefficients, and q is the moisture flux rate. Molecular diffusion is set using 1 cm^2/d for the solute diffusion coefficient in free water, which falls within the range of values listed for chloride in *Robinson and Stokes* [1965]; dispersion is determined using a dispersivity of 2 cm [*Cook et al.*, 1992].

Surface boundary conditions for (2-12)-(2-13) and the sink term (transpiration) in (2-12) are determined from daily meteorological inputs and vegetation parameters. The simple (non-dynamic) crop option of SWAP was implemented, for which vegetation parameters such root depth and leaf area index (LAI) over the growing season are user-specified. Details of the transpiration scheme are included in Appendix A. Soil evaporation is capped by potential evaporation (E_p), which is calculated from the Penman-Monteith equation [*Monteith*, 1981] (assuming no crop resistance and negligible crop height) and a decay factor based on crop foliage: $\exp(-0.45 * LAI)$. In many

models, actual evaporation under soil-limiting conditions is derived using soil properties of the top model layer (K_1) and the gradient between the surface soil pressure head (h_1 at depth z_1) and relative humidity in the air (equivalent to pressure h_{atm}) via Darcy's equation:

$$E_{Darcy} = K_1\left(\frac{h_{atm} - h_1 - z_1}{z_1}\right). \quad \textbf{(2-14)}$$

However, preliminary results found evaporation to be over-estimated by this approach, and an empirical option in SWAP based on *Black et al.* [1969] is used instead for actual evaporation E_a:

$$\Sigma E_{emp} = \beta * t_{dry}^{1/2} \quad \textbf{(2-15)}$$

$$E_a = \min(E_p, E_{Darcy,} E_{emp}),$$

where β is an empirical parameter, t_{dry} is time since a significant rain event, and t_{dry} is reset to zero when precipitation exceeds a pre-set limit of 0.5 cm/d.

The model domain was set to simulate both site profiles D06-02 and L05-01, which have maximum depths of 9.2 and 8.5 m, respectively. With respective water table depths of 10 and 36 m, we assume there is no significant interaction between the groundwater and the observed depths, and thus a free drainage bottom boundary condition was implemented below the measured depths. The 1-D vertical domain was discretized using 217 nodes; the top layer was set at 2 cm thickness, and lower layer thickness increased with a 1.05 factor until 10 cm thickness. Layer thickness was capped at 10 cm to achieve good numerical performance for transient fronts resulting from land-use change. While micrometeorological inputs are at the daily timescale, the variable numerical time steps were not permitted to exceed 0.2 days. These run specifications

were found to provide a good balance between computational time and numerical performance. The simulations began at the time of land-use change (1935 for D06-02 and 1930 for L05-01) and ended at the measurement date (February 14, 2006 for D06-02 and May 26, 2005 for L05-01).

In our estimation problem, the vector X of values to be estimated includes SWAP model states and inputs. Specifically, the model states include soil moisture, chloride concentrations, and flux over the entire simulation period. Although recharge is defined as the flux at the water table, deep percolation at 150 cm depth was considered instead. By analyzing percolation time series just below the root zone, it is possible to identify key surface dynamics that control fluxes that ultimately yield recharge. To produce model states for the prior distribution of X for importance sampling, Monte Carlo simulations are required: SWAP was run multiple times for each prior sample of model inputs. For this study, run sizes of at least $N = 30{,}000$ were used for each data profile ($N=30{,}400$ for D06-02 and $N=36{,}170$ for L05-01).

2.3.3. Model Inputs and Uncertainty

Proper characterization of prior model inputs and uncertainty is needed for any data assimilation problem to provide correct probabilistic results. Furthermore, because posterior state and parameter values are taken exclusively from the prior sample in our importance sampling approach, the prior model inputs must be particularly well-chosen in this study. The different inputs for the general model in (2-2) include the initial condition for the model states x_0, time-invariant parameters p, time-varying inputs (such as boundary conditions) b_i, and other model errors ε. For this study, we assumed that

uncertainty in the model is conveyed solely through parameter and boundary condition uncertainty, thus eliminating ε in equation (2-2). Remaining model inputs include initial condition matric potential and solute concentrations, vegetation and soil parameters, and meteorology.

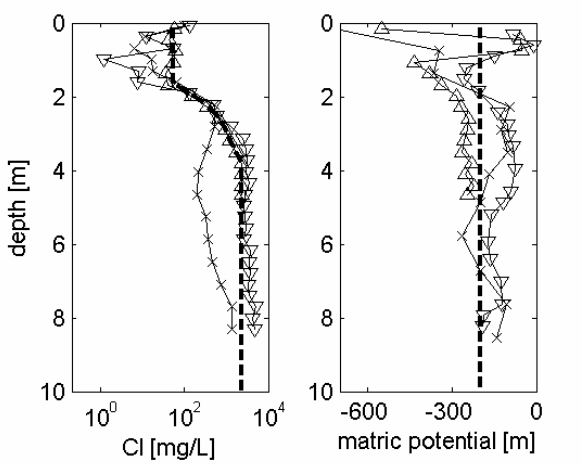

Figure 2-5: Dry and saline initial condition at the start of land-use change, shown with dashed lines, is based on natural grassland observations in SHP, shown with solid line and symbols.

Initial condition

Simulations started at the time of land-use change, and thus initial profile conditions reflected the dry and saline conditions under natural vegetation. SWAP requires matric potential and chloride concentration values to initialize runs; initial soil moisture is calculated from matric potential. Given the dissipative nature of the unsaturated zone well within the timescale of the simulation period (70+ years), uncertainty in the initial condition was not considered, and all simulations were initialized identically. Simulations are particularly less sensitive to the choice of initial

matric potential values, because wetting fronts propagate even faster than solute fronts when fluxes increase [*Jolly et al.,* 1989]. Initial matric potential and chloride concentrations used for this study were based on three observed profiles under natural grasslands that were also included in *Scanlon et al.* [2007]; these are shown in Figure 2-5.

Vegetation parameters

Because simulations began at the time of land-use change, vegetation parameters were only needed for cotton. We assumed that crop emergence began every year on May 15 and that harvest occurred on October 19 [*Keese et al.,* 2005]. For most vegetation parameters, a value was chosen based on the literature, and an independent uniform distribution of uncertainty was assigned about that nominal for the prior distribution. For ease of implementation, a time-invariant uncertainty factor was used for parameters specified over the growing season (root depth, LAI, and crop height). Because uncertainty introduced through the rooting depth was considered sufficient, root density distribution was set deterministically based on *Ritchie et al.* [2007].

Nominal parameter values and uncertainty ranges are summarized in Table 2-2. Preliminary tests showed low sensitivity to water and solute stress parameters, which were accordingly set to the deterministic values included in Appendix A. Sensitivity tests also indicated results are likely to be most affected by rooting depth of the other vegetation parameters, and thus a higher uncertainty range was assigned to it to allow for the full range of possibilities. Although the cited sources often report maximum rooting depths greater than the 1 m used here (e.g. *Bland and Dugas* [1989] and *Sarwar and Feddes* [2000]), smaller values were specified here to represent the active root zone.

Table 2-2: Vegetation parameters

	Nominal value	Literature Basis	Prior uncertainty
Root depth evolution	100 cm (max)	*Bland and Dugas* [1989], *Sarwar and Feddes* [2000], *Droogers* [2000]	Time-constant multiplicative uniform noise [0.5, 1.5]
LAI evolution	5 (max)	*Bland and Dugas* [1989]	Time-constant multiplicative uniform noise [0.75, 1.25]
Crop height evolution	90 cm (max)	*Askew and Wilcut* [2002]	Time-constant multiplicative uniform noise [2/3, 4/3]
Minimal crop resistance	90 s/m	*Kroes and van Dam*, [2003]	Multiplicative uniform noise [2/3, 4/3]

Soil parameters

SWAP uses the van Genuchten-Mualem soil retention and unsaturated conductivity model [*van Genuchten,* 1980] for its solution of equation (2-12):

$$\theta = \theta_{res} + \frac{\theta_{sat} - \theta_{res}}{\left(1 + |\alpha h|^{n}\right)^{m}} \quad \textbf{(2-16)}$$

$$K(\theta) = K_o S_e^{\lambda}\left[1 - \left(1 - S_e^{1/m}\right)^{m}\right] \quad \textbf{(2-17)}$$

with

$$m = 1 - 1/n \quad \textbf{(2-18)}$$

$$S_e = \frac{\theta - \theta_{res}}{\theta_{sat} - \theta_{res}}, \quad \textbf{(2-19)}$$

where θ_{res} (m^3/m^3) is residual soil moisture, θ_{sat} (m^3/m^3) is saturated soil moisture , α (cm^{-1}) and *npar* (-) are empirical parameters, λ is a parameter that depends on $\partial K/\partial h$, and K_o is usually saturated conductivity. Parameters needed for equations (2-16)-(2-19) were determined from soil texture (percent sand, silt, and clay) using the pedotransfer model Rosetta [*Schaap et al.,* 2001], a neural network program built on a large soil database. Note that while K_o is often set to saturated conductivity in (2-17), Rosetta provides lower, empirically-fitted values, which tend to result in significantly improved unsaturated conductivity estimates away from saturation [*Schaap and Leij*, 2000]. *Keese et al.* [2005] found soil layering to significantly affect recharge, and thus heterogeneous parameters are used with soil layers centered at available soil texture measurements. The soil evaporation parameter β describes evaporative properties for the surface layer in equation (2-15).

Uncertainty for the vertically heterogeneous soil parameters was attributed to two sources: the texture values entered into Rosetta and the Rosetta output parameters, as outlined in Figure 2-6. Because nearby soils can be expected to be similar, texture of adjacent layers should generally be more alike than distant layers. Thus, percent clay and silt distributions in the SHP were assumed to be first-order autoregressive processes (AR-1) with depth:

$$frac(z+dz) = \mu * frac(z) + \omega(z+dz) \qquad \textbf{(2-20)}$$

where *dz* is set to *-1 cm*, ω are independent Gaussian noise with zero-mean, and μ should fall between 0 and 1. If the texture distributions are further assumed to be stationary in their mean, it can be shown [*Priestly,* 1981] that the AR-1 distribution parameters can be

found from the texture autocovariance over depth increments $R(\zeta)$ via the following relationship:

$$R(\zeta) = \sigma_{\omega}^{2} \frac{\mu^{|\zeta|}}{(1-\mu^{2})}, \tag{2-21}$$

which also explicitly demonstrates the decaying correlation with distance. Accordingly, the coefficient μ and σ^2_{ω} were estimated based on the texture data collected over 24 boreholes in the SHP by *Scanlon et al.* [2007] to represent clay and silt profiles in the region.

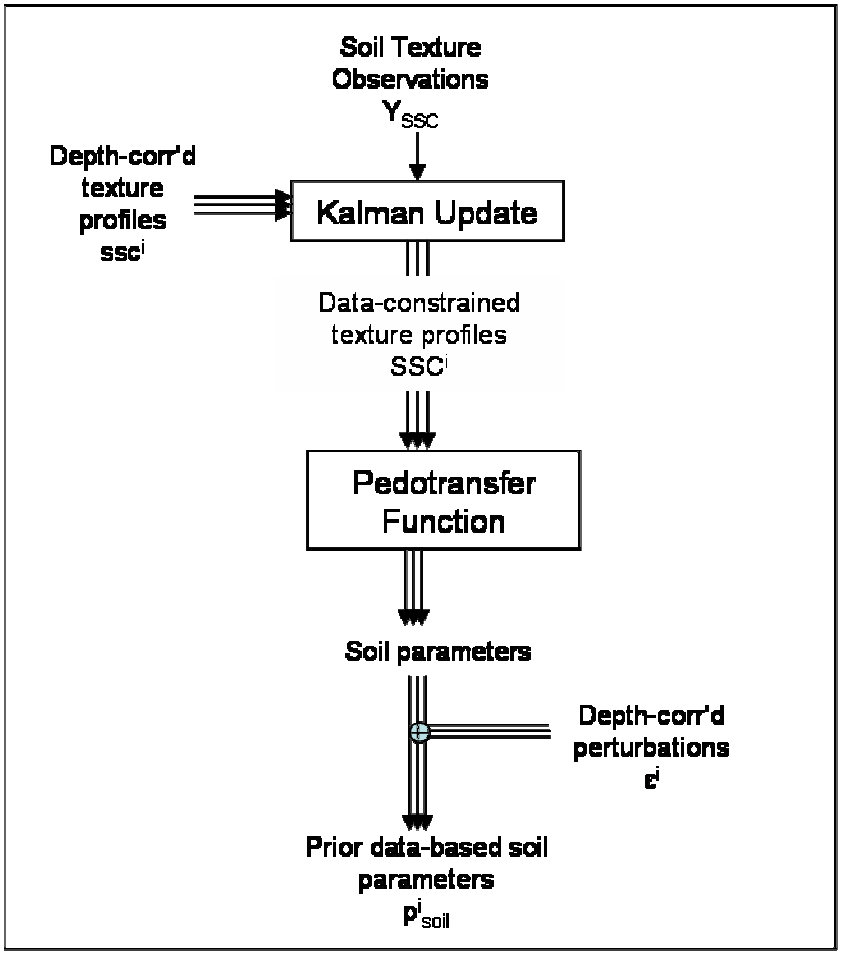

Figure 2-6 Soil uncertainty model

The percent clay and silt AR-1 profiles were then tuned to D06-02 and L05-01 by conditioning (2-20) on the data for those profiles. Because of the Gaussian nature of equation (2-20), the data-conditioned texture profile distributions could be found using the Kalman update estimator, which provides the posterior mean and covariance, as discussed in Section 2.2. The Kalman update scheme is included in Appendix B. The observations were assumed to have uncertainties of 5 percent clay and silt. A random draw was made from the conditional clay and silt percent distributions (truncated to fit the range of 0-100%), and sand percent was calculated from the residual. The texture samples were then averaged over the thickness of the heterogeneous soil layers (centered on measurement depths).

The resulting prior sample of percent clay, silt, and sand was inputted into Rosetta to obtain the prior sample of heterogeneous soil parameters. Although the Gaussian prior distribution of textures could be exactly represented by statistical moments, the output of the Rosetta neural network program is non-Gaussian, and thus only the discrete sample representation of the parameters exists. In addition to soil parameter estimates, Rosetta also outputs error measures. We assumed the parameter errors to be AR-1 with the same depth-correlation scale μ used for the texture profiles; the standard deviation was set to the Rosetta error values, inflated by a factor of 1.25 to account for other representativeness uncertainty. The final prior soil parameter samples included these AR-1 perturbations.

The prior sample for β for the evaporation model in equation (2-15) was drawn from the uniform distribution over [0.2, 0.6] cm/d$^{1/2}$. This range was based on the 0.33 to 0.51 cm/d$^{1/2}$ range found in *Ritchie* [1972], which reported empirical findings from

various studies using sand, clay, loam, and clay loam. Although the evaporation parameter is undoubtedly related to soil type, its prior distribution was assigned independent of texture because literature values were too sparse for inferring correlations, and because of the dependency on other factors such as tillage practices.

Meteorological input

Meteorological inputs needed for SWAP are chloride concentration in precipitation and daily records of precipitation, minimum and maximum air temperature (T_{min} and T_{max}), solar radiation, vapor pressure, and wind speed. The chloride concentrations in precipitation determined for the profiles D06-02 and L05-01 in *Scanlon et al.* [2007] were used here (listed in

Table 2-1). The four meteorological stations with long-term historical daily data available in SHP were Amarillo, Lubbock, Lamesa, and Midland (see Figure 2-3). Although long historical records of coarser time scale data would be easier to obtain, resolving precipitation intensities is important for simulating recharge in semi-arid climates. The sources and availability of daily data for the four stations are listed in Table 2-3.

Lamesa is 15 km from D06-02 and is its closest station; L05-01's closest station is Lubbock, at a greater distance of 77 km. Data from these nearest stations were used for the respective simulations. Reconstruction of missing historical micrometeorological data was needed for both stations (evident from Table 2-3), and the procedure used is outlined here. Days missing precipitation data were first determined to be rainy or dry depending on the precipitation condition at the next nearest station. Midland is closest to

Lamesa and Amarillo to Lubbock; the similarity of rain frequency for these pairs of stations supported the grouping, as shown in Table 2-4. If the day was reconstructed as rainy, daily rain intensity was assigned by randomly drawing from the monthly collection of historical intensities for that station; parametric distributions were avoided due to the strongly non-Gaussian nature of the intensities. Missing temperature data was then filled using data from the nearest station.

Table 2-3: Micrometeorological data availability and sources for 1930-2005 in SHP. SAMSON: Solar and Meteorological Surface Observational Network 1961-1990, available from GEM weather generator [*Hanson et al.,* 1994] dataset. NSRDB: National Solar and Radiation Data Base 1991-2005 Update [*National Renewable Energy Laboratory,* 2007]. NCDC: Daily surface data inventory [*NCDC*].

	Precipitation	**Temperature**	**Solar Radiation / Vapor pressure/ Wind**	**Data Source**
Amarillo	1948-2005	1948-2005	1961-2005	SAMSON, NSRDB
Lubbock	1930-2005	1930-2005	1961-2006	SAMSON, NSRDB
Lamesa	1930-2005 (~750 missing)	1930-2005 (~850 missing)	NONE	NCDC
Midland	1948-2005	1948-2005	1961-2005	SAMSON, NSRDB

Due to the sparse availability of the remaining meteorological fields, they were reconstructed based on historical data by month. Because data analysis showed solar radiation distributions to be very non-Gaussian and related to rain occurrence, it was reconstructed by randomly sampling the historical values according to the rain condition. Vapor pressure was found to be correlated with both rain occurrence and T_{min}; in particular, relative humidity and T_{min} records for each rain condition seemed jointly

Gaussian. Relative humidity, then converted to vapor pressure, was thus reconstructed by sampling the Gaussian distribution based on historical statistics and conditioned on the corresponding T_{min} record. Wind speed data was found to look non-Gaussian and unrelated to rain occurrence, and it was directly sampled from the historical records. Statistics of the filled meteorological data matched well with the available historical records.

Table 2-4: Historical rainfall statistics for 1961-2005 at SHP meteorological stations.

	Mean annual precip [mm]	**Percent rainy days [%]**	**Mean log-intensity [ln(mm/d)]**	**Std dev log-intensity [ln(mm/d)]**
Amarillo	470	17	1.17	1.37
Lubbock	450	16	1.20	1.39
Lamesa	470	13	1.42	137
Midland	350	13	1.13	1.40

To account for the distance between the meteorological stations and the data sites and for observation errors, uncertainty was included in the meteorological forcing. Sensitivity tests showed that the particular realization of reconstructed non-precipitation fields did not greatly affect the simulations. Thus, a single random sample of reconstructed non-precipitation values was used for all simulations, and prior uncertainty in the meteorological inputs was only introduced by varying precipitation. Furthermore, we assumed there to be greater confidence in the observation of precipitation occurrence than in detecting the actual rainfall amount, and only rainfall intensity was considered

uncertain. Chloride concentration in precipitation was set as deterministic, and thus the uncertainty in chloride deposition originated from precipitation amounts.

Two sources of uncertainty were injected into the rainfall intensity record, with the first being the random reconstruction of missing precipitation data. A simple random rainfall intensity model was constructed to add further uncertainty, where intensity for the sample *i* on rainy day *n* follows

$$\hat{I}_n^i = \exp(Y_n^i) \tag{2-22}$$

$$Y_n^i = (\log I_n - \overline{\log I_n})c^i + \overline{\log I_n} + d^i \tag{2-23}$$

$$c^i \sim U[1-\delta_c, 1+\delta_c] \tag{2-24}$$

$$d^i \sim U[-\delta_d, +\delta_d] \tag{2-25}$$

where I_n is the nominal intensity [cm/d] from the reconstructed historical record on rainy day n, the over bar signifies sample mean over the record, and $U[\cdot]$ is the uniform distribution over the specified range. While the above model is certainly not expected to generate the true rainfall series at the observation sites, it provides precipitation series varying in mean (with shift factor c) and standard deviation (with scaling factor d). Considering that early sensitivity tests showed recharge to be affected by total moisture input and high rain intensities, this model should capture the key rainfall characteristics that control subsurface fluxes. Parameters δ_c and δ_d were set based on the observed range of standard deviation and mean values for the four SHP stations; from Table 2-4, these can be found to be ~1.02 multiplicative range for the standard deviation and ~0.3 additive range for the mean, respectively. Due to the closer proximity, the assigned uncertainty

for Lamesa and D0602 was smaller at 1/4 the SHP-wide ranges, compared to 1/3 the ranges for Lubbock and L05-01.

2.3.4. Measurement Error

The importance sampling method determines posterior probabilistic weights according to the likelihood function $p(y|X)$, which indicates how likely the measured value is given the particular parameter set and model simulation under consideration. The likelihood function, in turn, is dependent on the measurement model and uncertainty (equation (2-4)) for soil moisture and chloride concentrations. Proper specification of the measurement uncertainty is critical in this probabilistic approach, because it determines how close model simulations must be to the data in order to be considered an acceptable estimate. For example, a small measurement error would create very stringent requirements. When assigning this uncertainty, procedural measurement errors and representativeness errors between the observations and model values should be considered. Also, assuming certain forms for the uncertainty facilitates likelihood function evaluations, such as use of Gaussian noise.

Measurements of gravimetric soil moisture were assumed to have additive 0-mean Gaussian observation noise $\omega_{\theta g}$ that is independent at different depths, and thus volumetric soil moisture observations follow

$$y_\theta = \rho_b * y_{\theta_g} = \theta + \rho_b * \omega_{\theta_g} \quad \textbf{(2-26)}$$

where the bulk density ρ_b is set to 1.6g/cm^3 [*Scanlon et al.*, 2007]. Considering the errors introduced from the soil collection, weighing, and oven-drying, we assumed an error of

$\sigma_{\theta g}$ = 0.03, which is about 25% of the observed values. As described in Section 2.3.1, measurements of chloride concentration in the pore water y_C were derived from the measurement of chloride in the sample supernatant y_S:

$$y_C = \frac{R_E * y_S}{y_{\theta_g}} = \frac{R_E * y_S}{\theta_g + \omega_{\theta_g}} \quad \textbf{(2-27)}$$

where the extraction ratio R_E is the mass of water added to the dried sample per mass of dried soil, and the density of water is assumed to be 1kg/m^3 for the units conversion. To account for the ±0.1g/mL instrument error for ion chromatography reported by *Scanlon* [2000] and the 9% mean difference between split tests for the chloride data [*Scanlon et al.,* 2007], both additive and multiplicative Gaussian measurement errors were represented in the supernatant measurements:

$$y_S = S + \omega_{S1} + S\omega_{S2} \quad \textbf{(2-28)}$$

where S (= $C^*\theta_g/R_E$) is the supernatant concentration and ω_{S1} and ω_{S2} are independent with means of 0 and 1, respectively, and standard deviations of σ_{S1} = 0.1 g/mL and σ_{S2} = 0.1.

Once the variance of $\omega_{\theta g}$ was specified, evaluating the likelihood function for $p(y_\theta|\theta)$ would be straightforward. However, evaluating $p(y_\theta,y_C|C,\theta)$ was made difficult because equation (2-27) is nonlinear in $\omega_{\theta g}$, making y_C non-Gaussian. We dealt with this problem by expanding (2-27) (with (2-28) substituted in) in a Taylor series around $\omega_{\theta g}$=0 and ignoring higher order terms. This resulted in:

$$y_C = C + C\varepsilon_1 + \varepsilon_2 \quad \textbf{(2-29)}$$

$$\varepsilon_1 = \omega_{S2} - \frac{\omega_{\theta_g}}{\theta_g} - \frac{\omega_{S2}\omega_{\theta_g}}{\theta_g} \quad \textbf{(2-30)}$$

$$\varepsilon_2 = \frac{R_E \omega_{S1}}{\theta_g} - \frac{R_E \omega_{S1} \omega_{\theta_g}}{\theta_g^2}. \tag{2-31}$$

Then,

$$E[\varepsilon_1 \mid C, \theta] = E[\varepsilon_2 \mid C, \theta] = 0 \tag{2-32}$$

$$\sigma_{\varepsilon_1}^2 = E[\varepsilon_1' \varepsilon_1' \mid C, \theta] = E[\varepsilon_1 \varepsilon_1 \mid C, \theta] = \sigma_{S2}^2 + \frac{\rho_b \sigma_{\theta_g}^2}{\theta} + \frac{\rho_b^2 \sigma_{S2}^2 \sigma_{\theta_g}^2}{\theta^2} \tag{2-33}$$

$$\sigma_{\varepsilon_2}^2 = E[\varepsilon_2' \varepsilon_2' \mid C, \theta] = E[\varepsilon_2 \varepsilon_2 \mid C, \theta] = \frac{\rho_b^2 R_E^2 \sigma_{C1}^2}{\theta^2} + \frac{\rho_b^4 R_E^2 \sigma_{C1}^2 \sigma_{\theta_g}^2}{\theta^4} \tag{2-34}$$

$$E[\varepsilon_1' \varepsilon_2' \mid C, \theta] = E[\varepsilon_1 \varepsilon_2 \mid C, \theta] = 0. \tag{2-35}$$

To facilitate our likelihood function calculations, we assumed that ε_1 and ε_2 were Gaussian with the means, variances, and covariance given in (2-32)-(2-35). The final calculation needed for evaluating $p(y_\theta, y_C|\theta, C)$ was finding the conditional covariance between soil moisture and chloride concentrations:

$$E[y_C' y_\theta' \mid C, \theta] = -\frac{C \sigma_{\theta_g}^2}{\theta}. \tag{2-36}$$

In summary, the likelihood function was assumed to be Gaussian with the following mean and covariance:

$$E\left[\begin{bmatrix} y_C \\ y_\theta \end{bmatrix} \mid C, \theta\right] = \begin{bmatrix} C \\ \theta \end{bmatrix} \tag{2-37}$$

$$Cov\left(\begin{bmatrix} y_C \\ y_\theta \end{bmatrix} \mid C, \theta\right) = \begin{bmatrix} C^2 \sigma_{\varepsilon_1}^2 + \sigma_{\varepsilon_2}^2 & -\frac{C \sigma_{\theta_g}^2}{\theta} \\ -\frac{C \sigma_{\theta_g}^2}{\theta} & \rho_b \sigma_{\theta_g} \end{bmatrix}, \tag{2-38}$$

where above entries are blocks including values for measurements at each observation depth.

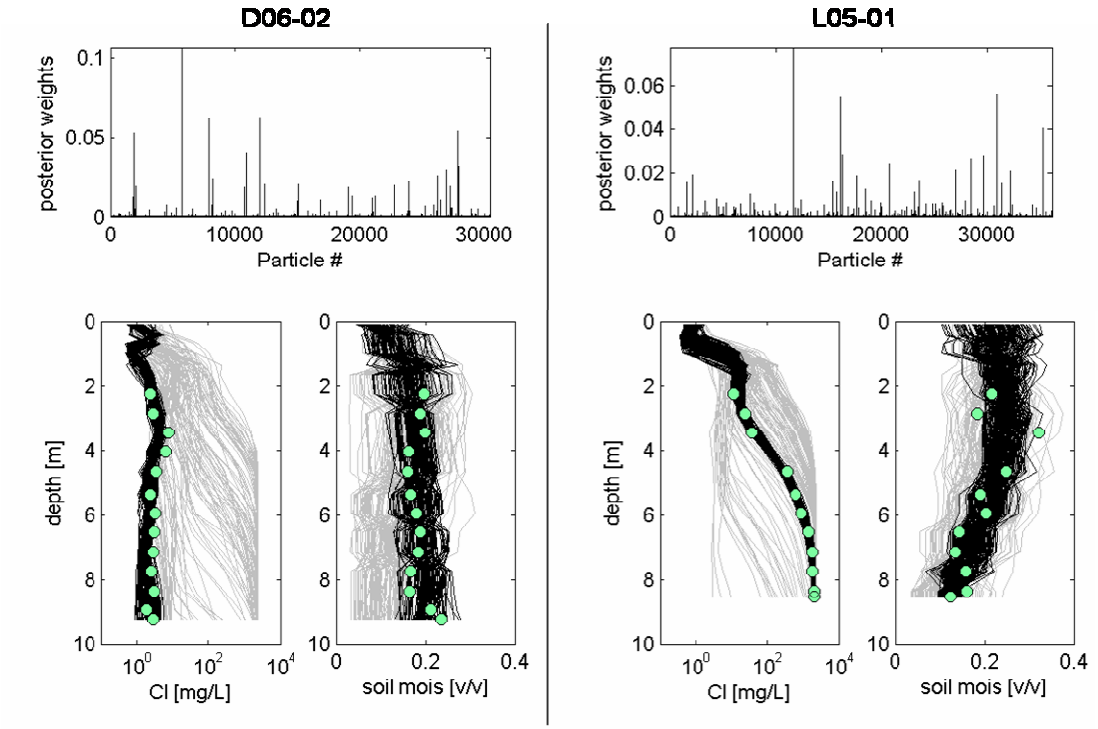

Figure 2-7: Top: Posterior (data-conditioned) particles have unequal weights, unlike the equi-probable prior particles. Bottom: Model states with significant posterior weights (black) are well-constrained by observations (green circles); prior model results are in gray.

2.4. Results and Discussion

2.4.1. Estimates of Model States and Long Term Recharge

Final model estimates are represented by sets of model inputs and simulations and corresponding probabilistic weights. While weights for all sets were equal before considering observations, signifying no greater confidence in any set over another, Figure 2-7 shows that high posterior weights were calculated with importance sampling for those

sets with soil moisture and chloride concentrations closely matching data points. It is evident from profile plots in Figure 2-7 that the prior range of input parameters, based on literature values, simulated a significant spread of soil moisture and chloride concentration profiles at the observation time; for both sites D06-02 and L05-01, the full range from highly concentrated to fully flushed chloride concentration profiles was produced for the prior. Some traditional calibration methods select a single model simulation set that best matches the observations, consequently ignoring other model results that also pass closely through data points. The probabilistic approach employed here recognized all model simulations that performed reasonably well, with the threshold for determining "good" matches set according to the uncertainty bounds of the observations.

As discussed earlier, deep percolation, or flux just below the root zone, is used as a proxy for recharge in this study; specifically, flux at a depth of 150cm was analyzed. To compare with traditional CMB results, long term average deep percolation was determined for each model run by dividing the simulated cumulative percolation following land-use change by the time since land-use change (until the observation date). Figure 2-8 shows that the prior percolation histograms have long distribution tails, demonstrating that numerical modeling alone may not provide good recharge estimates. Distributions for both data profiles peak around 10 mm/yr, although the high flux tail for D06-02 is somewhat wider, probably a result of the coarser soil texture there used in the pedotransfer function. Posterior histograms show that average percolation estimates were well-constrained by the data. Although the posterior peak for D06-02 is not higher than the prior peak, it shifted considerably to greater downward flux values, and the left-hand

tail is much tighter. As expected for L05-01, which had a partially-flushed chloride profile, the posterior percolation estimate shows less downward flux than D06-02. Although the posterior histogram mode does not differ as greatly from that of the prior, the peak is higher, and the long high flux tail seen in the prior distribution is mostly eliminated; confidence is thus greater for the low percolation estimate. The changes from the prior to the posterior percolation estimates at both sites confirmed chloride observations to be robust indicators of recharge.

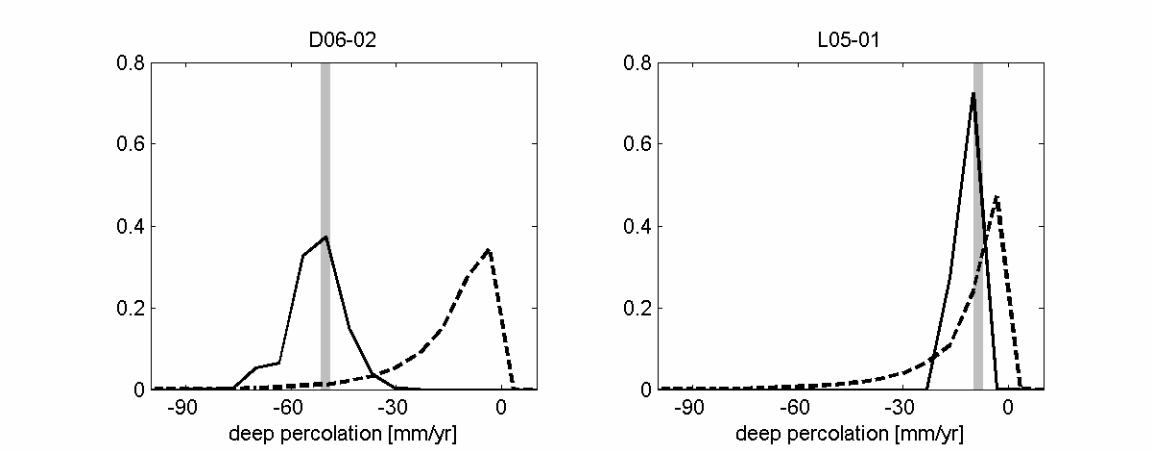

Figure 2-8: Histograms for prior (dashed) and posterior (solid) long term recharge; CMB estimate is indicated in gray.

The CMB recharge estimates are also included in Figure 2-8. CMB calculations for D06-02 included all assimilated data depths, while for L05-01 only the two chloride observation depths below the mixing layer (top 2m) and above the solute front were used. These resulting values differ slightly from those reported in *Scanlon et al.* [2007], which also used data depths from 100-200cm. As can be seen in Figure 2-8, the posterior distribution peak estimates agree well with the CMB values; this is expected, since numerical modeling also depends on mass conservation. An important difference

between our probabilistic approach to long term recharge estimation and the traditional CMB method is that our results directly generate uncertainty measures for recharge. Although CMB does not generally provide error estimates, *Scanlon et al.* [2000] calculated the uncertainty in CMB results by considering observation error in chloride concentrations and chloride input. In addition to observation uncertainty, data assimilation also accounted for the range of possibilities that were compatible with a physically-based moisture flux model in this work.

2.4.2. Estimates of Model Parameters

In the importance sampling framework presented in Section 2.2, the vector X represents values to be estimated based on observations. Typically, X contains model states, yet model parameters may also be estimated by including them in X; this approach is known as state augmentation in data assimilation. Parameter estimates make robust recharge predictions possible, which will be demonstrated in Chapter 3. As with flux estimates, probabilistic estimates of model parameters were produced with our approach, in contrast to the single parameter sets found using deterministic calibration methods. In importance sampling, posterior parameter estimates correspond directly to posterior state estimates. This is a significant advantage over Kalman-based methods, which generally would not guarantee that estimated parameters will simulate the estimated fluxes.

It is important to note that importance sampling assigns probabilistic weights to *sets* of models input, which means that rather than constrain any single parameter independently, it establishes relationships between model inputs that are critical for allowing the observed conditions. Consequently, identifying parameters with

significantly changed marginal posterior distributions can reveal important properties for simulations, yet it does not convey the full story on the conditional multivariate parameter distribution. For our data sites, despite the significant data-constraint shown in Figure 2-7, only a handful of the marginal parameter distributions were significantly changed, as documented in Appendix C. Of the two sites, D06-02 saw more significant marginal parameter changes, which could be expected from the considerable shift in the posterior recharge estimate. In particular, some of the shallow soil parameters and rooting depth were most heavily constrained, as indicated in Figure 2-9. Figure 2-9 also shows that rooting depth reduction was similarly important in producing the observed L05-01 conditions, though the only soil parameter notably changed was the evaporation parameter.

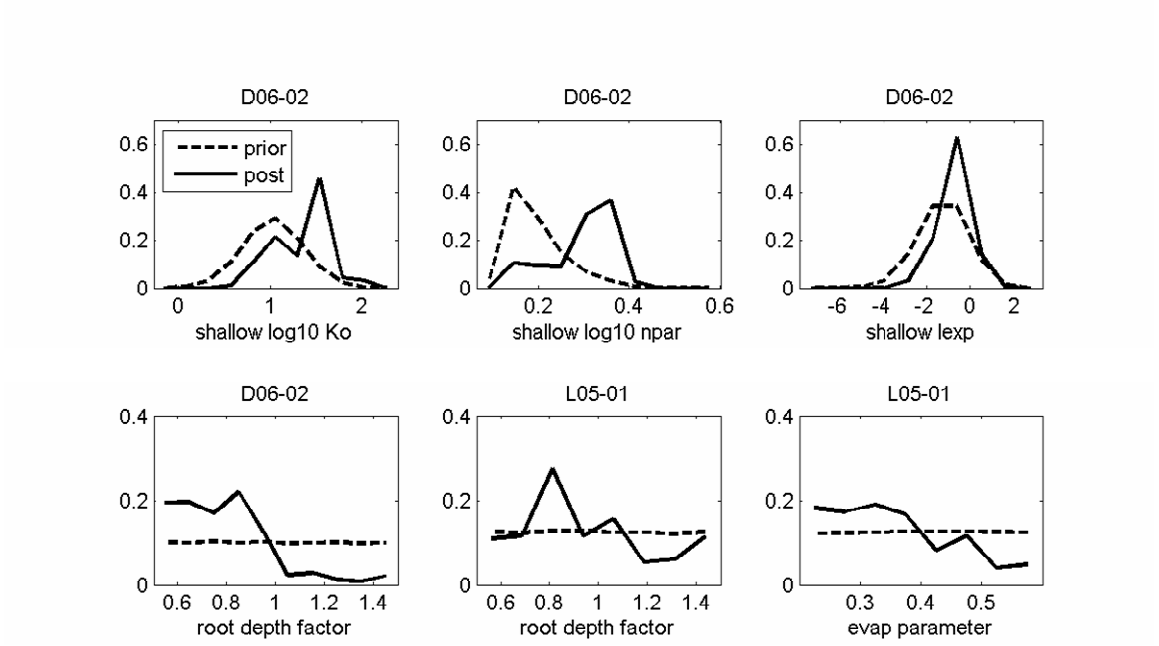

Figure 2-9: Sample of prior and posterior marginal histograms for parameters with greater constraints.

Although the largely unchanged marginal parameter distributions for other parameters may suggest unimpressive parameter estimation results, the emergence of posterior correlations between constrained parameters indicate that the parameter space had in fact been narrowed with data-conditioning. Examples of notable prior versus posterior correlations are show in Figure 2-10 and Table 2-5; the complete set of parameter correlations is included in Appendix C. For example, though the range of λ and *npar* soil parameter values at L05-01 changed little in the estimation procedure, their conditional values became significantly more correlated. Note that the smaller pre-existing correlation for prior parameters reflects soil relationships built into the Rosetta pedotransfer function. Even parameters with significant marginal constraints show further posterior narrowing in their relationship with other parameters, such as the rooting depth and evaporation parameter at L05-01. It is seen from (2-15) that more evaporation is simulated using a higher evaporation parameter, while similarly a greater rooting depth yields more transpiration. Thus, the observed conditions are possible only if these two competing elements are in balance to produce the proper amount of drainage.

Table 2-5: Samples of prior and posterior parameter correlations. Although marginal distribution constraints may be small, emergent posterior correlations indicate narrowing of posterior parameter space.

	Prior Correlation	Posterior Correlation
D06-02		
shallow npar & evap parameter	0	0.58
shallow K_o & shallow α	0.01	-0.60
deep K_o & deep lexp	0.05	0.56
L05-01		
evap parameter & root depth factor	0	-0.51
deep npar & deep lexp	0.15	0.59
evap parameter & shallow npar	0	0.40

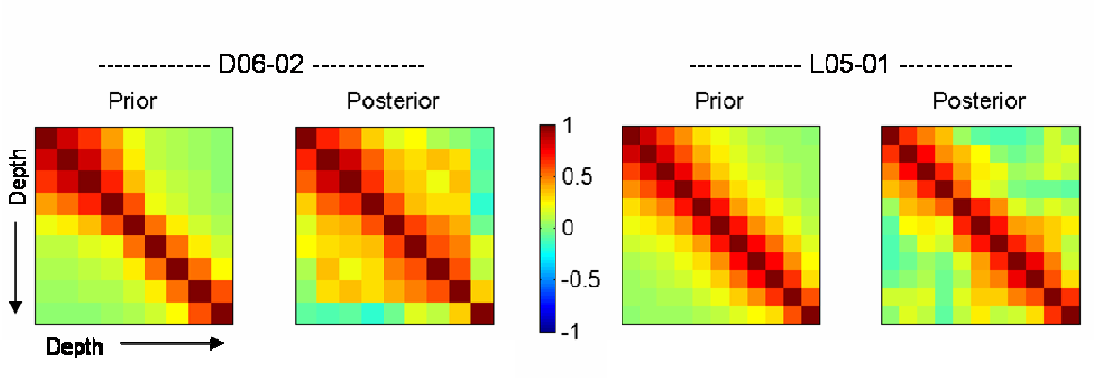

Figure 2-10: Correlation over depth for soil parameter K_o. Correlations build over depth for D06-02 with data-conditioning, while L05-01 appears to have less correlations and thus greater soil heterogeneity.

It is also apparent from Figure 2-10 that some correlation with depth was already present in the prior (due to the AR-1 soil uncertainty model described in Section 2.3.3), yet these correlations strengthened with data-conditioning for D06-02. Interestingly, the same building of posterior correlation with depth was less prevalent for the lower flux L05-01 site, suggesting a more heterogeneous soil profile there. This could corroborate other studies that found recharge to be less with soil layering [*Keese et al.,* 2005].

Although both profile sites contain cotton crops, estimation for the two sites were carried out independently of each other. Estimated rooting depths for both sites were both shallower than the prior depths, yet the posterior median for the coarser-textured D06-02 site was about 10% less than L05-01. While this is in line with the higher flux conditions found at D06-02, these results contradict studies showing rooting depth to be deeper in coarser soils to balance high drainage conditions [*Collins and Bras,* 2007; *Laio et al.,* 2006]. However, water usage at the two sites shown in Figure 2-11 compared reasonably with the range of measured SHP cotton ET in *Lascano et al.* [1987] and

Howell et al. [2004], suggesting realistic crop simulation at both locations despite the rooting depth difference. Our discrepancy with other studies on root depth and soil relationships could result from compensating effects for soil errors, though overall the rooting depths were not significantly different at the sites.

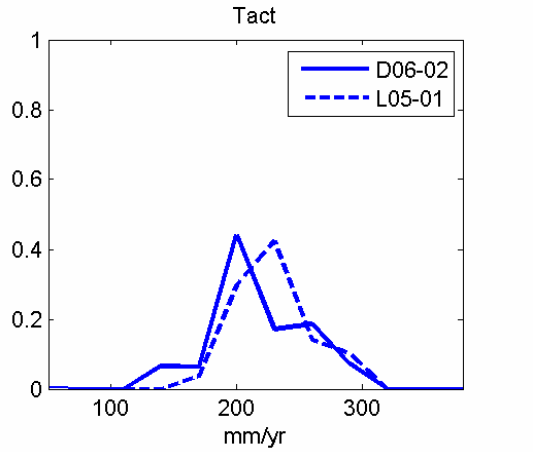

Figure 2-11: Posterior histograms of actual transpiration similar for data sites.

In addition to soil and vegetation parameters, the other uncertain model input was precipitation intensity (rainfall occurrence is deterministic). As shown in Figure 2-12, the changes from the prior were not significant, with the conditional rainfall at the fully-flushed D06-02 site only slightly higher. It is again the joint conditioning with other model properties that allowed model simulations to match observed data.

Overall, model input estimates showed poor constraints on many of the individual parameters, demonstrating that their effects could not be differentiated. However, the narrowing of the parameter space, indicated by emergent posterior correlations, established the types of interactions required among the soil, vegetation, and weather properties to generate the conditions seen at the data sites. Even the correlations shown

here do not display the full extent of the relationships in the multivariate parameter distributions. Without the conditioning on data, our prior understanding of the model inputs produced very uncertain recharge results.

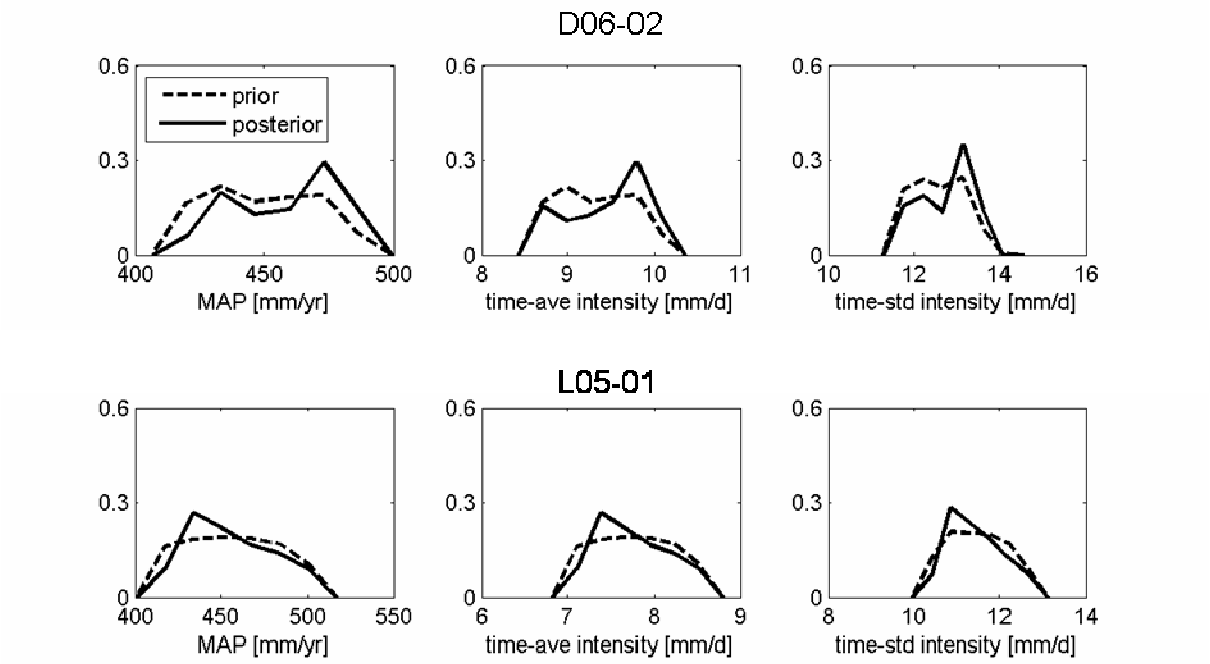

Figure 2-12: Prior and posterior histograms of precipitation statistics. Marginal distribution constraints are not significant.

2.4.3. Estimates of Recharge Time Series

Unlike classical CMB-based methods, the approach presented here allows for estimation of fine resolution flux time series. This can be important for understanding the control mechanisms that allow for recharge and for applications in which fine time scale dynamics are important, such as geochemical or contaminant transport. Estimating a historical time series leading up to the most current observation time is known as

"smoothing" in data assimilation, and it can be accomplished in two different ways for this recharge problem using importance sampling. The first option is to save the entire flux record from the land-use change until the observation date for each parameter/simulation set, and apply the posterior weight to the entire time series; this is equivalent to including model results at all times in the vector *X* of values to be estimated in equation (2-6). The disadvantage of this approach is the need to store in memory a potentially large amount of irrelevant data that may ultimately be assigned negligible posterior weights. A more favorable alternative for such cases is to estimate observation time model states and model inputs only. Then, only model inputs with non-negligible posterior weights are used to produce posterior fine scale time series. This latter approach was implemented here using the model input sets with the greatest posterior weights making up 97.5% of the total weights. For D06-02, these non-negligible weights consisted of 149 particles, and for L05-01, 355 particles.

Episodic recharge and interannual variability

Cumulative and weekly flux plots in Figure 2-13 and Figure 2-14 demonstrate that deep percolation has been significantly episodic, and far more so than precipitation. Although ripples in the cumulative precipitation record showed rainfall to be also irregular in occurrence, the corresponding cumulative percolation records was dramatically punctuated by occasional significant increases. Between high flux events, D06-02 was generally found to experience zero or very low downward flux, while it was possible that L05-01 saw upward flux at the reference 150 cm depth; thus, the finer soils in L05-01 were more likely to retain moisture at that depth for roots within the top 100

cm of the profile to tap into. The weekly percolation time series in Figure 2-14 shows flux events to have considerable interannual variability in occurrence and magnitude. While some years such as 1941 were dominated by exceedingly high percolation, some years such as the late 1950's at L05-01 experienced moderate percolation; yet other periods such as the early 1950's and mid 1990's saw virtually no percolation.

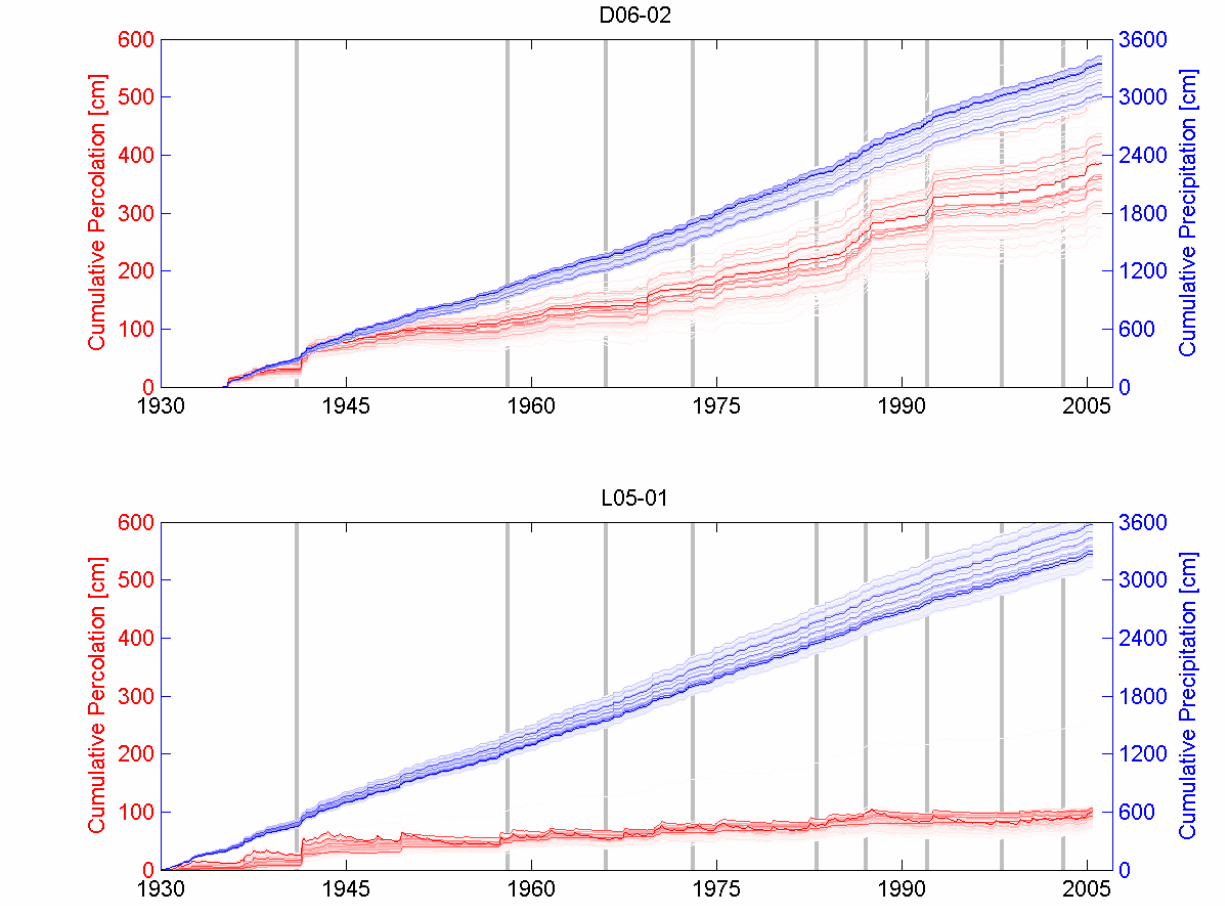

Figure 2-13: Cumulative precipitation and percolation starting from the time of land-use change until observation date; color intensities of time series scale with posterior weights (i.e. brighter line is more probable). Vertical lines indicate known ENSO episodes (winters of 1940-41, 1957-58, 1965-66, 1972-73, 1982-83, 1986-87, 1991-92, 1997-98, and 2002-03). Deep percolation is much more variable than precipitation.

Interannual variability in deep percolation could be caused in part by known interannual variability processes in the climate. Using a singular spectrum analysis approach, *Gurdak et al.* [2007] analyzed historical rainfall records and groundwater levels in the High Plains for known climate cycles and identified those characteristic of the Pacific Decadal Oscillation (10-25 years) and El Niño/ Southern Oscillation (ENSO) (2-6 year) to be present. Their findings suggested that those interannual climatic cycles could have significant impacts on vadose zone fluxes. In this study, we were able to directly estimate and compare deep percolation for known El Niño years, which typically bring wetter and cooler winters in this region. During the historical period considered here (1930-2006), there have been 9 significant El Niño episodes [Climate Prediction Center], which are indicated in Figure 2-13 and Figure 2-14.

Strikingly, the only two years in which both D06-02 and L05-01 experienced high intensity percolation events, 1941 and 1992, also happened to have El Niño events. While soil differences account for some of the dissimilarities in flux for D06-02 and L05-01, the non-coincident annual rainfall histories at the two sites shown in Figure 2-15 also gave rise to the diverse percolation series for the two sites. The profile D06-02 also saw a significant percolation event during the El Niño year 1987. Although most of the other El Niño years did not coincide with high magnitude percolation events at either site, some of those years had longer-duration, low intensity events, such as 1973 and 2003 for D06-02 and 1958 and 1987 for L05-01. Further relating fine time scale flux estimates to corresponding rainfall characteristics can help reveal how El Niño events and other types of precipitation events bring about the highly variable and episodic percolation found in the test sites.

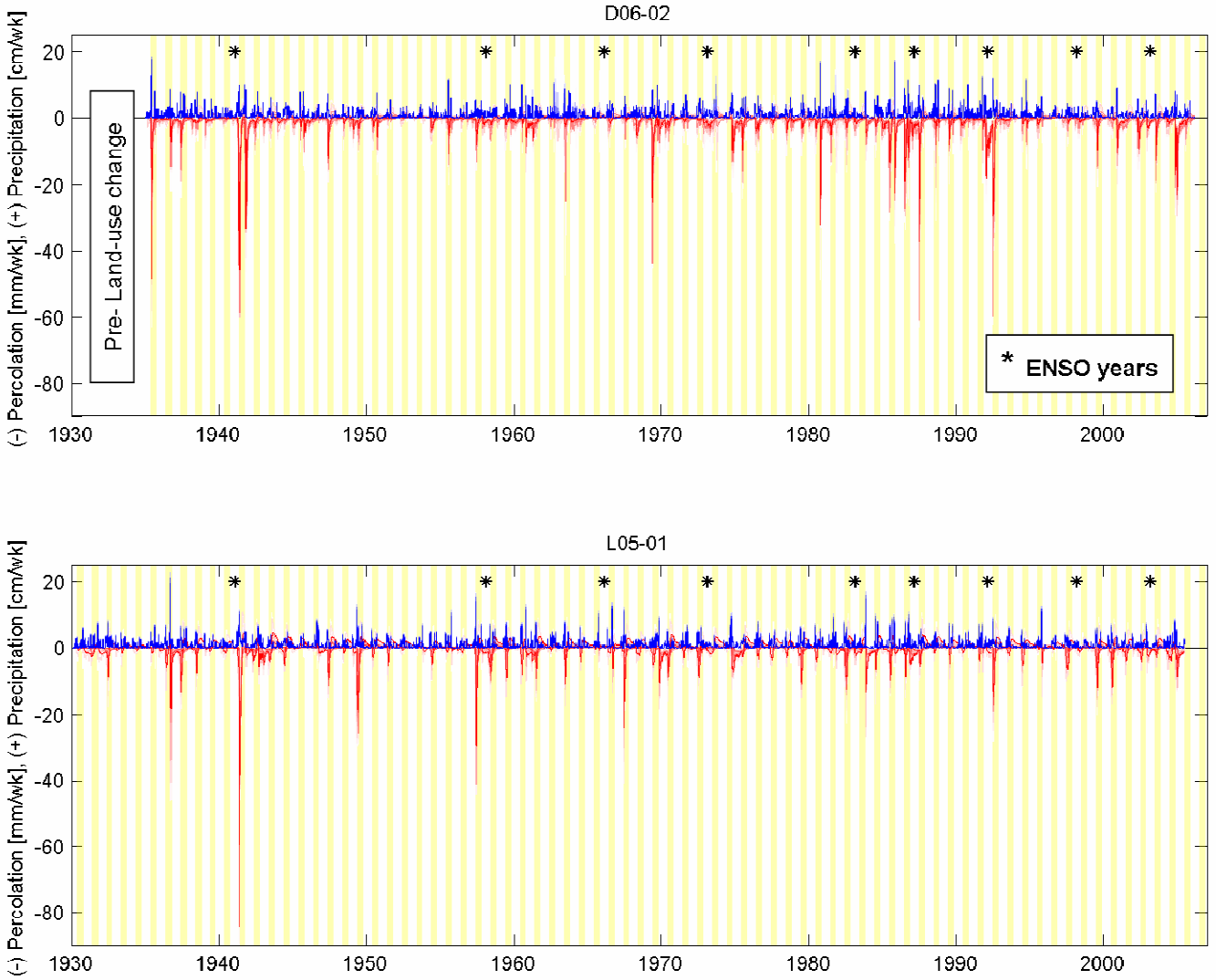

Figure 2-14: Weekly precipitation (blue) and percolation (red) time series, with growing seasons shaded yellow.

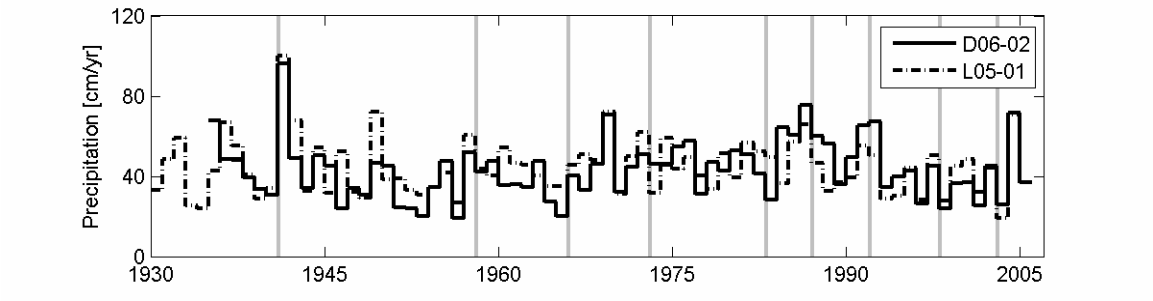

Figure 2-15: Annual precipitation for both sites; ENSO years indicated in gray. Some percolation time series differences arise from differences in precipitation at the two sites.

Sample time periods and recharge event mechanisms

Figure 2-16 focuses on example time periods from the full historical series for the two sites. From the flux histograms shown at selected time slices in Figure 2-16, it can be seen that between estimated high percolation events, there is high certainty that D06-02 experienced negligible or no flux. Similar certainty can be seen at L05-01 during dry periods for the absence of downward flux, though there is some probability of slight upward flux at 150 cm depth at the end of the growing seasons. Establishing this certainty of no downward percolation periods fortifies the argument that episodic percolation prevails at these sites. When percolation events do occur, their magnitudes can have important implications for subsurface chemical mobilization; however, it can be seen in Figure 2-17 that greater uncertainty lies in flux estimates during intense events. For example, although up to 60 mm of percolation could have occurred at D06-02 during the week ending at June 7, 1987, confidence in seeing such a strong spike was low. Also, the percolation timing was unsure, with possible start dates ranging over a couple of weeks. However, it is significant that histograms for June 14 and 28, 1987 confirm that a

major percolation event of at least 10 mm/wk strength did occur during that time. The histograms in Figure 2-17 also reveal that at the start of the percolation episode, it is possible that there was already a small amount of downward flux occurring. This suggests that sufficiently moist conditions could be critical for allowing extreme intensity percolation to follow.

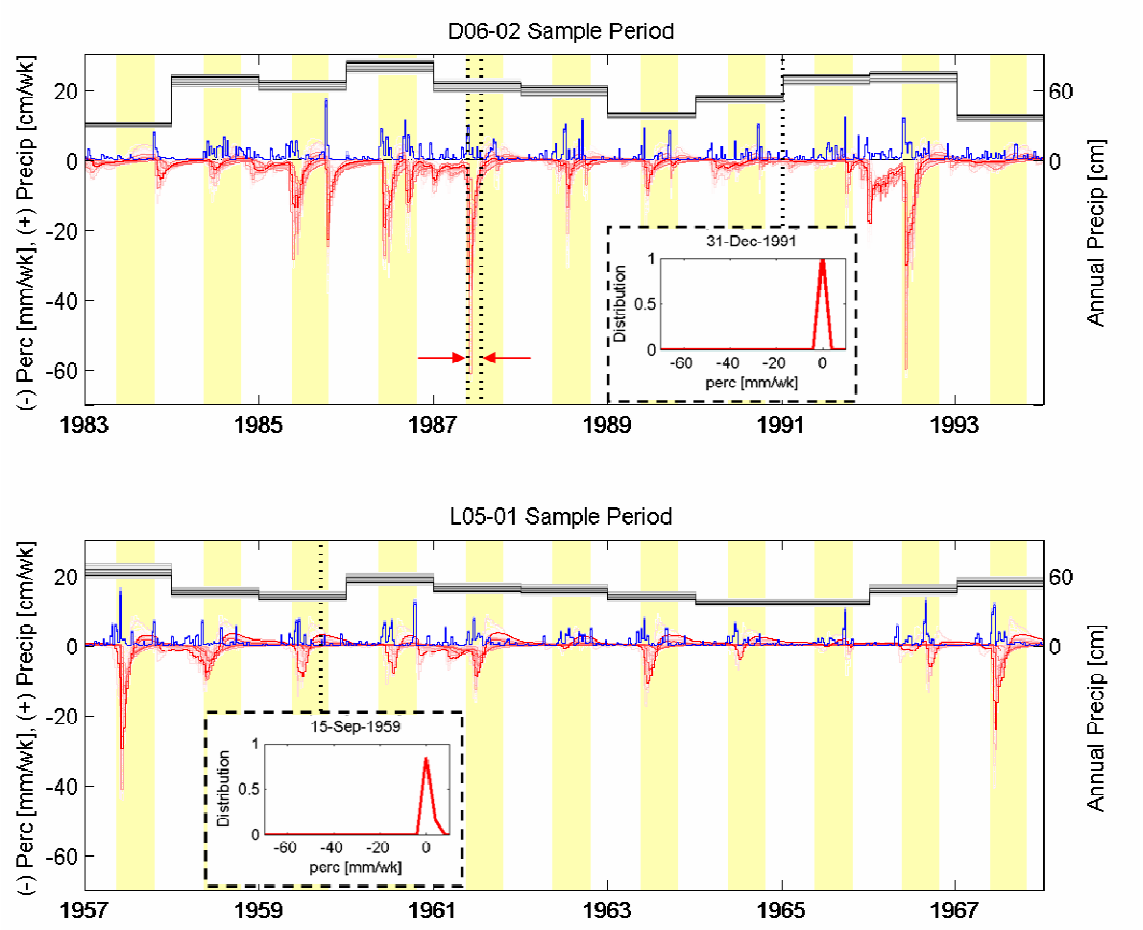

Figure 2-16: Sample time periods of weekly precipitation and percolation, with growing season shaded yellow. Color intensities of time series scale with posterior weights (i.e. brighter line is more probable). Insets: Histograms of weekly percolation at indicated time slices; date indicates end of week. The time period indicated by red arrows around percolation peak in D06-02 demark time range for histograms shown in Figure 2-17. Relating percolation time series to corresponding precipitation can reveal recharge control mechanisms.

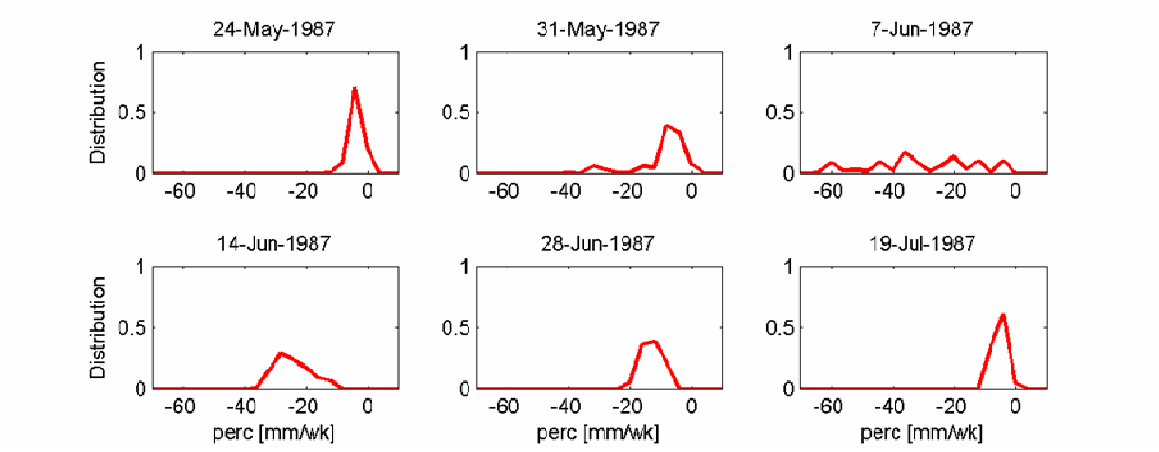

Figure 2-17: Weekly percolation histograms during the time range between red arrows in Figure 2-16 for D06-02; dates indicate ends of weeks. Although there is uncertainty in the exact peak percolation magnitude and arrival date, it is certain that a major percolation event did occur during this time.

A striking result from Figure 2-16 is that although annual precipitation might provide a convenient and tempting indicator for deep percolation, high flux events are clearly not entirely correlated with rainfall on that time scale. For example, 1991 and 1992 shared almost identical total precipitation amounts at D06-02, yet only 1992 was found to experience significant downward flux. Similarly, comparable annual rainfall fell at L05-01 in 1961 and 1962, with only the former having estimated deep percolation. It can be seen that intense concentrations of rainfall often provided the needed conditions for percolation events, such as in 1985 and 1992 at D06-02 and 1957 and 1967 at L05-01.

However, high weekly rain intensity was not sufficient for high percolation events either; strong rain events in 1991 at D06-02 and in 1965 and 1966 at L05-01 failed to produce any or particularly powerful flushing. Those strong rain episodes less capable of initiating flux events tended to occur in the mid to late part of the growing season, such as those years listed above. This suggested that heavy rainfall occurring when roots were at maturity tended not to be able to escape uptake at either site. In contrast, strong rain

pulses just at the start and sometimes also at the end of the growing season had potential for producing significant percolation events, such as in 1985 for D06-02 and 1967 for L05-01.

Although Figure 2-16 shows the non-growing season (late October – early May) to be generally drier, winter precipitation that did fall seemed to yield deep percolation even when the rain occurred at low intensity. This can be seen in 1984-1985, 1985-1986, and 1991-1992 for D06-02 and in 1957-1958 and 1960-1961 for L05-01. In all these cases, low to moderate intensity precipitation led to sustained, low percolation periods. Though the moisture contribution of these weak percolation events may not be significant, they often led to intense percolation spikes when stronger rainfall did occur at the start of the following growing season. This occurred for the highest magnitude percolation events at D06-02 (1987 and 1992). At L05-01, even moderate spring rainfall yielded notable flux events following the wet winter examples previously cited. In fact, the presence of winter rains seems the key difference between 1961 and 1962, which shared similar annual rainfall histories yet diverged significantly in flux histories. Even though the two strongest percolation events in the L05-01 sample period (1957 and 1967) did not have particularly rainy winters, the major rain events in both years were immediately preceded by light earlier spring rains. It thus seems that antecedent moisture, available following above-average winter rains, often played an important role in facilitating percolation events during big storms in late spring. In contrast, strong end-of-growing season percolation events were less common because of the typically drier conditions preceding it due to root uptake. These late-year percolation events seemed particularly rare at L05-01 due to the inertia of drying, upward fluxes typically seen then.

The implications of El Niño-type rain patterns on recharge can thus be understood by identifying the precipitation controls on deep percolation. Highest rainfall amounts and intensities typically occur during the growing season, and thus most percolation occurs at the start and end of the growing season, when root uptake is below its maximum. El Niño causes increases in low intensity winter precipitation, which would seemingly not affect recharge significantly. However, any additional rainfall during the non-growing season usually yields deep percolation. Furthermore, these winter rain episodes can create moist conditions at the start of the fallow season that greatly facilitate percolation when stronger spring and summer rains do arrive. Overall, the recipe for strong percolation events seems to be a combination of high total rainfall amounts, which allow for antecedent moisture, and intense rainfall.

Summary statistics

Although the variable nature of percolation limits the usefulness of average values to some extent, monthly trends and other summary statistics are helpful for characterizing dominating patterns of recharge for the sites. Figure 2-18 shows distributions of monthly average rainfall, rain intensity, and deep percolation over the historical period using box plots. Box lines indicate the first, second (median), and third quartiles, whiskers show data within another 1.5 times the interquartile range, and symbols represent outliers. Note that the spread represents uncertainty over the simulation ensemble and not variability over time. For both profile sites, May-July generally contributed most of the deep percolation, even though the rainy season extends from May through October. This confirms observations from the time series results that little moisture escapes fully

developed roots during the mid to latter part of the growing season. Although both sites match in their relative seasonal flux patterns, D06-02 generally experienced some winter percolation contribution while it was typically unlikely for notable amounts to occur at L05-01. Furthermore, based on the 25-75% confidence interval, L05-01 on average experienced a small net upward flux amount during the months of September, October, and November, while this was less likely for D06-02.

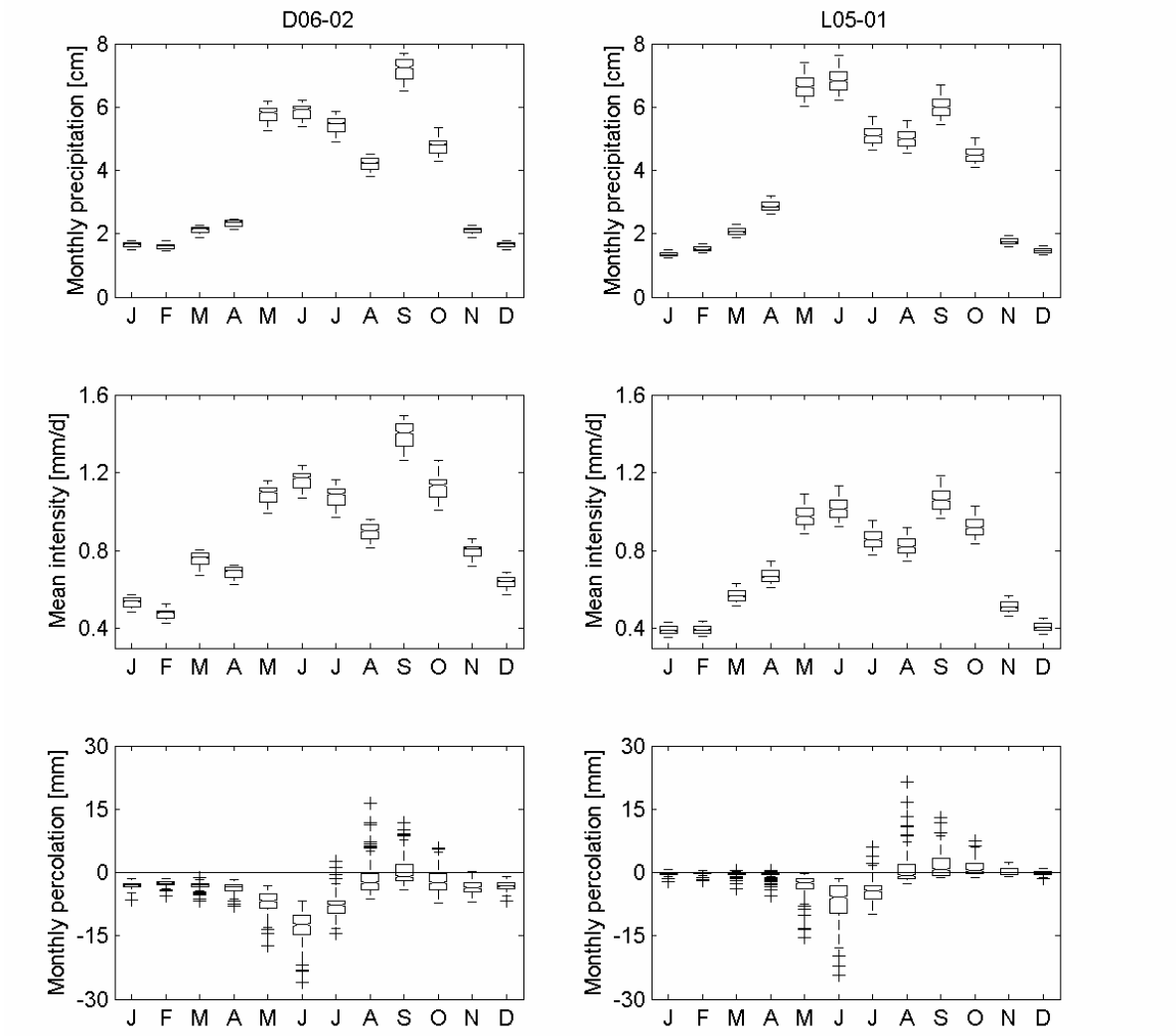

Figure 2-18: Box plots of mean monthly precipitation, intensity, and percolation. Spread shown is over ensemble of simulations, not time. Most percolation occurs in late spring / early summer at the sites.

To relate these monthly average flux estimates to precipitation, it was necessary to determine the lag time between rain occurrence and percolation. The wetting example shown in Figure 2-17 showed that percolation episodes can last at a few weeks following a rain event. Because of the considerable seasonal variability of both precipitation and flux, it could be expected that typical lag times between rainfall and percolation may vary for different months, and thus correlations between precipitation and subsequent flux are shown by month in Figure 2-19.

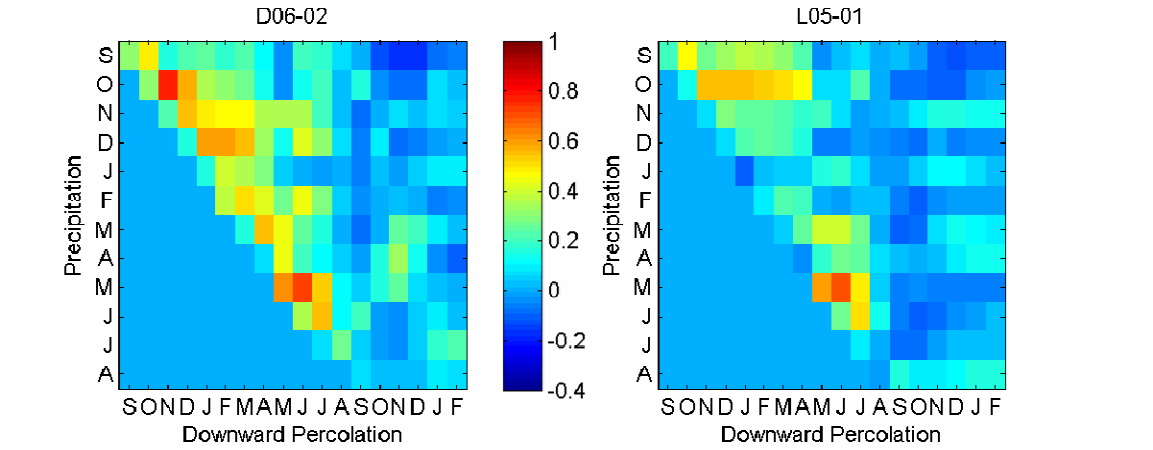

Figure 2-19: Correlation between monthly precipitation and downward percolation is same and following months. Months labeled with abbreviations, starting with September. Off-diagonal correlations indicate time lag between precipitation and resulting percolation.

Confirming a lag time for flux reactions, correlations were usually not strongest for precipitation and flux in the same month. Also, both sites showed an abrupt halt in correlations with August percolation, indicating the flux clock is in a sense reset because any previous moisture was almost all taken up by roots by then. Based on the correlations, May-July percolation at L05-01 was mostly controlled by rainfall occurring

since March, and May-July percolation at D06-02 may have been affected by rainfall since as early as the previous November. At both sites, May flux was mostly correlated with May rainfall, June flux with May rainfall, and July flux with both May and June rainfall. Overall, May rainfall seemed most important in determining recharge, probably because it is the only high rainfall month (in terms of total amount and intensity) without significant root density. June followed in importance, also before roots have reached full maturity. Non-growing season percolation at D06-02 seemed most strongly linked to rainfall in the previous month. Generally, correlations between rainfall and deep percolation were stronger at D06-02, further showing its soil to be more conductive and responsive.

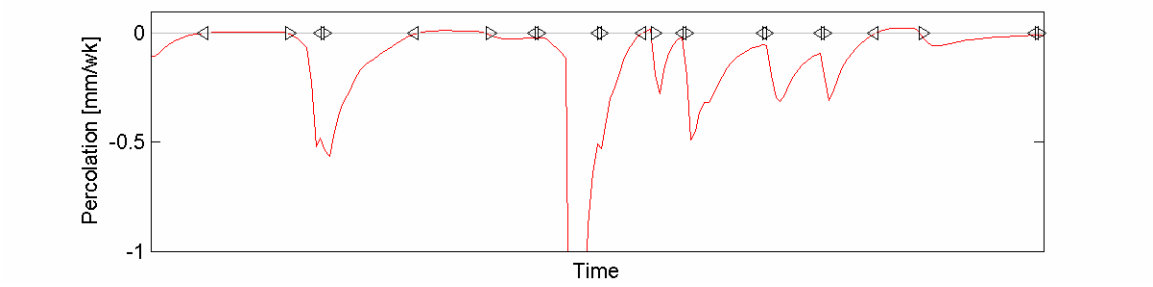

Figure 2-20: Demarcation of percolation events. Right-pointing triangles indicate starts of events, and left-pointing triangles indicate ends of events. Events are categorized according to their peak weekly percolation value.

To convey the overall episodic nature of percolation at the sites, the cumulative density plots in Figure 2-21 show how much of the net percolation at each site resulted from high intensity, infrequent flux events. These plots compare the cumulative fractional amount of net percolation for flux events of certain strengths, and they show the cumulative number of such strength events. Boundaries of percolation events were

identified by zero-flux crossings and by inflection points in the flux time series with negative concavity; Figure 2-20 shows an example of this. This analysis was done for each posterior simulation, and the first, second (median), and third quartiles of the ensemble distribution are shown.

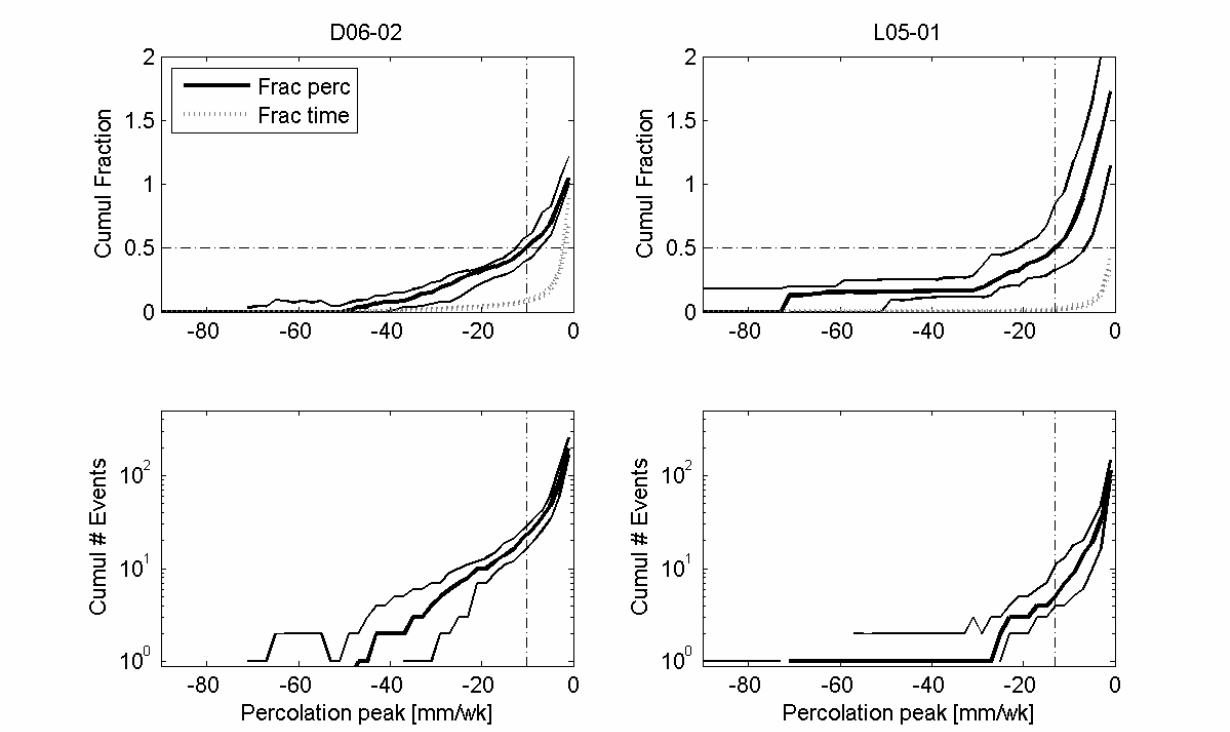

Figure 2-21: Top: Cumulative fraction of net percolation originating from percolation events of given peak intensities and stronger over the historical period (71-76 years), and cumulative fraction of time spent undergoing those percolation events. Bottom: Cumulative number of events of given peak intensities and stronger. Median and first/third quartiles over ensemble are indicated. For example, about half the total percolation at D06-02 originated from percolation events with at least ~10 mm/wk peak magnitudes; these 10 mm/wk events occur <10% of the historical time period over only about 15-25 events.

Profile D06-02 had about 50% of its net percolation at 150 cm depth occurring from percolation events of magnitude 10 mm/wk strength or greater, which only occurred

about 15-25 times over the entire period since the time of clearing, or on average about once every 3.5 years. In all, less than 10% of the time was spent undergoing an event of this 50th percentile flux magnitude. L05-01 similarly had about 50% of its net percolation originating from events of slightly over 10 mm/wk, though these occurred only about once every 15 years. Percolation at L05-01 could be characterized as more episodic than D06-02, considering less than 2% of the time was spent undergoing 10 mm/wk or greater events and percolation events are about 40% less common than at D06-02. Furthermore, the single most extreme percolation event at L05-01, which was traced to 1941, surpassed that of D06-02, and it contributed nearly a staggering 20% of the L05-01's net percolation. It should be noted, though, that D06-02 had overall more occurrences of moderately intense episodes, with over three times as many over 20 mm/wk events. These cumulative plots also show that L05-01 probably experienced about 20-150% more total downward flux than net percolation; this extra percolation was removed by upward flux toward the root zone during dry periods. Summarizing intense percolation risks, further analysis showed the maximum historic percolation peak to have first to third quartile ranges of 43 to 58 mm/wk at the D06-02 and 42 to 91 mm/wk at L05-01.

A similar episodic analysis was carried out on weekly precipitation; each weekly precipitation record was considered as an "event" for this analysis. Figure 2-22 shows that like percolation, weekly precipitation was also episodic in the sense that a disproportionately high fraction of total rainfall comes from large storms that take place more infrequently than small rain events. However, rain occurrence was far less episodic than percolation; there were on average four large rain events per year that contributed to 50% of precipitation, while it was likely that at most one flux event in every 3.5 years

made up half the net percolation. Thus, the irregular character of deep percolation can be partially traced back to episodic rainfall, yet other factors were at play. For example, the sequence of rain events, not conveyed through Figure 2-22, was critical for antecedent moisture conditions that allowed major percolation events. Furthermore, because the precipitation characteristics were shown to be very similar at the two data sites, it is largely the differences in the soil and root conditions at the two data sites that accounts for the disparity in episodic properties.

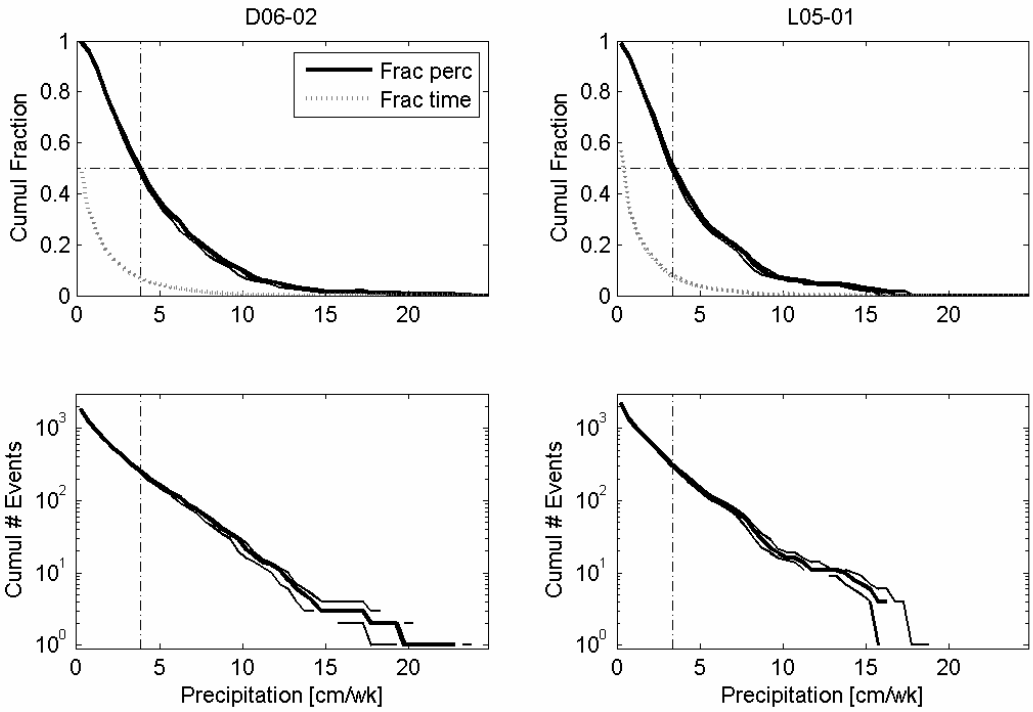

Figure 2-22: Top: Cumulative fraction of total precipitation originating from weekly events of given intensities and greater over the historical period (71-76 years), and cumulative fraction of time spent undergoing those precipitation events. Bottom: Cumulative number of precipitation events of given weekly intensities or greater. Median and first/third quartiles over ensemble are indicated. For example, about half the total precipitation at D06-02 originated from weekly events with at least ~4 cm/wk; these 4 cm/wk events occur ~5% of the historical time period over 250+ events.

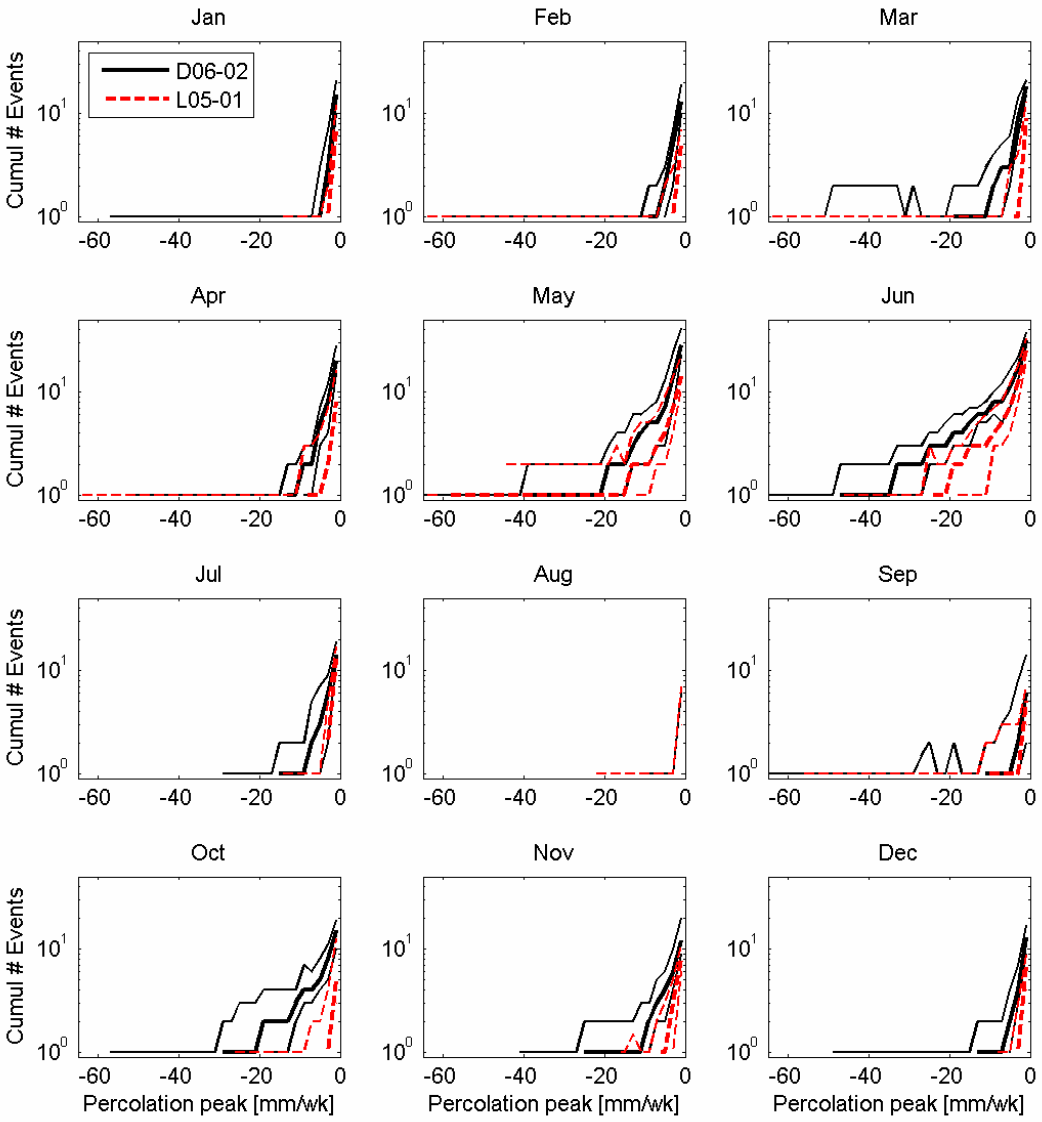

Figure 2-23: Monthly cumulative number of percolation events with given peak intensities. Late spring is most susceptible to rare, high intensity percolation events.

Monthly tallies of fluxes in Figure 2-23 allow us to further investigate when different types of flux events are likely to occur. There are similar patterns at both sites; hardly any percolation events were likely to have occurred in August, and only weak percolation events were ever seen in winter months. Although like in August, roots are fully developed in September, very occasional low to moderate flux events were

apparently able to infiltrate then as a result of extremely strong September rains. It is striking that neither site has near as high one event per year for any month for the entire 71-76 year historical period, showing that no month promises consistent percolation. Both sites showed May and June to be most susceptible to high magnitude percolation events, but as already suggested by the sample time periods examined, D06-02 also saw strong downward fluxes at the end of the growing season in October and November.

2.4.4. Comparison with Other Episodic Recharge Studies

Episodic recharge in semi-arid environments has also been examined using modeling in Australia, where increased recharge due to dryland agriculture has caused major salinization problems. The episodic recharge is of concern there because the infrequent and significant percolation events can limit how much agricultural management practices can curtail recharge. Thirty years of episodic recharge was estimated in Western Australia by *Lewis and Walker* [2002] using a simple water balance scheme; it was found that episodic recharge was commonly concentrated over only a few days in the wet (winter) growing season and 20-50% of episodic recharge occurred in the dry summer months of January-March. For our study sites, seasonal recharge patterns were more highly pronounced, with virtually no dry season (winter) percolation occurring at L05-01 and only about 10-25% of the total taking place in December-February in the form of mostly low intensity flux at D06-02. However, comparisons of our Richards model simulations with those from a simplistic bucket model are not very conclusive.

In a different episodic recharge study, *Zhang et al.* [1999a, b] employed another Richards-based model WAVES to investigate the effects of different crop rotation

practices on recharge in southeastern Australia. Their deterministic model was validated against vegetation and soil moisture data for various crops and two different sites. The SHP sites showed similar variability in monthly precipitation as one of their sites (Hillston), for which they concluded only 10% of annual percolation amounts contributed 50-75% of total percolation over the 35 years simulated for the tested crop rotation schemes. Estimates for our test sites were slightly less episodic with about the highest 10% of annual percolation amounts making up about 40% (D06-02) to 50% (L05-01) of the total since the land-use conversion. The inclusion of perennial pastures in one of the tested crop rotations in the Australian simulations accounts for their highly episodic estimate (10% of annual recharge amounts making up 75% of the total), though the lower range is quite high considering the use of fallow years. Analysis in this study extended beyond that of *Zhang et al.* [1999a,b] by considering modeling uncertainties and examining percolation events at sub-annual scales. While *Zhang et al.* [1999b] concluded that fallow years increase recharge by boosting moisture storage, this study found that it is very likely that even the dormant winter season in monoculture cotton practices in the SHP can provide antecedent moisture that facilitates later episodic recharge during intense rainy periods.

2.5. Summary and Conclusion

This chapter presented and demonstrated a probabilistic recharge estimation approach that integrates numerical modeling and data. Numerical modeling alone suffers from high sensitivity to parameter errors in dry environments, yet the traditional CMB methods using chloride data fail to generate fine time-scale recharge series estimates;

neither approach typically provides uncertainty measures of recharge. In our approach, model simulations for the semi-arid Southern High Plains region were conditioned on chloride concentration and soil moisture data using the importance sampling method. Although importance sampling requires a significant number of Monte Carlo simulations, its advantage is its ability to provide Bayesian conditional results for non-linear applications like the recharge problem. Critical to this probabilistic approach is the proper specification of uncertainty in the model and data. After developing uncertainty models for the soil and vegetation parameters, rainfall intensities, and the measurement error, distributional estimates of model inputs and deep percolation time series were produced.

For the two data sites considered, unconstrained long term recharge estimates showed significant spread. With the data conditioning, uncertainty was notably reduced for both, and the distribution peak for the wetter site was considerably shifted. These results confirmed that numerical modeling alone can lead to inconclusive or very misleading recharge estimates. The site with coarser soils was estimated to have about 40-65 mm/yr recharge, and the site with finer soils was estimated to have about 10-15 mm/yr recharge.

Model parameter results showed surface soil properties and rooting depth to be most sensitive to the calibration, while marginal distributions of most other parameters were not significantly changed. Correlations between some constrained parameters further revealed that the effects of certain individual parameters could not be differentiated using the available data. However, these correlations indicated that the full multivariate parameter distribution was altered with the data-conditioning, thus

establishing the combinations of soil, vegetation, and precipitation conditions needed for producing the observed conditions. This narrowing of parameter set uncertainty, rather than just individual parameters, was what improved recharge estimates.

The advantage of estimating fine time-scale percolation in this work is that unlike traditional CMB approaches, our approach provides insights into recharge mechanisms. At the two data sites, the deep percolation at 150 cm depth was found to be highly episodic and variable over the years, with 50% of long term percolation originating from recharge events occurring only once in about 3.5 years at the site with coarser soils and once in about 15 years at the site with finer soils. In fact, at the drier site, a single rare intense episodic event probably contributed almost 20% of the net percolation in 76 years.

Results also showed that on average, most deep percolation occurred in the early growing season (May-July), when rains are heavy yet roots have not reached full maturity. This time of year was also most susceptible to high magnitude percolation events, which typically follow high intensity rainfall. In contrast, heavy rains in the mid to late growing season rarely triggered appreciable percolation, especially at the finer-textured L05-01 site. Rain that did fall during the winter dry season led to weak but sustained percolation. Furthermore, these often provided antecedent moisture conditions that facilitate strong percolation peaks in the late spring, demonstrating that total rainfall amount in addition to rainfall intensity is important for major percolation events. This suggested that El Niño events can contribute to total and high intensity percolation by bringing wetter winters.

This work has demonstrated that a probabilistic data/model integration study of recharge can provide uncertainty bounds on long term recharge and episodic flux magnitudes in a semi-arid environment. Long term estimates can provide risk information for water resource concerns, while finer time resolution results can be important for chemical mobilization applications or other problems sensitive to intermittent dynamics in the subsurface. Together, constrained model parameter and percolation time series estimates revealed controlling factors of recharge. In addition to supplying historical recharge estimates, the conditional model parameters also provided stochastic recharge models for investigating recharge effects under varying conditions at the data sites. Impacts of climate change on recharge are evaluated in the following chapter using these constrained models.

Chapter 3

Probabilistic Recharge Predictions under Climate Change Scenarios

3.1. Introduction and Background

The most recent Intergovernmental Panel on Climate Change (IPCC) report [*IPCC*, 2007] indicates strong consensus that the climate is changing due to heightened atmospheric CO_2 from anthropogenic sources, but how the terrestrial hydrologic system will be impacted remains uncertain. Of particular concern is the fate of subsurface water resources in moisture-limited regions. Although the global average precipitation is expected to increase with a warmer climate, local rainfall amounts are likely to decrease in parts of the subtropics and mid-latitudes, which are often already dry. In other mid-latitude regions, different general circulation model (GCM) forecasts disagree in their predictions of rainfall. Further complicating the changes, precipitation is also expected to vary in ways other than total amount; higher intensity rainfall is possible for all latitudes, and shifts are not expected to apply evenly over the seasons [*Trenberth et al.*, 2003].

Changed climate is linked to groundwater impact via recharge, making the prediction of this moisture flux across the water table key to understanding potential groundwater vulnerabilities. How much rain water will escape evapotranspiration to reach aquifers in the future depends on changes in precipitation – both total amounts and intensities – and other meteorological variables. In addition to surface forcing, recharge is also a complex function of soil conditions, vegetative cover, and topography. Numerical models using water balance calculations can provide recharge simulations based on physical conditions. However, simulations can be very sensitive to model errors, especially in dry environments where the magnitude of recharge can be small [*Hillel and Gee,* 1988*; Allison et al.,* 1994]. Thus, the uncertainty in projecting future recharge rates lies not only climate change predictions, but also in the characterization of the other recharge controls and their link to recharge.

In recent years, a number of studies have tackled the problem of connecting GCM climate change predictions to potential impacts on local groundwater systems around the world. The approaches varied in how GCM predictions were incorporated and what type of hydrological model was employed. Most studies calculated meteorological change factors from GCM outputs. Some directly applied the factors to historical meteorological data for use in hydrological models [*Kirshen,* 2002*; Eckhardt and Ulbrich,* 2003*; Croley and Luukkonen,* 2003*; Brouyere et al.,* 2004*; and Serrat-Capdevila et al.,* 2007], while others used the change factors to calibrate stochastic weather generator models to produce their model inputs [*Rosenberg et al.,* 1999*; Scibek and Allen,* 2006*; Green et al.,* 2007*; and Herrera-Pantoja,* 2008]. *Loaiciga* [2003] derived scaling factors directly for runoff, and *Jyrkama and Sykes* [2007] used meteorological change ratios based IPCC

summaries rather than direct calculations from GCM results. Recharge models used in the studies ranged from simple water balance calculations based on the residual of precipitation and evaporation [*Kirshen,* 2002*; Herrera-Pantoja,* 2008], to multi-layered distributed models [*Rosenberg et al.,* 1999*; Eckhardt and Ulbrich,* 2003*; Brouyere et al.,* 2004*; Scibek and Allen,* 2006*; Jyrkama and Sykes,* 2007], to full Richards-based models [*Green et al.,* 2007]. More empirical approaches were used by *Loaiciga* [2003] and *Serrat-Capdevila et al.* [2007] to predict recharge from channel transmission loss and mountain front recharge.

Many studies looking at climate change and impact on groundwater systems acknowledged the uncertainty in future meteorological forcing by considering different climate predictions [*Rosenberg et al.,* 1999*; Kirshen,* 2002*; Eckhardt and Ulbrich,* 2003*; Croley and Luukonen,* 2003*; Brouyere et al.,* 2004*; Jyrkama and Sykes,* 2007*; Serrat-Capdevila et al.,* 2007]. Furthermore, studies that employed stochastic weather generators also accounted for uncertainty from natural weather variability within a given climate prediction; though, rather than report the resulting spread in recharge as done in *Green et al.* [2007], most averaged over the realizations. However, uncertainty in non-meteorological control factors of recharge was seldom explored. Many climate change and groundwater impact studies used uncalibrated models with single parameter sets based on the literature, which entirely overlooks model errors that can significantly affect results. Even though some models were calibrated and/or validated using groundwater level or stream flow data [*Rosenberg et al.,* 1999*; Krishen,* 2002*; Eckhardt and Ulbrich,* 2003*; Croley and Luukkonen,* 2003*; Brouyere et al.,* 2004*; Herrera-Pantoja,* 2008], their

use of single parameter sets still failed to represent the uncertainty due to the non-uniqueness of the calibration problem.

This study presents an approach to predicting climate change impacts on diffuse recharge that explicitly accounts for uncertainty in future meteorological conditions and in the other physical controls on recharge. To our knowledge, no other study of climate change impacts on recharge has provided such thorough treatment of uncertainty. For a range of GCM climate predictions, our approach provides probabilistic predictions of recharge based on natural variability of weather and uncertainty of soils and vegetation. Because of the significant sensitivity of recharge to model errors, the soil and vegetation parameter distributions were conditioned on current unsaturated zone data.

This probabilistic impact study is demonstrated using the data-conditioned stochastic recharge model that was developed in Chapter 2 for the semi-arid SHP region. In that chapter, recharge was found to largely originate from episodic percolation events allowed by the coincident occurrence of particular precipitation, vegetation, and soil conditions. This chapter examines the sensitivity of those recharge mechanisms to potential future climate changes. Future climate change predictions for the sites were considered for 16 GCMs participating in the World Climate Research Programme's (WCRP's) Coupled Model Intercomparison Project phase 3 (CMIP3) multi-model dataset[1], and a subset of those GCM results were used for recharge simulations. By providing probabilistic recharge predictions for a range of climate forecasts, this

[1] We acknowledge the modeling groups, the Program for Climate Model Diagnosis and Intercomparison (PCMDI) and the WCRP's Working Group on Coupled Modelling (WGCM) for their roles in making available the WCRP CMIP3 multi-model dataset. Support of this dataset is provided by the Office of Science, U.S. Department of Energy.

approach makes it possible to analyze the changes and risks to subsurface water reservoirs in the future.

3.2. Stochastic Recharge Model

The stochastic recharge model developed in Chapter 2 for two dryland cotton sites in SHP were used here for demonstrating the probabilistic approach to recharge prediction under climate change scenarios. As presented in that chapter, recharge distributions can be simulated by running the deterministic and physically-based unsaturated zone model SWAP with conditional distributions of soil and vegetation parameters. The conditional parameter distributions were constrained using chloride concentration and soil moisture data. By using soil and vegetations parameters conditioned on recent observations, we assumed there would be no major changes in soil or vegetation conditions at the sites in the future. The propriety of this assumption is discussed later. In this work, deep percolation below the root zone at 150 cm depth was simulated as a proxy for recharge at the water table. Time-averaged percolation should compare closely with average recharge, and temporal distributions of percolation provide information about surface controls.

Certain aspects of the recharge model developed in Chapter 2 are critical for proper probabilistic representation. Firstly, in this work, full parameter distributions were available for the Monte Carlo simulations. Simple distributional properties such as mean or standard deviation of parameter distributions are inadequate for inferring corresponding simple statistics of model outputs because of the significant non-linearity of unsaturated zone dynamics. Recharge impact studies that calibrate their hydrological

models using a single parameter set implicitly aim for using the mean or mode of a conditional parameter distribution; thus, they not only fail to account for uncertainty in their recharge predictions, but they may not even be capturing the average or most likely recharge value. Note that for Monte Carlo simulations, equi-probable parameter sets are needed, yet the importance sampling method described in Chapter 2.2 provided different conditional probabilistic weights for the different parameter sets. The resampling algorithm outlined in *Arulampalam et al.* [2002] was applied to the results to generate an equi-probable random sample of the conditional distributions; this is described in Appendix D.

Another key feature of our recharge model is that it is data-conditioned. It is possible to make probabilistic predictions using unconditioned, prior soil and vegetation parameters based on literature values. However, numerical model simulations are very sensitive to parameter errors, especially in semi-arid environments, and consequently parameter uncertainty may overwhelm efforts to narrow recharge predictions. In fact, in the historical recharge estimation of Chapter 2, the prior deep percolation distribution differed significantly from the data-conditioned distributions. For both sites, especially L05-01, the prior uncertainty was substantially greater. Even more striking, the prior mean percolation for D06-02 was considerably different from the constrained range. Thus, without probabilistic conditioning on data, it would have been unlikely to make informative predictions of recharge at these sites. Furthermore, the non-linearity of unsaturated zone dynamics could render even relative recharge change predictions unreliable for unconstrained recharge simulations.

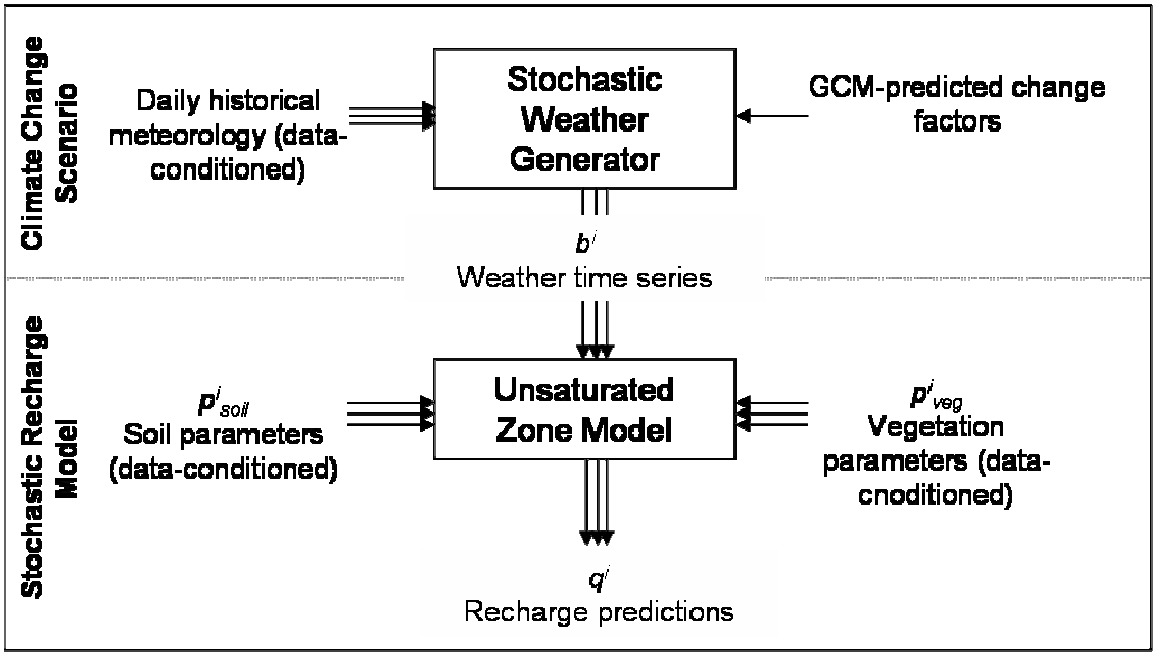

Figure 3-1: Diagram of probabilistic recharge prediction approach. Recharge distribution, discretely represented by the ensemble of flux simulations q^i, incorporates natural weather variability and uncertainty from soil and vegetation parameters. Model parameters are constrained with unsaturated zone data in Chapter 2.

3.3. Generating Climate Change Scenarios

Generating climate change scenarios for recharge predictions entails examining climate projections for the region and translating those climate projections into forcing inputs for the stochastic recharge model. Complex global circulation models (GCMs) have been developed by various research institutes to predict climate conditions under future CO_2 concentrations. However, these models involve great uncertainty and represent coarse time and space resolutions, making it inappropriate to use their results directly as daily point-scale inputs for a land-surface model. A procedure was thus needed for mapping GCM predictions to scales required for diffuse recharge simulations in a way that produces realistic weather patterns. Our approach to identifying potential

climate change scenarios from GCM predictions and linking them to recharge modeling is described in the following sections and outlined in Figure 3-1.

3.3.1. GCMs

GCMs are numerical coupled models of the atmosphere, ocean, and land surface that simulate conditions on a global scale. The models considered in this work were found from the CMIP3 dataset, which includes results from 25 GCM models. We selected 16 of those models and analyzed them for the range of future climate conditions predicted for the SHP region. These 16 models, listed in Table 3-1, were chosen because of the availability of daily output (needed for predicting rainfall intensities, which could be important for recharge changes) and their inclusion in Table 8.1 of the IPCC AR4 [*2007*] for being among the most often cited models in their report. Due to the water-limited nature of the study site, we preliminarily focused on the predictions of precipitation change. We considered only the SRES A1B scenario [*IPCC,* 2000], which is a mid-range emissions scenario that was most commonly simulated in the CMIP3 dataset and depicted in the *IPCC AR4* [2007]. For our work, the future period of 2080-2099 was compared with the baseline of 1980-1999, as was done in most of the *IPCC AR4* [2007] summaries. Of the 16 models examined for their precipitation predictions, five were selected for recharge predictions. This subset of GCMs was selected to cover the diverse range in predicted total precipitation amounts and seasonal changes. In addition to precipitation, predicted changes in air temperature, solar radiation, wind speed, and vapor pressure were also incorporated.

Table 3-1: List of all GCMs considered, (*) indicates GCMs used for recharge predictions

	Model Name	Sponsor(s), Country	Annual precip change factor^
a	*ECHO-G	Meteorological Institute of the University of Bonn, Meteorological Resrach Institute of the Korea Meteorological Administration (KMA), and Model and Data Group, Germany/Korea	1.12 (↑)
b	CCSM3	National Center for Atmospheric Research, USA	1.03 (~)
c	*CGCM3.1(T47)	Canadian Centre for Climate Modelling and Analysis, Canada	1.02 (~)
d	CSIRO-Mk3.0	Commonwealth Scientific and Industrail Research Organization (CSIRO) Atmospheric Research, Australia	0.99 (~)
e	*BCCR-BCM2.0	Bjerknes Centre for Climate Research, Norway	0.96 (~)
f	FGOALS-g1.0	National Key Laboratory of Numerical Modeling for Atmospheric Sciences and Geophysical Fluid Dynamics (LAGS)/Institute of Atmospheric Physics, China	0.95 (~)
g	CGCM3.1(T63)	Canadian Centre for Climate Modelling and Analysis, Canada	0.93 (~)
h	ECHAM5/MPI-OM	Max Planck Institute for Meteorology, Germany	0.89 (↓)
i	INM-CM3.0	Institute for Numerical Mathematics, Russia	0.84 (↓)
j	PCM	National Center for Atmospheric Research, USA	0.83 (↓)
k	GFDL-CM2.0	U.S. Department of Commerce/ National Oceanic and Atmospheric Administration (NOAA)/ Geophyiscal Fluid Dynamics Laboratory (GFDL), USA	0.75 (↓)
l	CNRM-CM3	Météo-France/ Centre Natinoal de Recherches Météorologiques, France	0.73 (↓)
m	*MIROC3.2(medres)	Center for Climate System Research (University of Tokyo), Natinoal Institute for Environmental Studies, and Frontier Research Center for Global Change (JAMSTEC), Japan	0.73 (↓)
n	GISS-AOM	National Aeronautics and Space Administration (NASA)/ Goddard Institute for Space Studies (GISS), USA	0.72 (↓)
o	*IPSL-CM4	Institut Pierre Simon Laplace, France	0.62 (↓)
p	GISS-ER	NASA/GISS, USA	+

^ Multiplicative change factor predicted for grid cell containing D06-02 data site; arrows indicate increase or decrease in predicted annual precipitation; changes within 10% considered approximately unchanged (~).

+ Current climate precipitation outcome considered suspect; change factor not computed.

3.3.2. Downscaling GCM Predictions

As global scale models, GCMs typically use grid cells with resolutions of 2-4°, and even though the CMIP3 dataset includes simulations with 3-hourly output frequencies, there is generally little confidence of GCM results below a monthly resolution [*Prudhomme et al.*, 2002]. These resolutions are too coarse for capturing most hydrological processes, which are often influenced by land features on the scale of 10s of meters and daily or sub-daily meteorological dynamics, and thus GCM outputs cannot be directly used in hydrological studies. A number of spatial and temporal downscaling techniques have been developed to modify GCM predictions for appropriate use with hydrological models; a review of these can be found in *Fowler et al.* [2007]. Regional climate models (RCMs), which operate on a finer scale than GCMs and use GCM results for their boundary conditions, provide an appealing option that is physically-based; however, comprehensive RCM simulations are not yet widely available. In contrast, statistical downscaling methods are based on stronger empirical assumptions, yet are readily applicable; used in most other studies on the climate change impacts on recharge, this type of approach was adopted for this work.

The simplest variety of statistical spatial downscaling is the application of change factors to historical point data. The change factor (multiplicative or additive) of a meteorological variable is calculated from GCM outputs for a certain future scenario and GCM outputs for a baseline (current) time period. The GCM grid cell used should contain the location of the historical data. The assumption is that the relative change within a GCM grid cell should be the same everywhere. The other advantage of using change factors relative to GCM baseline outputs is that it helps reduce the effects of some

GCM short-comings. For example, the over-simulation of drizzle in GCMs [*Sun et al.*, 2006] is less problematic when considering GCM future simulations with respect to GCM current simulations. *Scibek and Allen* [2006] tested two more sophisticated statistical spatial downscaling methods using regression models and found them to sometimes produce substantially different results. Given the significant uncertainty of those more complex methods, this study implements the simple change factors for calculating future monthly meteorological values predicted under climate change.

Similar to spatial downscaling, the most straight-forward temporal downscaling method is the application of monthly change factors to daily historical data, with the assumption that variability within a month will not change; this approach is common in a number of climate change impact studies [*Kirshen,* 2002*; Eckhardt and Ulbrich,* 2003*; Croley and Luukkonen,* 2003*; Brouyere et al.,* 2004*; and Serrat-Capdevila et al.,* 2007]. However, the *IPCC AR4* [2007] warns that longer dry periods and higher intensity precipitation could occur where the total amounts decrease. Neither change phenomenon, which could greatly affect recharge, can be generated by directly scaling daily historical data with monthly change factors. Because it is considered important to capture such features in this study, temporal downscaling was carried out using a stochastic weather generator that was calibrated with daily historical data and modified to emulate the predicted monthly statistics, including precipitation amounts and dry spell lengths. Weather generator downscaling has been used in a number of other climate change and recharge studies [e.g. *Rosenberg et al.,* 1999*; Scibek and Allen,* 2006*; Green et al.,* 2007*; and Herrera-Pantoja,* 2008]. In addition to producing daily resolution data, using a stochastic weather generator allows for exploring the uncertainty of recharge

predictions due to natural variability of weather within a climate scenario. In contrast, directly applying change factors confines the analysis to the particular sequence of rain events found in the historical record.

3.3.3. Stochastic Weather Generator

Stochastic weather generators are statistical models that generate time series of daily meteorological data that are each different but fulfill the same climatic statistics. The review by *Wilks and Wilby* [1999] provides some background and describes the two main classes of stochastic weather generators: those that model precipitation occurrence as a Markov process and those that explicitly model spell-lengths (number of consecutive rainy days and number of consecutive dry days). First-order Markov processes tend to under-simulate long dry spells [*Wilks and Wilby*; 1999], and thus the spell-length model LARS-WG v. 4.0 [*Semenov*, 1998] was selected for use in this semi-arid study site. Full weather generators extend beyond rainfall models by also simulating other meteorological data in a consistent manner; generating a weather series with realistic combinations of precipitation, temperature, and solar radiation values etc. can be important for modeling recharge in dry conditions, where rainfall only occasionally exceeds ET under the right conditions.

LARS-WG generates daily time series of precipitation, maximum and minimum air temperature (T_{max} and T_{min}), and solar radiation based on a calibration set of historical daily data. Wet and dry spell lengths and precipitation intensities are modeled using a semi-empirical distribution based on the calibration data, temperature is modeled as an AR-1 Gaussian process conditioned on precipitation occurrence, and solar radiation is

modeled using a semi-empirical distribution conditioned on precipitation occurrence with a one day autocorrelation factor; further details are found in the LARS-WG manual (available at http://www.rothamsted.bbsrc.ac.uk/mas-models/larswg.php). Good performance for LARS-WG was demonstrated for diverse climate conditions [*Semenov*, 1998], and it was shown to satisfactorily simulate extreme precipitation (e.g. annual maximum precipitation) [*Semenov*, 2008], which was shown in Chapter 2 to play an important role in recharge at our study sites. LARS-WG has been previously used in a number of climate change scenario studies (e.g. *Semenov and Barrow*, [1997]; *Semenov*, [2007]; and *Scibek and Allen*, [2006]). To simulate changed climates, it applies monthly change factors for mean precipitation totals, mean wet and dry spell lengths, mean minimum and maximum temperatures, standard deviation of temperature, and mean solar radiation to its output. Daily GCM outputs are required for calculating change factors for wet and dry spell lengths. Note that daily precipitation intensities are indirectly changed when modifying mean precipitation totals and wet and dry spell lengths.

Past studies have shown LARS-WG to perform competitively with other weather generators, yet because these models are constructed to match only certain statistics, none can be expected to realistically reproduce all characteristics of weather at their target site. For example, LARS-WG tends to underestimate interannual variability [*Semenov*, 1998], as do other generators [*Wilks and Wilby*, 1999], and this could be important for generating episodic recharge. Although weather generators may not capture all features of true weather dynamics, they should at least produce correctly those that are important to the application of interest. Thus, it is important to not only validate base case (no climate change) weather simulations against historical weather observations, but also to

evaluate recharge simulations using the simulated weather. A preliminary test was carried out with an example SHP parameter set for weather simulations from LARS-WG and also the weather generator GEM [*Johnson et al.*, 1996], a first-order Markov chain weather generator that uses parametrically fitted precipitation distributions. Figure 3-2 shows that GEM almost exactly simulated the observed mean precipitation, but LARS-WG far out-performed GEM in capturing the mean annual maximum precipitation intensity with its semi-empirical precipitation scheme. Although mean precipitation is often used as the key descriptor for a site, it can be seen that recharge simulated with the GEM weather matched very poorly with recharge simulations using observed weather data. In contrast, LARS-WG results compared very well, thus supporting its use in this recharge impact study.

The SWAP model used for simulating recharge requires two meteorological variables not generated by LARS-WG: vapor pressure and wind speed. Historical records throughout SHP showed that within any month, daily vapor pressure was correlated with rain occurrence and T_{min}. In particular, relative humidity (relative to T_{min}) and T_{min} records for each rain condition seemed jointly Gaussian for each month. Thus, relative humidity, then converted to vapor pressure, is simulated by sampling the Gaussian distribution conditioned on the T_{min} record, with the mean and covariance calculated from the historical data. Because relative humidity is not expected to change with rising temperatures [*Allen and Ingram*, 2002], no change factors are applied to relative humidity when simulating climate change scenarios. However, vapor pressure is implicitly affected by changes in T_{min}. Historical wind speed data was found to look non-Gaussian and uncorrelated to rain occurrence, and thus it is simulated by randomly

sampling the historical records of wind speed (regardless of rain) for the corresponding month. Multiplicative climate change factors are used instead of additive to prevent negative wind speed values.

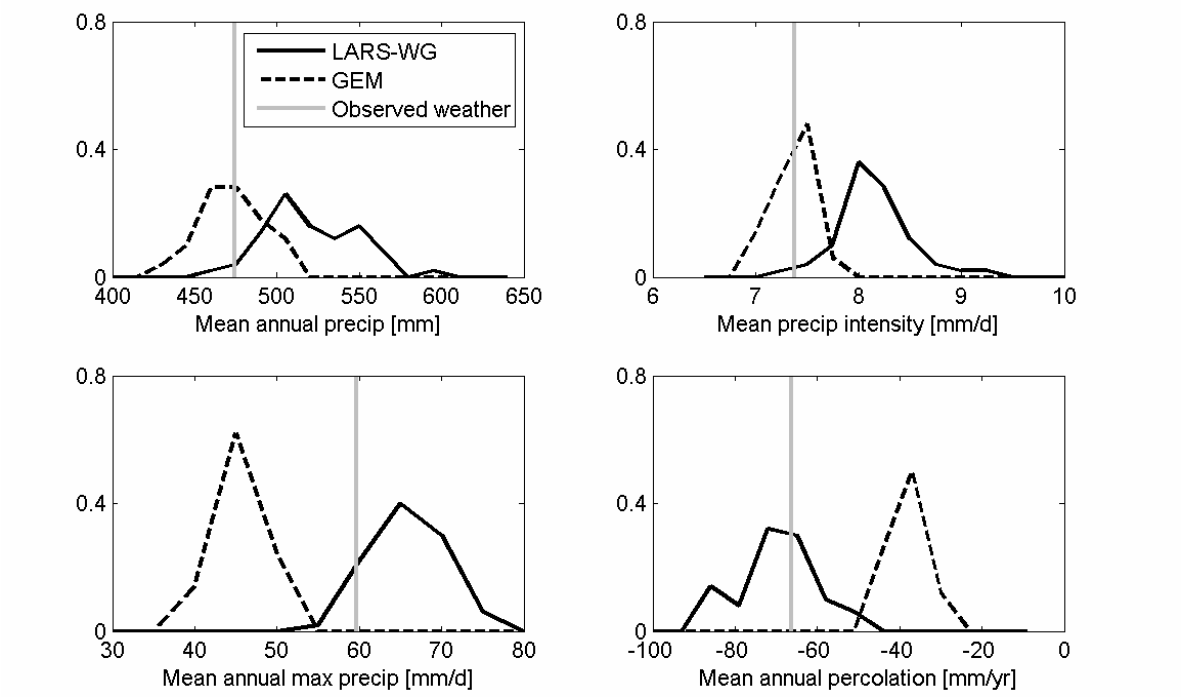

Figure 3-2: LARS-WG and GEM-generated precipitation compared with an observed precipitation series; percolation simulated with the model-generated meteorology compared with percolation simulated with observed meteorology. Percolation simulated with LARS-WG-generated precipitation matches better with percolation simulated with historical observations because capturing high precipitation events is important for recharge.

In addition to this extra wind and vapor pressure generator, solar radiation outputs from LARS-WG generator were slightly increased. LARS-WG imposes a range constraint on the solar radiation based on latitude that is calibrated using European data sites [*Semenov*, personal correspondence, 2008]. Possibly due to the clearer atmosphere in the High Plains, the imposed range constraint fell below that of SHP observations, and simulations were adjusted accordingly. Overall, correct simulation of non-precipitation

variables were expected to be less important than precipitation simulations in this water-limited study region.

3.3.4. Application for Recharge Predictions

Distributions of recharge were predicted for a range of GCM future outputs using the stochastic weather generator downscaling approach described above. Specifically, for each GCM climate scenario, 200 realizations of weather time series of 75 years length were generated using the stochastic weather generator LARS-WG and historical data. A distribution of 200 recharge series was then simulated using the weather series realizations and the data-conditioned soil and vegetation parameter distributions. Although change factors were calculated from predictions for 2080-2099, the 75 year time length was chosen to parallel the historical estimates made in Chapter 2 over 71-76 years. Some studies also considered transient climate change scenarios [*Brouyere et al.*, 2004; *Kirshen*, 2002; *Serrat-Capdevila et al.*, 2007; *Herrera-Pantoja and Hiscock*, 2008; *Scibek and Allen*, 2006], yet this study applied constant climate predictions and instead focused on probabilistic analysis.

Note that our work differs slightly from other recharge studies using stochastic weather generators in that the historical meteorological record used here for calibrating LARS-WG was not entirely deterministic. The data-conditioning carried out in Chapter 2 not only constrained uncertain soil and vegetation parameters, but also uncertain historical meteorological forcing; to account for instrument errors and mismatch between rain conditions at the data site and meteorological station, daily rainfall amounts on rainy

days in the historical record were treated as uncertain. As a result, for a certain soil/vegetation parameter set in the Monte Carlo recharge simulation, the corresponding conditioned historical precipitation series was used to calibrate the stochastic weather generator.

For consistency, future recharge impacts were ultimately assessed by comparing recharge predictions under climate change with recharge forced with LARS-WG-simulated weather for current "base case" conditions. The former were carried out using LARS-WG outputs calibrated to conditional historical data and altered with GCM change factors, and the latter were found using LARS-WG outputs without change factors. In the rest of this thesis, "base case" refers to LARS-WG weather simulations without climate change factors. Thus, in total, recharge predictions were made for 6 climate scenarios: the base case + 5 GCM-predicted change scenarios.

3.4. Results and Discussion

3.4.1. GCM Results

GCM predictions

Based on their map coordinates, D06-02 and L05-01 fall in different, neighboring grid cells in the north-south direction for many of the GCMs considered. The present-day precipitation gradient runs east-west, and if relative climate dynamics in the region remain largely similar in the climate predictions, precipitation change factors for the two grid cells should resemble each other. Figure 3-3 confirms that indeed most precipitation projections for the two grid cells are similar. Because of this, and to facilitate

comparisons, climate predictions for the grid cell containing D06-02 were applied to both test sites. Those GCM predictions with more notable differences between the two grid cells (CGCM47, BCCR, CGCM63, and INM) are still within the range of uncertainty covered by the 16 models.

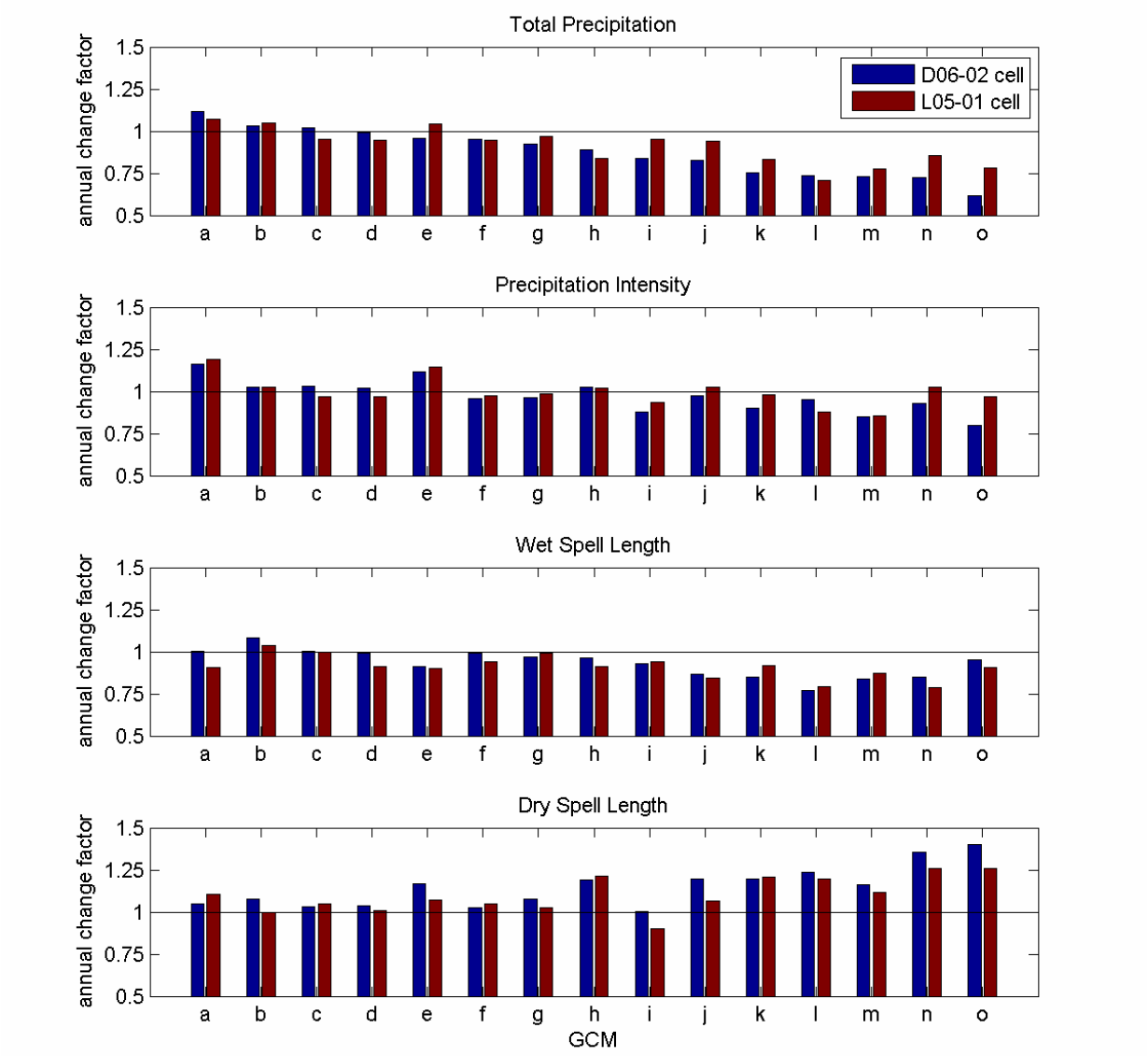

Figure 3-3: Multiplicative change factors predicted by GCMs for mean annual precipitation, precipitation intensity, wet spell lengths, and dry spell lengths for grid cells containing D06-02 and L05-01 data sites. GCM letters correspond to Table 3-1.

The 16 GCMs considered in this study demonstrate the uncertainty in future precipitation predictions in the SHP. Note that GISS-ER was considered suspect due its very high current-climate precipitation simulation and was thus omitted in the study. As shown in Figure 3-3, a little over half the GCMs predicted a decrease in mean annual precipitation in the future, while most of the remainder project total precipitation to remained about the same (within a 10% change); only one GCM predicted a slightly wetter future. Although many studies propose widespread increases in future precipitation intensities (e.g. *Allen and Ingram* [2002]; *Gutowski et al.* [2007]; *Kharin and Zwiers* [2004]; *Easterling et al.* [2000]; *Trenberth et al.* [2003]), only a couple of GCM predictions examined here showed such an increase. Other GCM predictions for the D06-02 grid cell agree with *Sun et al.*'s [2007] multi-model comparison study, which found general decreases in intensity predictions with lower totals. However, mean intensities were not projected to decrease as much as total precipitation, which also was evidenced in the general increase in predicted mean dry spell lengths and decrease in predicted mean wet spell lengths.

Seasonal patterns of precipitation change predictions were even more varied than annual values, as shown in Figure 3-4. Although only one GCM of the 16 projects increased annual precipitation, over a third predict at least one season with increased precipitation. Summer precipitation uncertainty seemed greatest, with some GCM outputs showing substantially drier conditions and others showing notably wetter summers. Spring results seemed most consistent, with many GCMs predicting slightly lower rainfall amounts. Seasonal precipitation intensity changes mostly mirrored total

precipitation changes, except values were slightly higher, due to generally longer seasonal dry spell lengths.

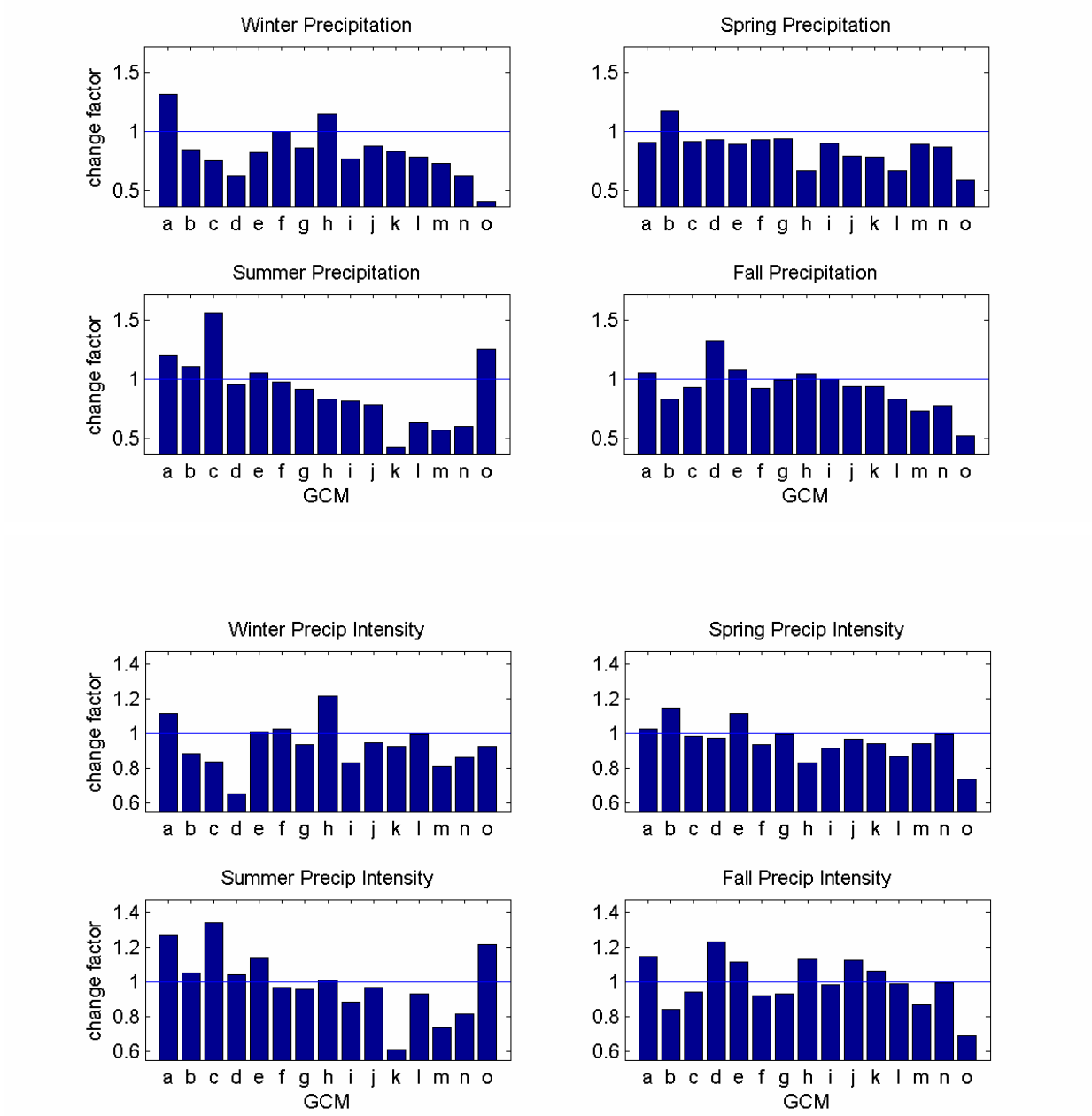

Figure 3-4: Seasonal multiplicative change factors predicted by GCMs for average precipitation and precipitation intensity for grid cell containing D06-02 site. GCM letters correspond to Table 3-1.

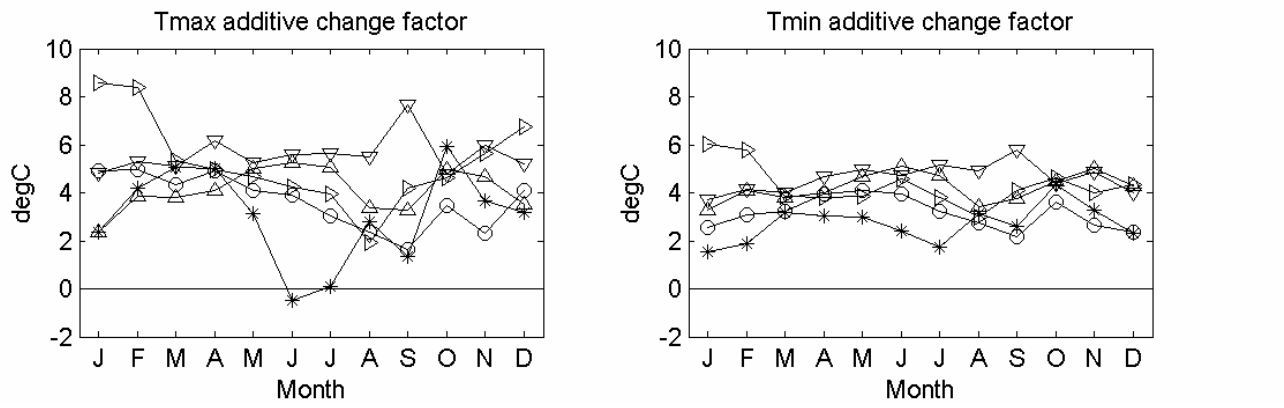

Figure 3-5: Monthly temperature additive change factors predicted by GCMs for grid cell containing D06-02 site. Upward pointing triangle: a. ECHO; asterisk: c. CGCM47; circle: e. BCCR; downward pointing triangle: m. MIROCm; right pointing triangle: o. IPSL. In contrast to the significant uncertainty in precipitation predictions, all models project a warmer future.

Predictions from 5 GCMs were selected for the recharge predictions, which are indicated in Table 3-1. Because of the significant differences among the GCM outputs, the group was chosen to represent different features among the climate predictions. Overall, the aim of this work is not to make absolute predictions on how much recharge will occur in the future, but instead to examine the sensitivity of recharge to possible climate changes projected by GCMs. Our diverse subset of GCMs included two models with drier futures: IPSL-CM4 ("IPSL"), which showed the driest total outcome, and MIROC3.2(medres) ("MIROCm"), which was among the few GCMs predicting decreased precipitation for all months. ECHO-G ("ECHO") was chosen to represent a wetter future scenario for the region. Also included were two GCMs representing those that project similar annual precipitation as current conditions: BCCR-BCM2.0 ("BCCR"), which projected more intense rains, and CGCM3.1(T47) ("CGCM47"), which predicted drier winters and wetter summers. All GCM models predicted increased

T_{max} and T_{min} (shown in Figure 3-5), and overall solar radiation and wind speeds were not expected to change significantly (not shown here).

GCM performance

Given the uncertainty in climate modeling, different GCMs are generally considered equally accurate or inaccurate. To help alleviate the effects of climate modeling errors, change factors were found relative to current climate model outputs rather than to actual meteorological observations. However, comparing current climate GCM simulations with observations can provide a metric for assessing GCM performance. Comparisons for the monthly values inputted into LARS-WG are shown in Figure 3-6 for historical observations and the five GCM simulations used for recharge predictions. Although precipitation is considered the most important forcing in this semi-arid environment, performance of all meteorological fields should be considered due to the complex interactions of climate dynamics. Note that a perfect match between observations and GCM outputs should not be expected, because downscaling was not used to map the large grid cell resolution of the GCM to the point observations. However, meteorological observations for two SHP locations (closest to the two data sites) were included for a wider representation of the regional meteorology.

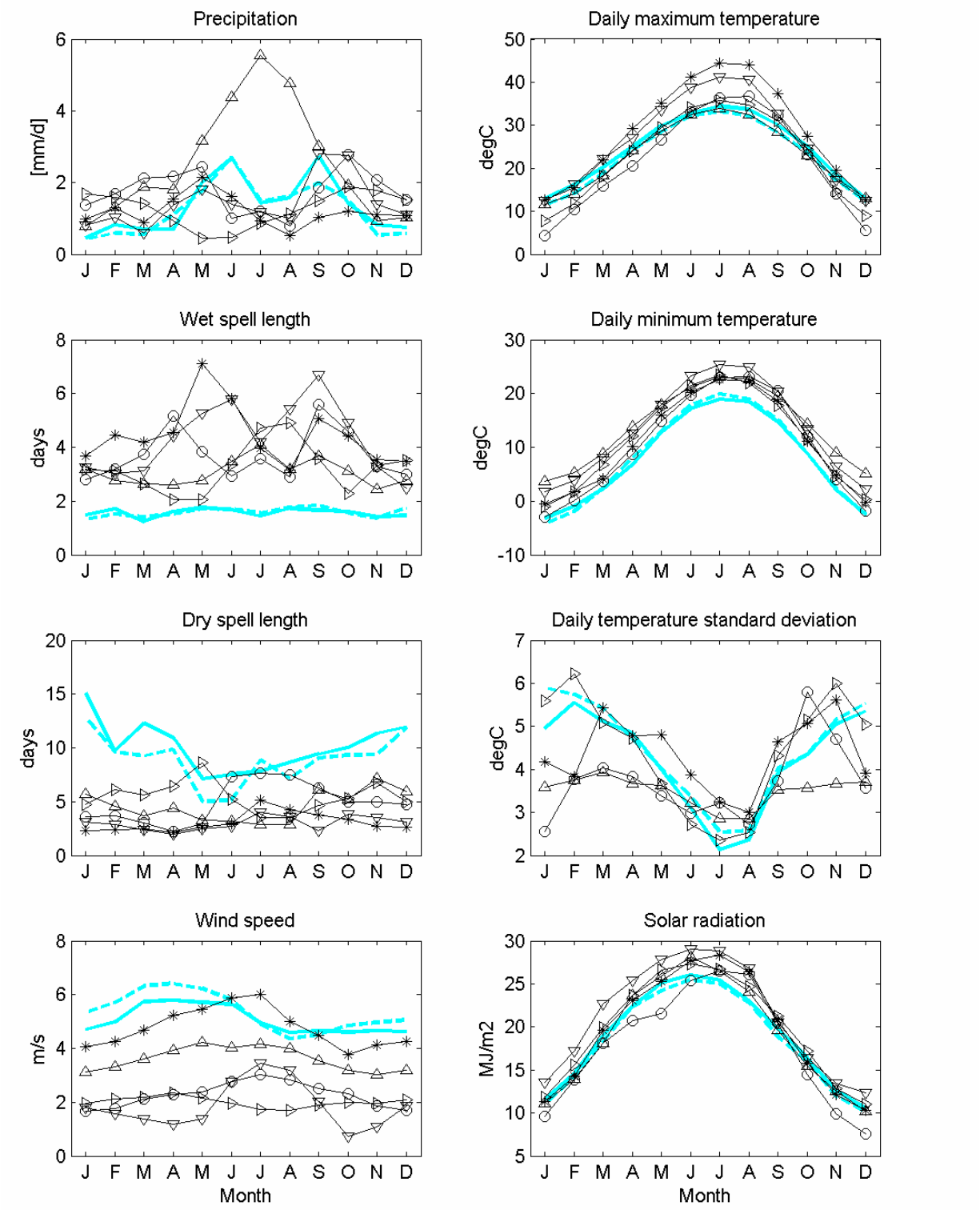

Figure 3-6: Comparison of current-condition (~1981-2000) mean monthly GCM outputs (symbols) with SHP observations (cyan). Upward pointing triangle: a. ECHO; asterisk: c. CGCM47; circle: e. BCCR; downward pointing triangle: m. MIROCm; right pointing triangle: o. IPSL. Solid cyan line: Lamesa observations; dashed cyan line: Lubbock observations.

Nearly all five GCMs accurately simulated more rain during the growing season, even though the monthly distribution was generally not as good a fit. IPSL, which actually provided the best match for observed annual precipitation, was the main exception with a simulated winter rainy season. ECHO also stood out for its unusually high summer precipitation total. Greater errors persisted for wet and dry spell lengths in the GCMs, with wet spell lengths consistently showing a high bias and dry spell lengths showing a low bias. This likely reflects the over-simulation of very low intensity rains known to plague GCM results [*Sun et al.*, 2006]. It could also suggest difficulty in simulating high daily precipitation intensities, which is in agreement with other studies that found deep convective storms of the region to be poorly represented in GCMs [*Deng et al.*, 2007]. ECHO and IPSL were the most successful in capturing the observed seasonality of dry spells in this region, which currently experiences long dry periods in the winter.

Monthly patterns were very well simulated for air temperature and solar radiation, as could be expected by the dominance of seasonal forcing. For actual temperatures, all analyzed GCMs outputted minimum temperatures higher than observed. Many GCMs simulated maximum temperatures very well, though CGCM47 and MIROCm generated overly warm summers. All GCMs successfully simulated lower monthly air temperature variability in the summer, with IPSL results matching remarkably well with the standard deviation of observed monthly temperature. Except MIROCm, all GCMs modeled higher winds in the spring as observed, though only CGCM47 was close in following observed magnitudes.

It was thus determined that although none of the GCMs included in the recharge study perfectly modeled the current climate, all successfully captured some of the observed features. Of the five, IPSL could be considered the most suspect due to its failure to correctly simulate precipitation seasonality. However, it is noteworthy that it provided satisfactory to very good results for all other meteorological properties considered, including dry spell lengths. More importantly, it should be cautioned that success in simulating current climate conditions does not guarantee accuracy in simulating emergent future climate conditions.

3.4.2. Weather Simulation Validation

Although stochastic weather generators are designed to emulate specific meteorological statistics, actual simulated weather series were evaluated to ensure they perform as expected. Box plots for the 200 realizations of 75-year monthly means are shown for base case LARS-WG weather simulations (no change factors) and conditioned historical data in Figure 3-7. In these and other box plots in this thesis, box lines indicate the first, second (median), and third quartiles, whiskers extend to values within another 1.5 times the interquartile range, and symbols indicate outliers. Spreads in the simulated precipitation results are often greater due to random variability that is not present in the historical series. Although each historical precipitation series differed slightly to account for uncertainty in intensity measurements, all series had the same sequence of rain events. In contrast, simulated precipitation series used random draws of wet and dry spells, and took different realizations of intensities. As a result, recharge base case predictions

should reflect greater uncertainty than historical estimates due to this natural weather variability.

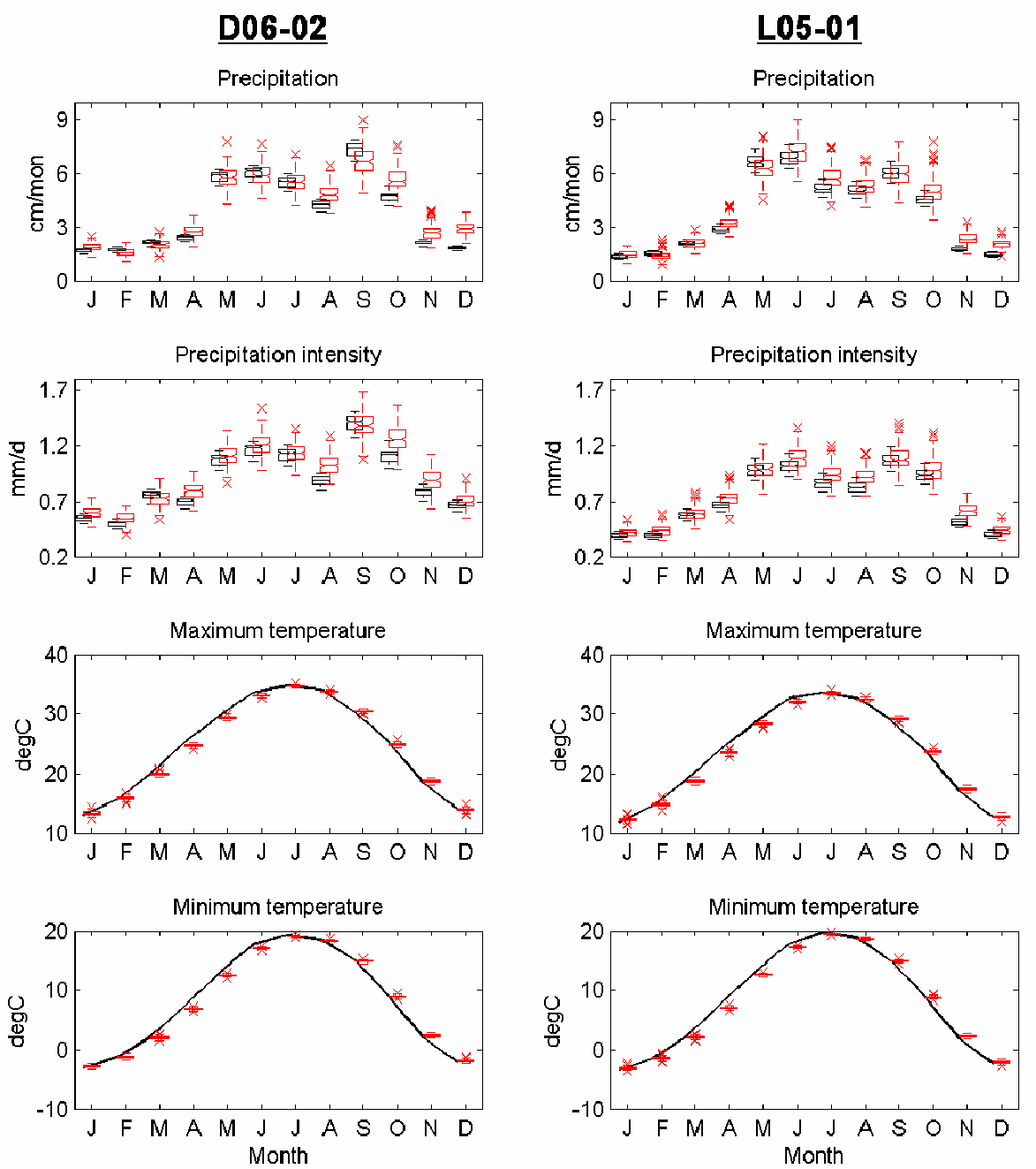

Figure 3-7: Mean monthly historical observations (black) and LARS-WG-simulated base case results (red). Means are taken over 71-76 year periods and box plots show spread over the ensemble of realizations.

Simulated base case precipitation generally matched observed statistics, although some months seemed not as well reproduced as others. Most months that do not match the historical record as closely tend to have over-simulated rainfall amounts, yielding a slight high bias in the mean annual precipitation in Figure 3-8. High simulated monthly totals usually resulted from higher than observed mean daily intensities. Analysis of individual intensity records showed that although most of the simulated intensity distribution overlapped that of the observations, the wet bias may have originated from the way LARS-WG fills the sporadic representation of very high intensity rainfall at the sites. The only months in which total rainfall was somewhat under-simulated was September for D06-02 and May for L05-01. Energy demand was well-simulated, as shown in the mean annual potential ET distributions in Figure 3-8.

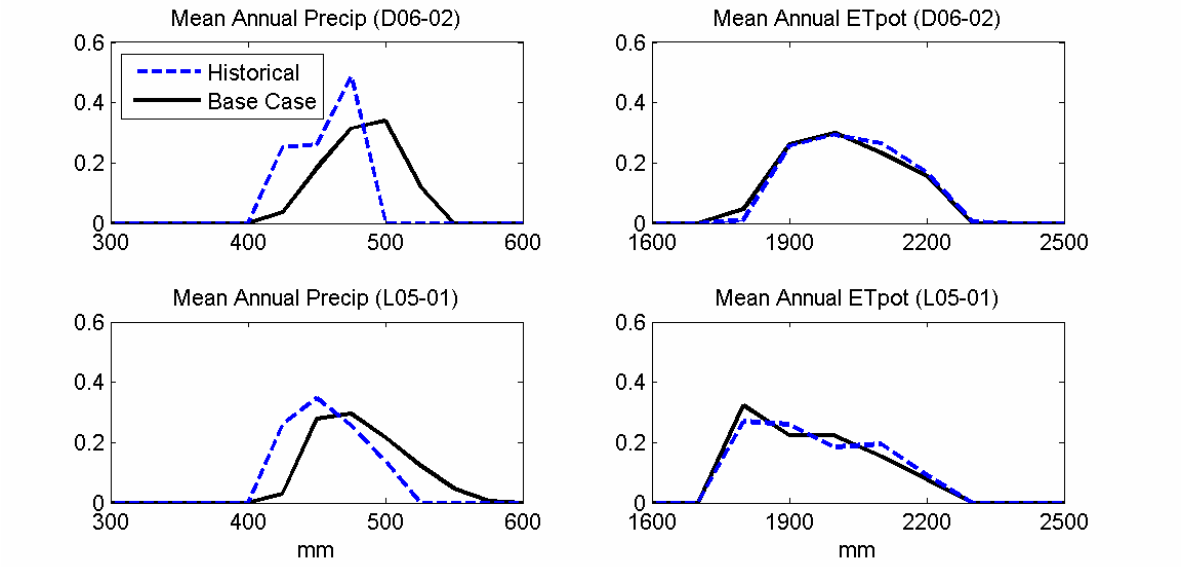

Figure 3-8: Mean annual precipitation and potential evapotranspiration for historical period and LARS-WG-simulated base case period. Histograms show distribution over ensemble of realizations.

While Figure 3-7 and Figure 3-8 compare average statistics, Figure 3-9 compares the interannual variability of monthly precipitation by examining maximum values during the 75-year period, which are known to be under-simulated by stochastic weather generators yet potentially important for recharge. It can be seen that despite the generally good matches with observed mean rainfall statistics, the usually high rainfall records in the late spring and early fall were generally missed by the weather model. These were monthly rainfall episodes that occurred once or only a few times in the entire historical 75-year period. Note, however, that the tail of the maximum monthly rainfall distribution beyond the upper quartile (not shown here) indicated a minority of 75-year realizations do include these extreme monthly amounts. While it is possible that an even longer historical data record might show the return time of those unusual months during 1930-2005 to coincidentally correspond with the distributions generated by LARS-WG, the weather generator should ideally reflect the statistics of the data period to which it is calibrated.

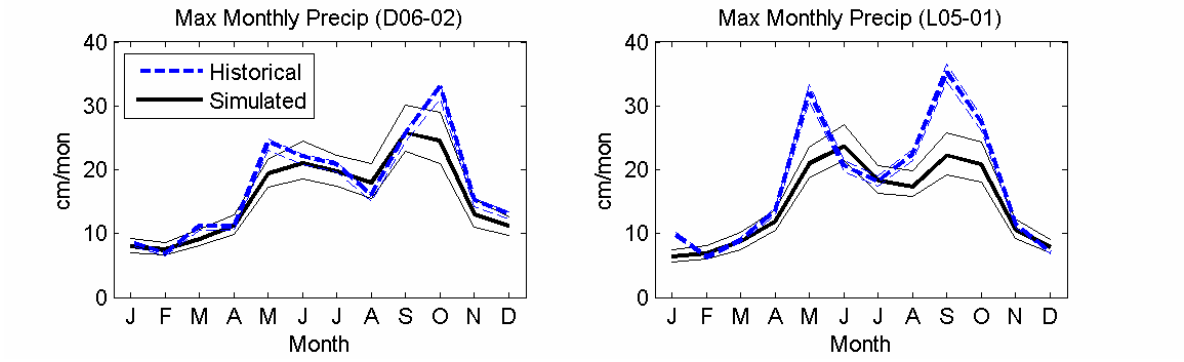

Figure 3-9: Maximum monthly precipitation in historical and LARS-WG-simulated time periods. Median and first and third quartiles are shown over the ensemble of realizations. LARS-WG under-simulates rare wet events in late spring and early fall, which could be important for recharge simulations.

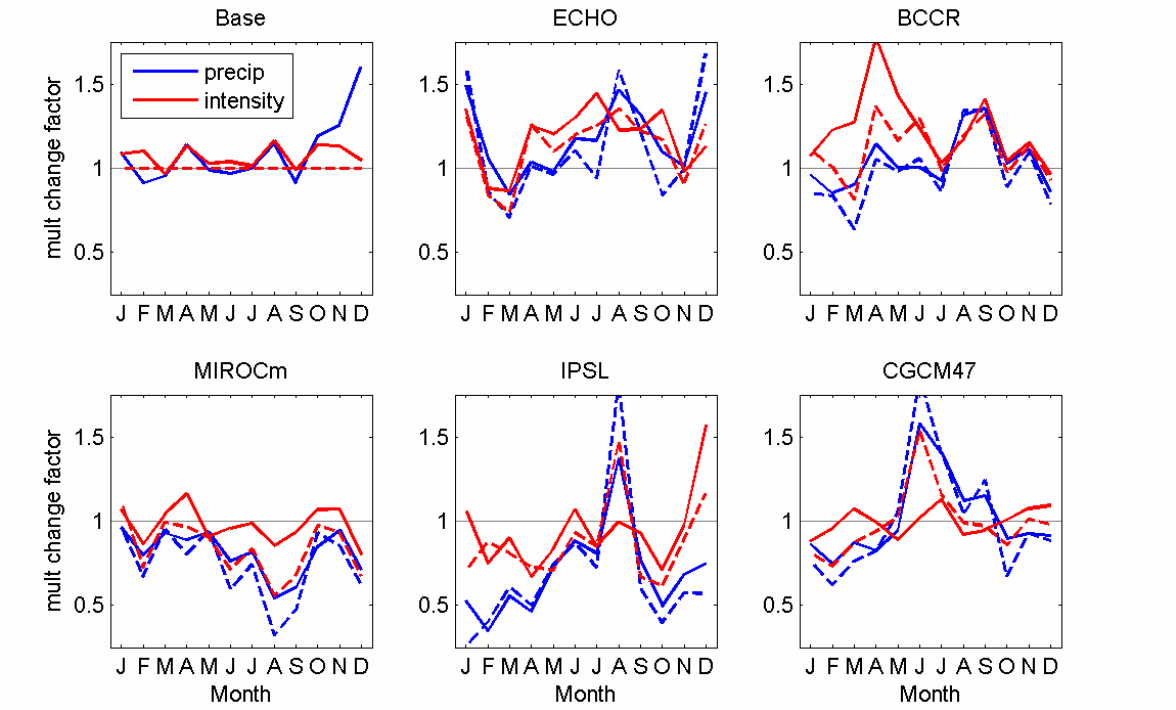

Figure 3-10: Multiplicative change factors for mean monthly precipitation (blue) and mean precipitation intensity (red). Target factors from GCM predictions indicated with dashed lines, and actual simulated change factors from LARS-WG indicated with solid lines.

To evaluate the performance of LARS-WG in simulating target precipitation statistics for the climate change scenarios in addition to the base case, average monthly change factors were calculated for the ensemble of simulated time series (200 realizations x 75 years) and compared with the target values. For the climate change scenarios, the target change factors are those calculated from the GCM results and inputted into LARS-WG, and for the base case, the multiplicative change factor should of course be equal to one. Ideally, the actual change factors found from the simulations should match these target values. The monthly change factors assessed are for total precipitation and mean

daily intensity, which should be the most critical elements in this semi-arid test region. Note that while the total precipitation change factors were inputted into LARS-WG, the weather generator was only indirectly calibrated to intensity change factors via the mean wet and dry spell change factors. For the base case test, the historical series are used as the reference, while the base case provides the reference for the climate change tests in the change factor calculations. Comparison of the change factors for D06-02 precipitation is shown in Figure 3-10; the test was also carried out for L05-01, and the simulated change factors were nearly identical to those of D06-02.

Figure 3-10 shows that actual change factors realized in the simulated series generally agree with the target values. Overall, target monthly total change factors were better reproduced than mean intensity, which is expected because the latter was only indirectly specified in LARS-WG. The main exceptions to this were November and December for the base case, for which error in the total monthly precipitation was greater. For these months, the very long dry spells characteristic of the SHP was not captured by LARS-WG, which seemed to assume dry spells to be contained within the calendar year during the calibration process. Typically for monthly precipitation, the weather model had the most difficulty in generating peak changes, which can be seen in ECHO December, IPSL August, and BCCR March. Mismatches for intensity change factors were more common and diverse in nature. Although the general trend of the intensity change factors was usually followed, simulated changes either disagreed in sign with the target or failed to capture a significant change for MIROCm late summer, IPSL August, and CGCM47 June. When assessing the predicted recharge changes, the actual simulated climate changes should be referenced for consistency.

3.4.3. Recharge Simulation Validation

While an initial test in Section 3.3.3 supported the use of LARS-WG for recharge simulation, a more thorough validation test using the full range of the recharge model uncertainty and 75-year period is necessary to determine whether it should be used for the probabilistic recharge analysis at our data sites. The under-simulation of maximum precipitation values shown in the weather validation section suggested there could be difficulty in simulating the episodic percolation conditions found in Chapter 2. In validation tests, predicted recharge distributions using base case weather simulations (no change factors) were compared with historical recharge estimates. The distribution of mean annual simulations were compared to assess the overall performance, and mean monthly percolation distributions were also examined to check that recharge is occurring by the same mechanisms. Although both SHP locations (D06-02 and L05-01) experienced similar meteorological features and earlier comparisons of simulated base case and observed precipitation were similar, the validation test was carried out for both sites because their diverse soil conditions could make them susceptible to different meteorological features. Validation tests to assess the use of stochastic weather generators to simulate recharge have not been (at least explicitly) carried out in other climate change and recharge studies.

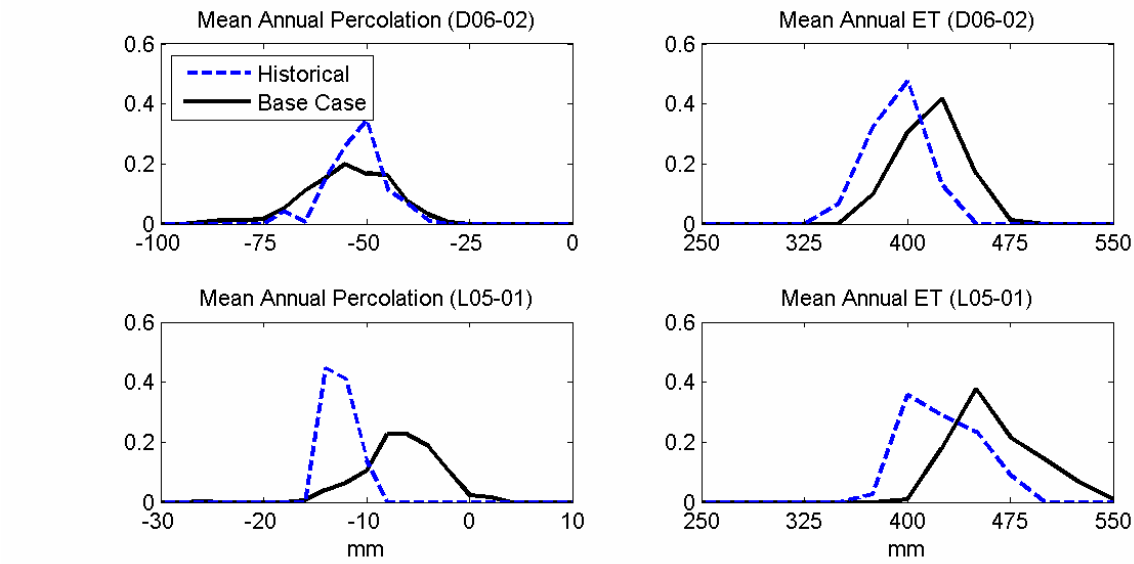

Figure 3-11: Verification of mean annual results with historical vs. LARS-WG-simulated base case forcing. Histograms show distribution over ensemble of realizations. L05-01 site fails validation test.

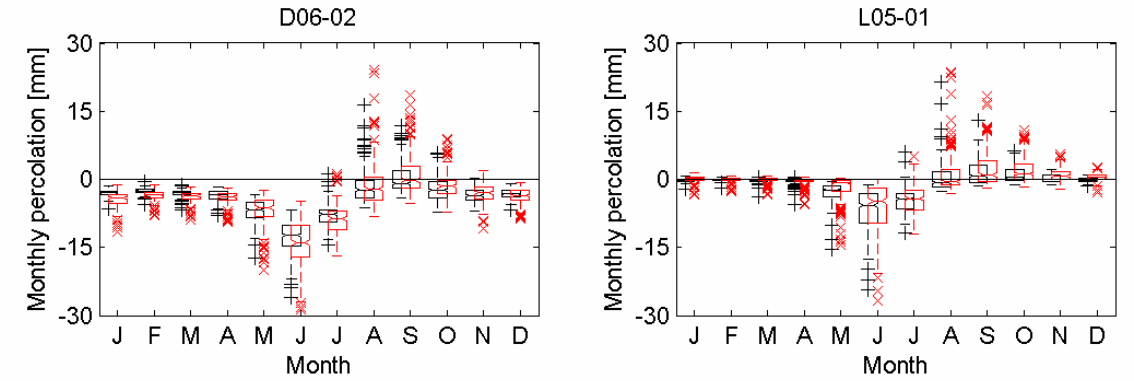

Figure 3-12: Box plots of mean monthly percolation for the historical estimate (black) and the prediction from LARS-WG-simulated base case weather (red). Box plot shows distribution over the ensemble of realizations.

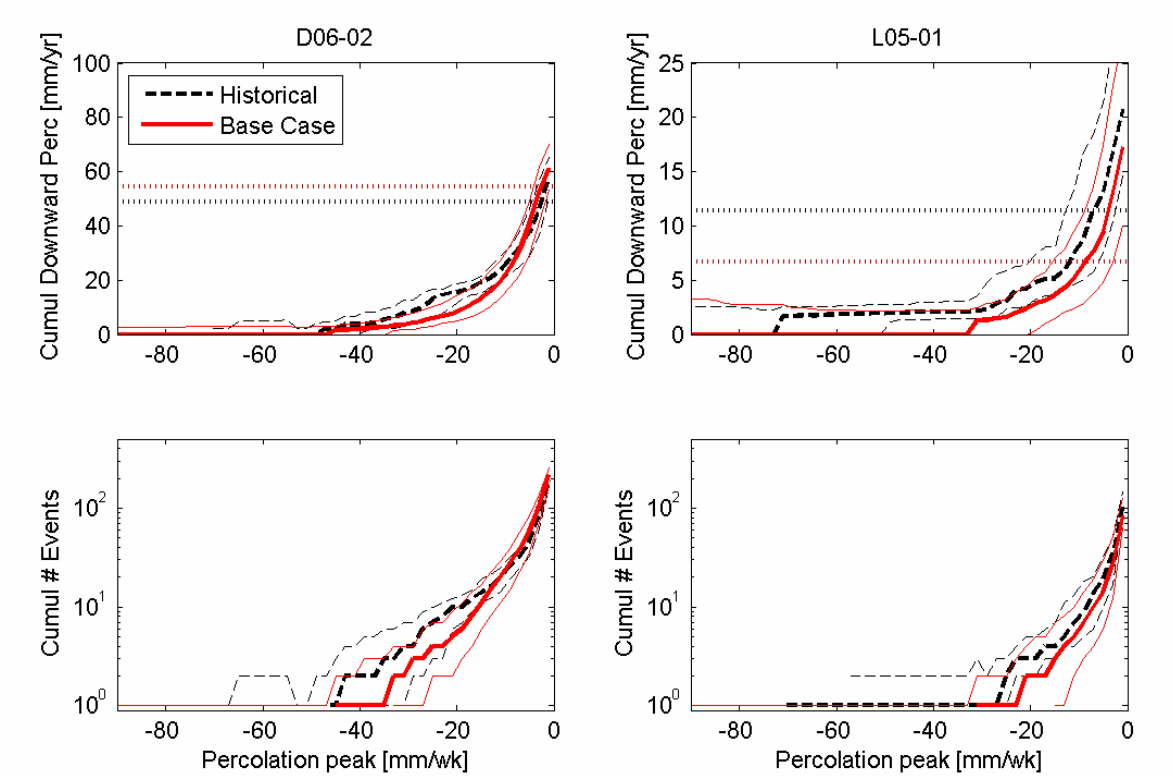

Figure 3-13: Top: Cumulative downward percolation originating from weekly events of given intensities and stronger over the historical period (71-76 years) and the base case simulation period (75 years); cumulative percolation is normalized by length of time period. Median and first/third quartiles over ensemble are indicated. Dotted horizontal lines show the median value of the mean annual (net) percolation from Figure 3-11. Under-simulation of rare, episodic percolation events does not significantly impact overall recharge amounts at D06-02, but it notably compromises total recharge predictions at L05-01. Over-simulation of upward flux with the LARS-WG base case for L05-01 also leads to low recharge results, as shown by the significant difference between total and net percolation.

D06-02 site

Results for D06-02 in Figure 3-11 show that although mean precipitation has a slight high bias in the simulations, annual average percolation compares favorably with the historical estimate. Most of the excess rain simulated seemed to be evapotranspired despite the unbiased energy demand, suggesting that the extraneous rainfall generally lacks the features of recharge-yielding rain events. Box plots of mean monthly

percolation values in Figure 3-12 show that the base case predictions match historical estimates well in their general seasonality. Uncertainty in the base case recharge predictions was generally greater than that of the historical estimates, which could probably be traced to the variability in meteorological forcing not found in the historical-based forcing. It could also be seen that the amount of spread in mean monthly flux correlated more with the amount of precipitation than mean flux magnitude, which likely reflected the different responsiveness of the uncertain land-surface parameters during rain events. Correspondingly, when mean monthly rainfall was under-simulated by LARS-WG in September, predicted uncertainty was reduced from the historical spread in October percolation due to the weaker excitement of the soil properties, despite the variability in simulated base case forcing.

It was found in the previous chapter that recharge in the region is characterized by episodic percolation. If events are categorized by their peak weekly flux magnitude and are demarcated by 0-flux crossings and inflection points (shown in Figure 2-20), then the cumulative plot of recharge event contributions in Figure 3-13 shows that historically at D06-02, probably 20% of total percolation over 76 years originated from four intense events of about 25 mm/wk peak magnitude or higher. LARS-WG's difficulty in simulating rare wet episodes could adversely affect the ability to realistically predict recharge peaks at the site, and accordingly, Figure 3-13 shows that indeed strong percolation events were less frequent with the LARS-WG-simulated base case weather series. However, in order to maintain the mean rainfall characteristics of the historical data, LARS-WG compensated for the missed high-end events by slightly over-simulating moderately strong rain months, which consequently yielded greater occurrence of mid-

sized flux events with 10-20 mm/yr peaks. Thus, although predictions with LARS-WG may under-account for extreme percolation events at D06-02, it should overall provide acceptable measures of deep percolation dynamics.

L05-01 site

In contrast to D06-02, validation test results for the L05-01 site demonstrated the limitations of using a stochastic weather generator for recharge impact studies. The distribution of predicted base case mean annual percolation for this site differs substantially from the historical estimate in Figure 3-11. Uncertainty in the prediction was notably greater, and its mode was about half the flux magnitude of the well-constrained historical distribution. Comparison of the cumulative flux plots for the historical estimates and base case predictions reveal why L05-01 fails the validation test.

Due to the higher holding capacity and lower conductivity of the fine soils at this site, percolation was even more episodic than at D06-02, making it even more susceptible to the under-simulation of extreme wet periods by LARS-WG. In particular, Figure 3-13 shows that one extreme historical flux event alone made up nearly a third of the difference between the mean annual historical percolation and the low predicted amount. Without that single rare event, total historical and predicted downward flux were close, which means the remainder of the difference between the base case and historical long term net percolation must have been due to over-simulation of upward flux in the base case (recall from Chapter 2 that upward flux at 150 cm depth sometimes occurs during the late growing season at L05-01). Correlations found in Chapter 2 between historical monthly rainfall and percolation indicate May, October, and September rains to be the

most important for percolation at this site (see Figure 2-19); accordingly, while heavy May rains probably sparked strong percolation events before roots set in, big October and September rains helped prevent upward flux toward the mature root zone. Thus, under-simulation of extreme rains in May by LARS-WG (seen in Figure 3-9) seemed to lead to a low bias in summer percolation, and under-simulation of extreme rains in early fall seemed to lead to the high bias in upward flux simulations at the end of the growing season.

Although the base case simulations for L05-01 were clearly a poor match with the historical estimate, it is noteworthy that the large spread in base case precipitation and deep percolation do cover the historical estimates (see histograms and quartile plots). This suggests that it is within the range of chance that with the right soil conditions, LARS-WG can generate the types of extreme conditions that are critical for recharge at L05-01. Thus, if the return times of those rare events observed in the last century in SHP were known, it could be possible to constrain the LARS-WG output to produce target interannual variability statistics. Most stochastic weather generator studies that focus on simulating correct interannual variability condition their output on measured large-scale physical indices such as sea surface temperature and sea level pressure [*Wilby et al.*, 2002; *Katz and Parlange*, 1993]. This type of approach, however, is more difficult for future scenario simulations.

These validation tests established that LARS-WG should not be used to produce the precipitation characteristics important for recharge for L05-01. Although most annual recharge realizations using LARS-WG forcing for the site matched well with typical

annual percolation, the handful of missed rare events over nearly a century makes up a major fraction of total long term recharge. However, LARS-WG provides adequate precipitation series for simulating recharge with D06-02 soil properties because the rare events not captured are not likely to significantly affect overall recharge amounts. The remainder of the climate change analysis was thus carried out for site D06-02. We assumed that recharge would also be properly simulated using model-generated precipitation under climate change scenarios for this site.

3.4.4. Recharge Predictions

Mean annual results for all GCMs

Results for the 5 different future climate scenarios are summarized by their mean annual characteristics in Figure 3-14 and Figure 3-15. Although overall wetter meteorological conditions yielded higher recharge and drier conditions less recharge, it can be seen that changes in annual rainfall cannot provide accurate predictions of recharge changes. For most of the cases examined, relative changes in recharge outpaced changes in rainfall, with one scenario even predicting a change with the opposite sign. For those with agreeing signs, the difference in relative changes for rain and recharge ranged from over ~1.5 to over ~3.5 times greater percent change in percolation than rainfall.

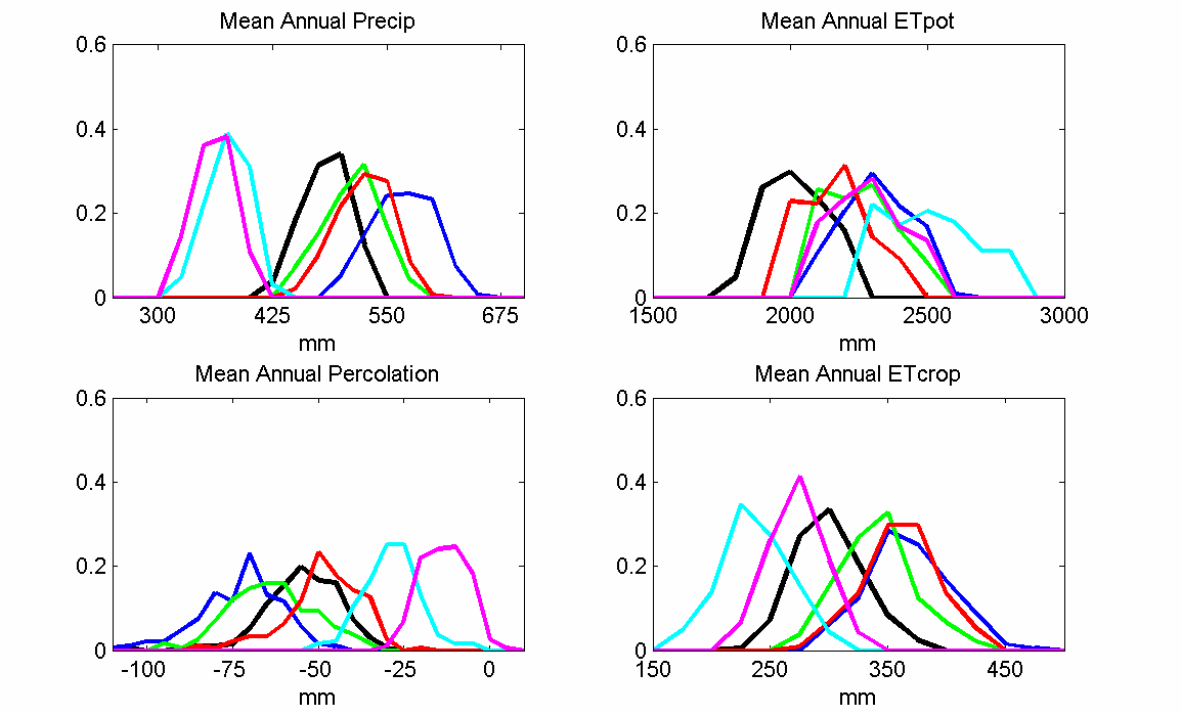

Figure 3-14: Mean annual precipitation, potential ET, percolation, and crop ET for all prediction scenarios: base case (black), ECHO (blue), BCCR (green), CGCM47 (red), MIROCm (cyan), and IPSL (magenta).

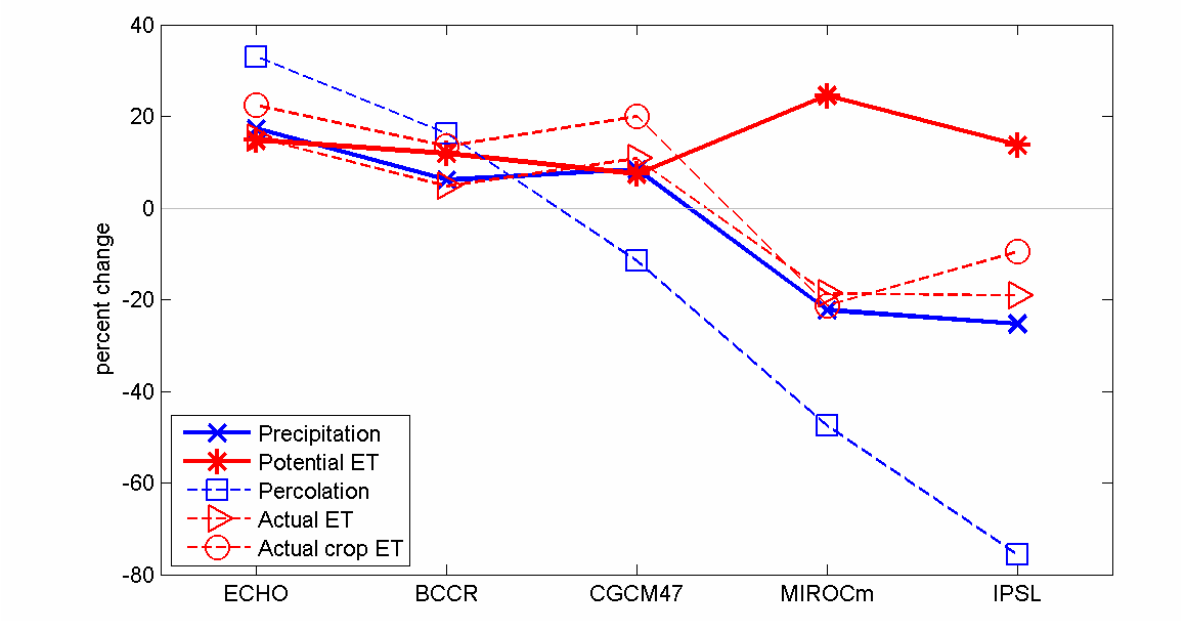

Figure 3-15: Percent change in mean of mean annual fluxes (precipitation, potential ET, percolation, and actual ET) from base case.

The probability distribution shape for percolation predictions also varied greatly for the different scenarios. Like the base case, the uncertainty was fairly symmetric for ECHO, MIROCm, and IPSL predictions. BCCR differed in that most of the probability mass was concentrated around 60-80 mm/yr, though future recharge for this case could be as little as ~40mm/yr. CGCM47 prediction uncertainty was similarly unbalanced, with higher probability concentration at percolation rates weaker than the mode. It can also be observed that uncertainty decreased slightly for the dry scenarios.

Potential evapotranspiration, which represents energy demand, was found to increase for every future climate prediction in Figure 3-14. This resulted from the consistent increase in predicted air temperature seen in all GCM outputs. However, changes in actual evaporation and transpiration seemed entirely uncorrelated with potential ET; instead, changes in rainfall provided a better indicator. This signifies that the study site is moisture-limited, which greatly marginalizes the temperature affect on the hydrologic response, as expected. Although actual ET changes followed annual rainfall changes with striking similarity in Figure 3-15, relatively small differences are what gave rise to the changes in the small recharge rates in this semi-arid setting; this underscores the sensitivity of recharge estimates to errors in surface input measurements at the annual scale in dry conditions. Most notable among the differences between rainfall and ET changes, the driest scenario IPSL did not produce significantly less transpiration than the base case, and CGCM47 with similar future annual rainfall would likely undergo the same amount of ET as the wettest ECHO scenario.

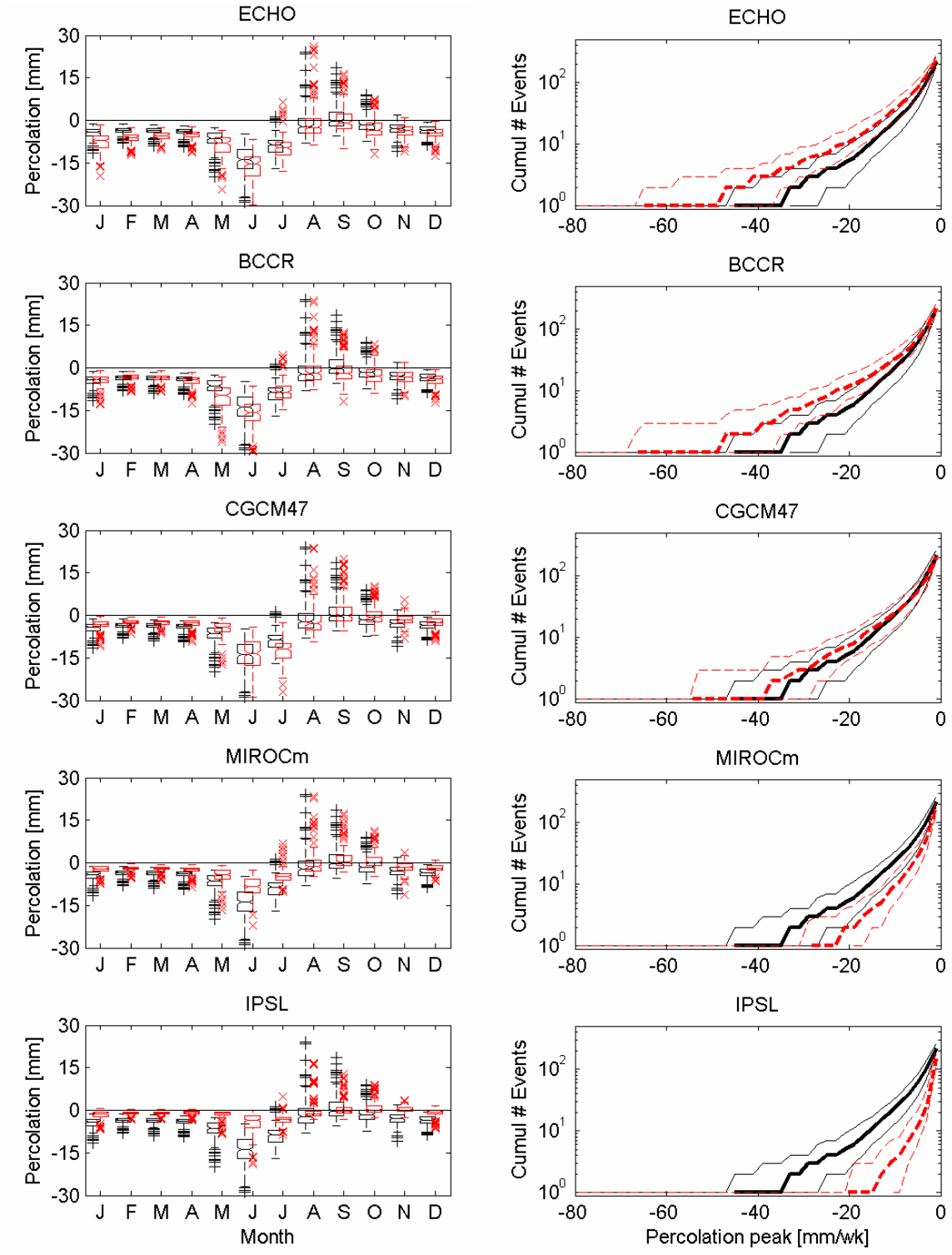

Figure 3-16: Left: Box plots of mean monthly percolation for base case (black) and change scenarios (red). Right: Cumulative number of percolation events in 75 years with given peak intensities and stronger.

The unpredictable nature of future recharge and evapotranspiration from annual meteorological changes stem from the nonlinear behavior of the land-surface system that makes the timing of these changes very important. In the following, each scenario is examined to identify the driving components of these changes. Considered in the analysis were seasonal forcing dynamics and predicted changes in precipitation intensity. In addition to considering the impacts on average percolation shown in Figure 3-16, predicted changes in the occurrence of high magnitude episodic percolation events were also assessed; how these change may affect the vulnerability of groundwater resources to chemical mobilization and different agricultural practices.

ECHO (wetter scenario)

ECHO was the only GCM of the 16 considered to predict an increase in future annual precipitation, with the increases occurring in the rainy June-October period and the relatively dry December-January period. Also significant, daily rainfall intensity was predicted to increase in almost all months apart from late winter. With these changes, average monthly percolation was predicted to increase in every month other than August. Most notable percolation increases were generally found for the winter and May-June, even though much of the greatest precipitation increase (total amount and intensity) was expected for late summer. As suggested by the higher crop ET projection, much of the increased rainfall in the late summer appeared unable to bypass the mature roots; such impacts could be a bonus for cotton production in the region. The most dramatically increased percolation in May and June seemed not as much a result of more total rainfall but of higher rain intensities in April through June. In fact, stronger percolation events

were seen with this scenario following higher intensity rain months than in the base case, including the end of the growing season. In contrast, for the months when intensity did not rise (February and March), affected percolation months (March and April) probably saw higher flux due to more low intensity flux events.

Overall, the typical incidence of very intense percolation events, defined by those with peak magnitudes of at least 20 mm/wk, increased two-fold from 5 times under the base case scenario to 10 times under the ECHO future scenario in 75 years. About an 18% increase in future rainfall was predicted to yield a ~20% increase in crop ET and ~30% increase in recharge.

BCCR (approximately unchanged annual precipitation)

BCCR predicted annual precipitation to remain about the same as present-day, with wetter totals in late summer balanced by drier winters. A small annual change of ~5% drier future in the GCM outputs was realized in the LARS-WG simulations as a slight ~5% wetter future. However, a key feature of BCCR was the predicted increase in rainfall intensity, despite a largely unchanged total. Future intensity simulations were particularly higher in the spring, which was shown to be important for recharge in present conditions in Chapter 2. Percolation responded to the greater late summer rains by increasing slightly on average in September and October, but the most impressive jump in percolation occurred in May and June. Because total rain amounts in March-June were not expected increase, this change resulted directly from the higher concentration of rain in time. Indeed, while base case April-June percolation was only weakly correlated with rain in the same month, zero-month lag correlation for BCCR future runs were stronger

for late spring, indicating that high intensity storms are quickly transported deep into the subsurface, as seen in Figure 3-17.

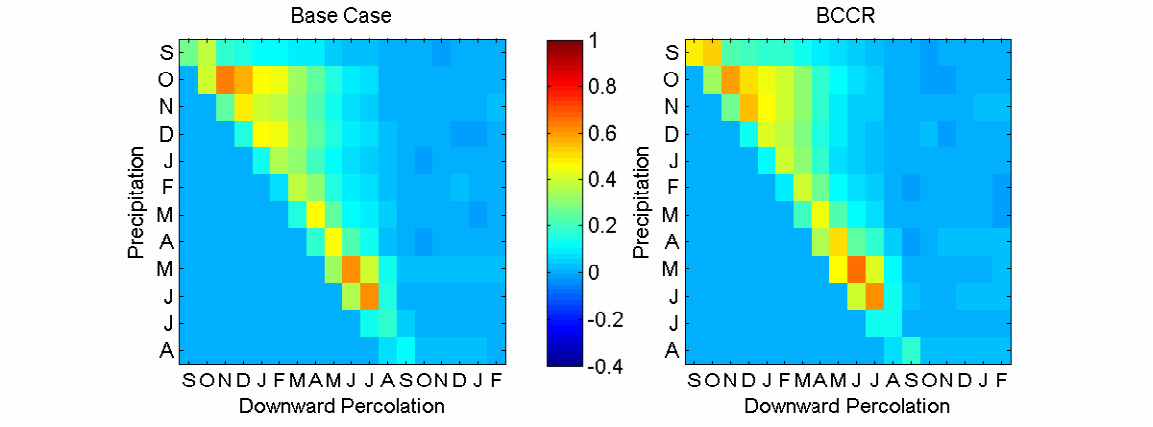

Figure 3-17: Correlation between monthly precipitation and downward percolation in same and following months for the base case and BCCR scenario. Months labeled with abbreviations, starting with September. The higher correlations at shorter time lags in the late spring for BCCR indicate stronger intensity percolation events.

Significantly, although ECHO overall provided the wetter future scenario, BCCR percolation simulations showed comparable occurrences of very high magnitude flux events. An increase in annual average percolation of ~18% for BCCR again exceeded the relative change in rainfall, and by an even more dramatic margin than ECHO. Furthermore, the distribution of predicted annual recharge bulges toward high percolation values, in the range of predicted annual recharge for ECHO. However, unlike ECHO, predicted crop ET for the BCCR scenarios was only about 10% higher than the base case.

CGCM47 (approximately unchanged annual precipitation)

Like BCCR, CGCM47 also predicted mean annual precipitation to remain about the same as the present conditions, although almost a 10% increase was generated with LARS-WG. Monthly precipitation was expected to decrease in winter but increase throughout the summer; this differs from BCCR, which only predicted more rain in August and September. Because June rains were the most important for strong percolation events only after May rains, such a change could potentially have a large effect on recharge. Accordingly, July did have greater predicted percolation after the June rains, yet most other months had less percolation projected under this climate scenario. The net change in percolation was a 10% decrease, which is in the opposite direction of the predicted annual rainfall change. Thus, the increased July percolation past the root zone was insufficient for making up for the decreased percolation the rest of the year. Although predicted summertime rainfall and crop ET were similar for ECHO and CGCM47, the earlier concentration of CGCM47 rain before maximum rooting depth was reached would have suggested more percolation and less crop ET for this scenario. It is possible that dry antecedent conditions in CGCM47 curtailed additional recharge early in the growing season.

Unlike ECHO and BCCR scenarios, which had more intense storms, precipitation intensities were largely unchanged in the simulations for the CGCM47 scenario. Strikingly, though, the typical occurrence of high magnitude flux events (greater than 20 mm/wk peaks) was a little higher at ~7 times versus ~5 times for the base case over the 75 year simulation period. Many of the additional high flux events followed June rains, which were predicted to increase in total precipitation but not intensity. Thus, an increase

in total precipitation alone without higher intensity seemed to facilitate strong flux events. To result in an overall decreased annual percolation for the CGCM47 scenario, smaller flux events became less frequent, mostly due to the decrease in the weak winter rains that give rise to minor percolation rates. Note that although the mean value of mean annual recharge is expected to decrease, much of the full distribution overlaps the base case distribution.

MIROCm (drier scenario)

MIROCm predicted a drier future with a decrease in total precipitation in every month. Most of this decrease occurred June-September, which was likely to impact crops significantly. MIROCm outputs also predicted a decrease in intensity, though less than for total precipitation; however, LARS-WG produced intensities not significantly different than that for the base case for most months. As could be expected for this scenario, predicted percolation was reduced in every month. Although small amounts of percolation were still predicted in the winter, it was on average unlikely that September and October would see any net percolation at 150cm depth anymore. As discussed early, percolation uncertainty scaled with rainfall amount due to its excitement of soil and vegetation parameter distributions. Thus, spread in flux predictions was reduced for every month, resulting in a more certain mean annual prediction.

Generally for this scenario, there would no longer be any extreme intensity flux events above 30mm/yr, and there would only be about half as many events of 10mm/wk magnitude or greater than the base case. Total number of percolation events of any size is also expected to drop about 25%. Overall, the ~25% drop in total rainfall resulted in

~50% drop in recharge and over 20% drop in crop ET. Since dryland cotton is already near the limit of economical feasibility under current semi-arid conditions [*Howell et al.*, 2004], such a reduction in water supply for the crop would likely end dryland cotton growing practices.

IPSL (drier scenario)

IPSL predicted the driest future of all the GCM outputs examined. It differed from MIROCm (the other dry GCM used for recharge prediction) in its seasonality; IPSL expects August to become much wetter and winter to be dramatically drier. However, LARS-WG under-simulated the increase in total August rain, and simulated only a slightly drier annual average than MIROCm. Based on the simulated IPSL scenario, average percolation will likely decrease from the base case amount in every month except September, with winter percolation is almost reduced to zero. Due to the high August rains, September will on average maintain a roughly zero net flux as in the base case. No increase was seen in downward percolation probably because of the dry antecedent conditions.

Although percolation uncertainty typically scales with the amount of rain, predicted August and September percolation for this scenario seemed to be an exception with substantially lower uncertainty than the base case. It is possible that the upper profile was so dry as to prevent significant flux for any of the soil and vegetation parameter values used. No notable percolation increase resulted from the significantly higher August rains, indicating that the extra moisture is taken up by ET. In fact, mean actual crop ET for IPSL was only a little more than 10% less than the base case, despite

the 25% lower annual precipitation. Furthermore, the peak of the actual root uptake distribution for IPSL predictions fell just within the wider peak of the base case distribution, suggesting that even in this drier climate, dryland cotton may remain possible. However, it would be very certain that mean annual recharge would drop considerably (~75%), and percolation events of magnitudes beyond even 10 mm/yr would be unlikely.

3.5. Summary and Conclusion

We have presented a probabilistic approach to studying climate change impacts on recharge that takes into account uncertainty in weather and land-surface conditions. While previous impact studies have considered the uncertainty of GCMs, this is to our knowledge the first to also include uncertainty of soil and vegetation parameters. Due to the non-linearity of soil moisture dynamics, resolving the full uncertainty distribution of model inputs is particularly important. We considered climate conditions for the region by evaluating predictions from 16 frequently-cited GCMs, 5 of which we selected for recharge predictions based on their diverse outcomes. Most of the 16 GCMs predicted for this region either lower or approximately unchanged annual precipitation with increased dry spell lengths.

This work demonstrates the importance of validation tests in hydrologic impact studies to ensure stochastic weather generators used to downscale GCM predictions simulate the properties most important to the process of interest; this is a procedure that is never (at least explicitly) carried out in other recharge impact studies. We also showed validation test results to be dependent on soil and vegetation properties, not only

meteorological conditions, with opposite outcomes for the two SHP test sites. When performing the validation test, it is necessary to include a sufficiently long time period to test the effects of interannual variability. We found that LARS-WG tends to under-simulate very rare (few times a century) rain events, which produce a disproportionate fraction of long-term recharge at the site with finer soil. While these rare events also impact the coarser-textured site, leaving out these contributions did not substantially affect overall percolation simulations. Thus, recharge predictions were only made for the latter site.

Although potential ET was projected to increase in every GCM prediction scenario, this seemed to have little effect on recharge and actual ET, which instead roughly followed patterns of precipitation changes. Thus, in moisture-limited regimes such as the semi-arid SHP, hydrologic impacts will possibly be greatest due to changes in precipitation rather than temperature. For the scenarios examined here, higher predicted annual precipitation generally yielded higher percolation predictions and vice versa, as could be expected. However, recharge was very sensitive to precipitation changes, with relative recharge changes generally greater than the corresponding precipitation changes. Furthermore, in one case, a slight increase in total precipitation actually led to a decrease in future recharge. The tenuous connection between total precipitation changes and percolation was traced to the timing of the predicted changes.

It was universally found for all scenarios that any change in winter precipitation translated directly to a corresponding change in percolation, due to the low ET during those fallow months. However, because most percolation occurred during the rainy summer season, changes during that time could significantly impact recharge. In

particular, increases in May-June rainfall sparked rises in the high mean monthly percolations amounts in the early growing season. Similarly, changes in September-October rains affected mean monthly percolations at the end of the growing season, though these changes were less pronounced due to the dampening effect from root uptake. Increased rainfall in the peak growing season (July-August), however, added little to recharge because it was mostly taken up by the crops. Summer percolation may also have been impacted by changes in winter rain due to the latter's effect on antecedent moisture, which facilitates percolation during the growing season.

This study is also unique in its analysis of not only average recharge dynamics, but also the distribution of flux event magnitudes, which could be critical for chemical mobilization or agricultural management concerns. As discussed in Chapter 2, high magnitude percolation events can be found at D06-02 under current climate conditions in the early growing season and end of the growing season, when rain events are strong and root uptake is either before or past its peak. Accordingly, our predictions showed that sufficiently greater rainfall in the early and late growing season made the site more susceptible to high magnitude events, such as those with peaks exceeding 20 mm/wk, even when total annual percolation did not increase. Interestingly, either higher monthly rainfall with unchanged rain intensities or greater rainfall intensity alone was capable of increasing the occurrence of these high magnitude percolation peaks. In contrast, greater winter percolation due to increased winter rains led to higher frequency of low magnitude percolation events. Note, however, that rare and extreme percolation events were generally under-simulated using precipitation series produced by the stochastic weather generator used here.

The probabilistic approach used here showed that uncertainty in percolation tends to scale with precipitation amount. Thus, the distribution of flux values generally narrowed for drier predicted months and widened for wetter months. It was also shown that the shape of the percolation distribution for some scenarios was substantially skewed, even though the base case uncertainty was mostly symmetric. This demonstrates that deterministic recharge predictions could be misleading.

A drawback of this study was its simplistic static vegetation model. In the most extreme case, future conditions may no longer allow for cotton cultivation. As a first order check, comparison of crop ET for the different scenarios with base case ET suggested all scenarios but one of the drier ones to be within the range of crop feasibility, with wetter summer scenarios potentially bringing higher yields. However, a more subtle short-coming is the model's pre-specification of the crop development schedule independent of meteorological conditions. Although our study found non-precipitation variables to have little effect on recharge, *Rosenzweig* [1990] found that increased temperatures could shorten the growing season. Furthermore, changed CO_2 levels could impact water usage through CO_2 fertilization effects [*Allen et al.*, 1996]. These issues could be handled with the use of a dynamic vegetation model, as done in *Green et al.* [2007].

Rather than propose any definitive hydrologic predictions for a specific location, the focus of this study was to introduce a probabilistic approach to analyzing climate change impacts on recharge. By using a data-conditioned stochastic recharge model, we were able to analyze the possible changes in recharge for an example SHP site. Proper probabilistic specification is necessary due to the non-linear dynamics of the unsaturated

zone. The approach demonstrated the importance of shifts in forcing seasonality and precipitation intensity on both long-term average recharge and major episodic percolation events. Characterizing both aspects of subsurface fluxes will be critical for understanding and managing groundwater systems.

Chapter 4

Conclusions

This thesis proposed a probabilistic approach to analyzing recharge in a semi-arid environment. By conditioning an unsaturated zone numerical model on chloride concentration and soil moisture data, distributional results were found for historical recharge and potential future recharge under predicted climate change scenarios for data sites in the Southern High Plains of Texas. Main results and original contributions are summarized below.

4.1. Principle Findings

Historical recharge in SHP

Deep percolation below the root zone was found to be highly episodic and show significant interannual variability at the two SHP data sites considered, with 50% of long term percolation originating from recharge events occurring on average about once in

3.5-15 years over the last ~75 years. Recharge was found to be more episodic at the finer-textured site. Conditions that allow major percolation events were found to be high intensity rains, moist antecedent soil conditions, and below-maximum root density. The most susceptible time of year is the early growing season, when rains are heavy yet roots have not reached full maturity. Historical estimates also showed occasional intense percolation events in the fall at the coarser-textured site only; stronger drying prevented similar occurrences at the finer-textured site. El Niño events can contribute to interannual variability of percolation by bringing wetter winters. Increased light winter rains during the non-growing season (winter) were found to readily produce low-grade percolation events. Additionally, such rains often provide wet antecedent conditions for heavier spring and summer rains to trigger high magnitude percolation events. Bracketing the range of possible episodic percolation intensities can be critical for chemical transport problems and other applications sensitive to intermittent and variable subsurface dynamics.

Climate change impacts on recharge in SHP

Most climate models predicted less or similar future annual precipitation for SHP; all predicted higher temperatures. Results for various predicted climate change scenarios suggested that in moisture-limited environments, changes in precipitation can have greater hydrological impact than temperature rises. For most of the tested scenarios, relative changes in recharge exceeded relative changes in rainfall, demonstrating high sensitivity to climate change. Predictions indicated the temporal distribution of rainfall changes to be most critical for recharge. All scenarios showed that changes in winter

precipitation directly affect percolation during the non-growing season. In contrast, predicted rainfall increases in the mid-growing season affect recharge negligibly due to greater root uptake. Our results suggested that both increased total monthly precipitation with unchanged rain intensities and more intense daily rain rates with unchanged total monthly precipitation in the late spring and early fall can make the site more susceptible to strong percolation peaks. Uncertainty in recharge predictions generally scaled with the amount of precipitation.

4.2. Original Contributions

- Introduced data and model integration approach to recharge estimation

Chloride concentrations in the soil are generally considered to be among the most robust measurement types for estimating recharge in semi-arid settings. However, the traditional variants of the chloride mass balance method and the chloride front displacement method only provide long-term average recharge estimates. In contrast, numerical modeling can produce estimates at any time scale, yet it is very sensitive to errors in dry conditions. This work proposed and demonstrated the application of data assimilation to downscale chloride concentrations with model simulations and produced data-conditioned estimates of recharge time series.

- Considered uncertainty in land-surface properties for recharge predictions under climate change scenarios

Previous studies examining climate change impacts on recharge acknowledge uncertainty in climate model predictions, yet they fail to account for uncertainty in soil

and vegetation properties. Considering the sensitivity to model errors, this uncertainty can significantly affect recharge predictions. A probabilistic approach to recharge prediction that includes uncertainty in both land-surface conditions and future weather was introduced using the data-conditioned model parameters found in the data and model integration portion of this thesis. Findings that the recharge distribution shape can vary for different climate scenarios confirm that deterministic predictions can be misleading.

- Demonstrated the importance of validation tests when using stochastic weather generators for hydrological studies

Stochastic weather generators designed to produce meteorological time series are commonly used for incorporating climate model predictions in hydrological studies. They are also often used when real data is unavailable. While they typically perform well in producing statistics to which they are calibrated, we showed that validation is critical to ensure that they capture features important to the process of interest. Such tests were never (at least explicitly) carried out in past climate change impact studies involving recharge. Our validation tests showed that depending on land-surface conditions, recharge in a semi-arid setting may not be properly simulated using a stochastic weather generator that is unable to produce realistic high monthly rainfall amounts or interannual variability.

- Identified main recharge controls and mechanisms in a semi-arid environment

A key advantage of estimating time-distributed recharge is being able to infer from them the main recharge controls and mechanisms of the data site. Although diffuse

recharge is well known to be controlled by soils, vegetation, and meteorology, how these factors interact to affect recharge is complex. Examining the timing of deep percolation relative to precipitation events revealed how recharge is generated at the two data sites with differing soil conditions. As discussed in greater detail in the Principle Findings section, analysis of historical estimates and future predictions suggested episodic percolation events to dominate.

4.3. Future Research Directions

The main elements allowing for probabilistic analysis of recharge in this work are the model, observations, and the estimation method. The innovative aspect of this thesis has been to bring together these three elements to better characterize recharge. However, future work on each part can further improve our understanding of recharge. Some possible extensions are outlined here.

Model

The recharge model used here provides the physics of subsurface dynamics and uncertainty characterization through model inputs. Assuming that Darcy flow describes moisture flow at the test sites, a more physically-based crop model can be the most important improvement to model physics. The static model used in this work pre-specifies crop development independent of weather conditions, and this is particularly limiting for the climate change impact predictions. Although a dynamic crop model has significant parameter requirements, it can capture emergent effects due to higher temperatures, increased atmospheric CO_2, and varied precipitation patterns.

Model uncertainty can be improved by better calibrating prior distributions to the study sites. For example, in this thesis, cotton crop parameters were derived using some data from outside the SHP region. Similarly, the soil layer boundaries implemented may not match with actual conditions. For forcing uncertainty, the simple historical rain intensity error model can be changed to also incorporate uncertainty in rain events.

Improving the stochastic precipitation model for the climate change study can expand the types of recharge mechanisms we can consider. Specifically, the precipitation model can be adapted to be able to simulate interannual variability by conditioning it on target interannual statistics. This will allow for improved predictions of rare and high intensity percolation, and for the assessment of future recharge under changed interannual climate variability.

Observations

Chloride concentrations provide robust indication of subsurface fluxes, yet assimilation of other data types can help further constrain recharge estimates if available. Other tracers often measured for recharge studies include environmental and historic isotopes. Nitrate and sulfate are inconveniently more reactive, yet they are also commonly measured at agricultural sites. This work has demonstrated that chloride data at a single observation time provides temporal information, but additional observation times can provide added value, especially for the partially-flushed site. Since plant uptake is found to be a key controller of recharge, surface crop data and root zone observations can improve crop parameter estimation, even though they measure dynamics that are much more transient than subsurface fluxes leading to recharge.

However, the value of crop-related measurements can be limited by the quality of the crop and root zone model (where considerable non-Darcian mixing can occur).

Estimation method

Importance sampling proved effective for parameters and flux estimation for this highly non-linear problem. Its main drawback, however, is its need for a large number of Monte Carlo simulations to produce conditional distributions. This results from its inability to change state values from those specified by the prior distribution, which can differ substantially from the target posterior distribution.

Markov Chain Monte Carlo (MCMC) methods [*Chib and Greenberg*, 1995] offer a promising alternative that can lower the number of simulations while providing a good discrete approximation to the posterior distribution. These methods allow for exploration of the state-parameter space through a candidate-generating density. For example, in a common variant of the method, a random walk is executed through the state-parameter space to generate a discrete representation of the posterior distribution. However, MCMC methods do not guarantee fewer simulation runs than importance sampling. They require a "burn-in" time to converge on the target posterior distribution, and how many simulations this requires depends on the candidate-generating density used. Furthermore, most implementations of MCMC for Bayesian estimation require closed forms of the prior distribution and likelihood. A likelihood model has already been developed in this work, but the soil parameter uncertainty model would require further adjustments to fit a closed form representation.

Further applications

This recharge study examined diffuse recharge in an agricultural semi-arid setting, yet little to no diffuse recharge is believed to occur in many other dry environments, especially under natural vegetation. In those regions, the predominant recharge mechanism is typically focused recharge, which results when sufficient moisture collects in topographic lows. Recharge in those settings is probably even more difficult to simulate, and applying a data assimilation approach like that used here with an appropriate physical model can improve recharge characterization. Surface data such as distributed surface soil moisture and aerial channel images over time can help constrain runoff simulations, and unsaturated zone profiles within topographic lows can help estimate the resulting focused recharge. Also with the proper model and observations, regional analyses of recharge can be carried out that consider various recharge mechanisms throughout a watershed. Controlling computational load will be even more critical in such studies.

Appendix A

Simple Crop Model in SWAP

In the simple crop growth model of SWAP, root depth, LAI, and crop height over crop development stages are user-specified. Values used for those crop parameters and minimal crop resistance are discussed in Chapter 2.3.3. The precipitation interception and transpiration scheme of the model are outlined here, with further details contained in SWAP user's manual [*Kroes and van Dam*, 2003].

Rainfall Interception

In the SWAP model, rainfall intercepted by crops (P_{int}) is found using *LAI* at the current crop development stage and gross daily precipitation (P_{gross}):

$$P_{\text{int}} = 0.25 * LAI * \left(1 - \frac{1}{1 + \frac{4 * P_{gross}}{3}} \right) \quad \textbf{(A-1)}$$

Potential Transpiration

Daily potential evapotranspiration (ET_p) is calculated from meteorological inputs, minimum crop resistance, and crop height parameters using the Penman-Monteith equation [*Monteith,* 1981]. Daily potential transpiration (T_p) is partitioned from total ET_p according to

$$T_p = (1 - W_{frac}) * ET_p - E_p, \quad \textbf{(A-2)}$$

where E_p is potential evaporation and W_{frac} is the fraction of the day that the canopy is wet from rainfall interception. The assumption is that transpiration is negligible while intercepted rainfall is evaporated. W_{frac} is calculated from the intercepted rainfall and the evaporation rate of the intercepted rainfall (E_{int}):

$$W_{frac} = \max\left(\frac{P_{\text{int}}}{E_{\text{int}}}, 1\right), \quad \textbf{(A-3)}$$

where E_{int} is calculated using Penman-Monteith with no crop resistance. Potential transpiration is then distributed throughout the root zone according to user-specified root density.

Actual Transpiration

Actual transpiration T_a (root uptake) is then calculated by

$$T_a(z) = \alpha_w(h)\alpha_s(c) * T_p(z), \quad \textbf{(A-4)}$$

where the functional relationships of water stress α_w and solute stress α_s with matric potential and solute concentration are shown in Figure A-1. Water stress parameters used for cotton in this work are based on *Sarwar and Feddes* [2000], with h_1 = -10 cm, h_2 = -

25 cm, $h_{3,H}$ = -500 cm, $h_{3,L}$ = -900 cm, and h_4 = -16,000 cm. Solute stress parameters from the SWAP manual, Appendix 4 were used: EC_{max} = 7.7 dS/m and EC_{slope} = 5.2 %/dS/m. Electrical conductivity is converted from solute concentration.

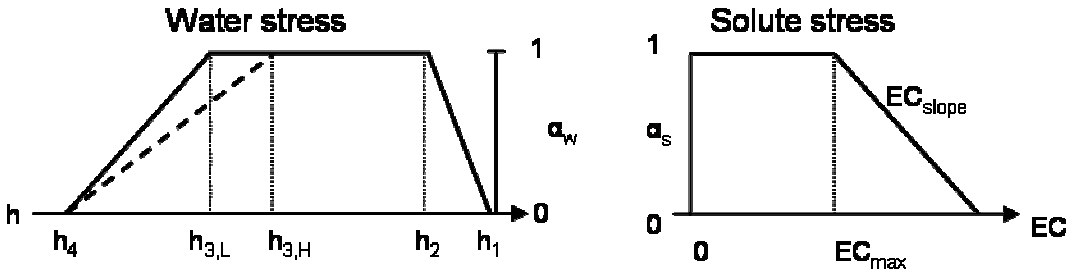

Figure A-1: Water and solute stress scheme for transpiration. Actual h_3 is interpolated from $h_{3,L}$ and $h_{3,H}$ between T_p = 0.1 cm/d and 0.5 cm/d. For the solute stress function, solute concentration is expressed in electrical conductivity.

Appendix B

Kalman Update

For problems in which the state and observations are jointly Gaussian, the Kalman update provides the optimal state estimator based on observations [*Gelb*, 1974]. Assuming the observation can be expressed as a linear function of the state with additive noise v, i.e.

$$Y = HX + v\,, \tag{B-1}$$

the Kalman update provides the following posterior state mean $\widehat{X}$ and covariance $\widehat{P}_X$ estimate:

$$\widehat{X} = \overline{X} + P_{XY} P_Y^{-1} (Y_{obs} - H\overline{X}) \tag{B-2}$$

$$\widehat{P}_X = P_X - P_{XY} P_Y^{-1} P_{XY}^T \tag{B-3}$$

where $\overline{X}$ and P_X are the prior state mean and covariance, and Y_{obs} is the observed value of Y. The Kalman update provides central estimation step in the sequential Kalman Filter [*Kalman and Bucy*, 1961].

Appendix C

Parameter Estimation Plots

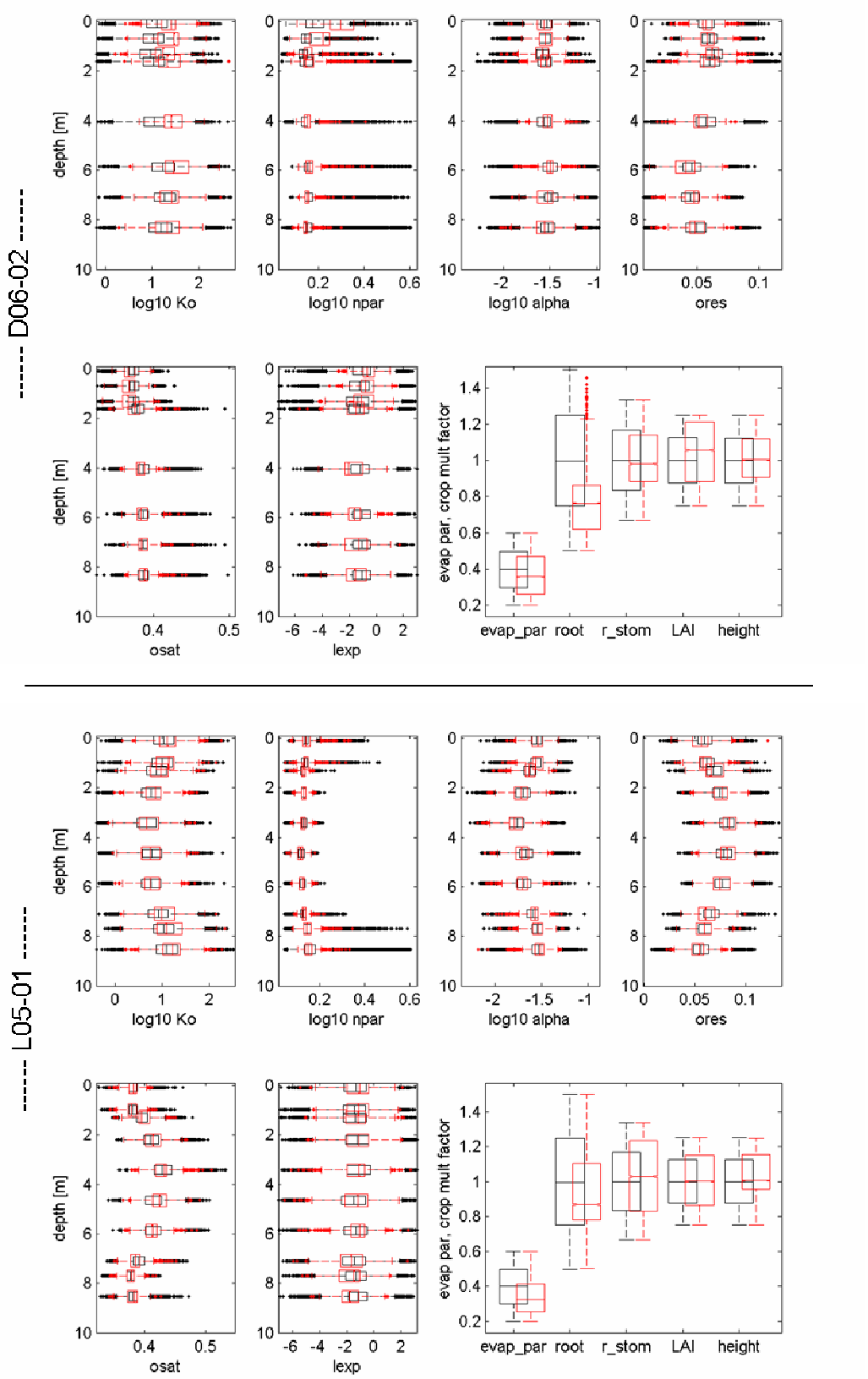

Figure C-1: Box plots of prior (black) and posterior (red) parameters for soil and vegetation.

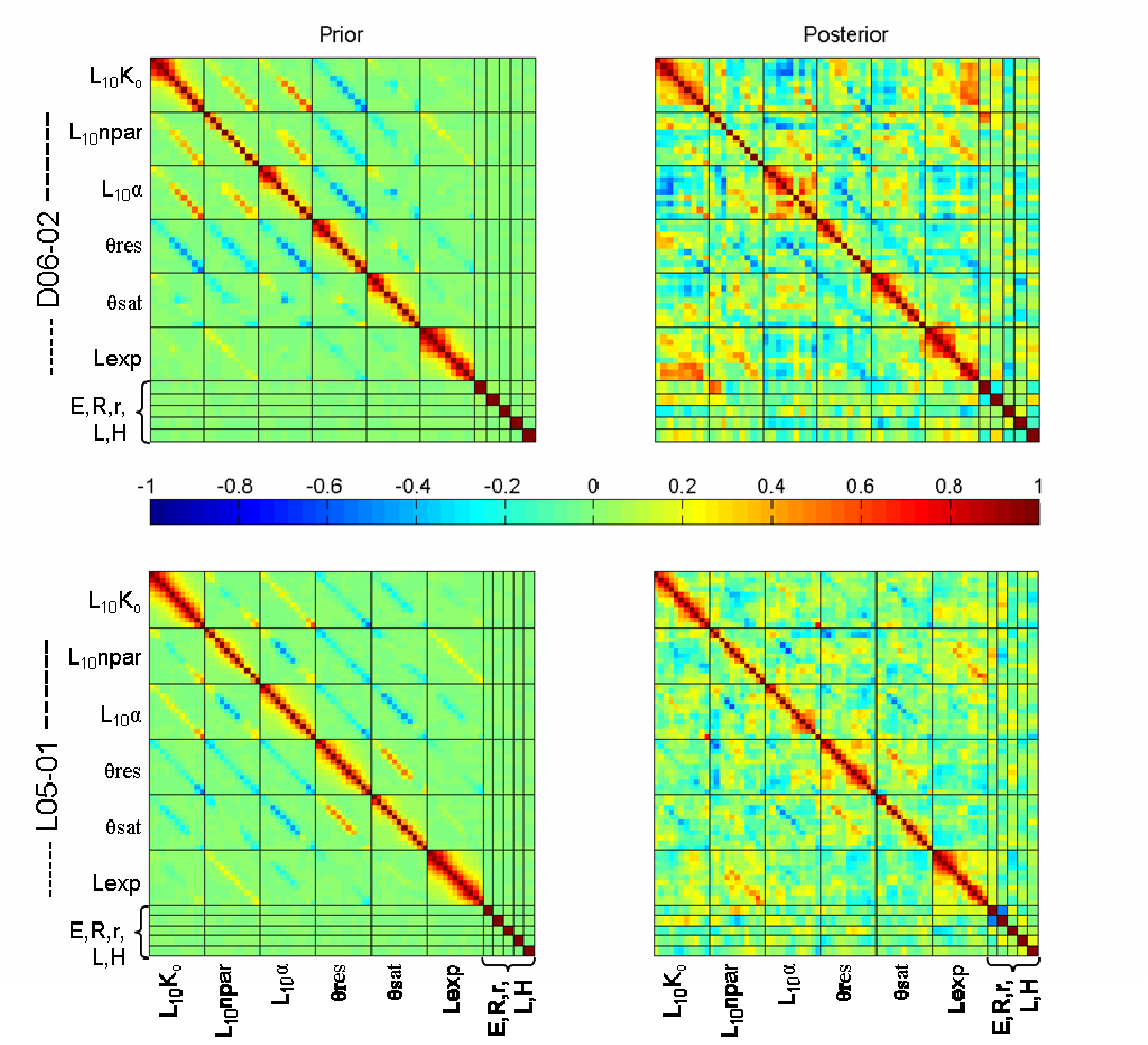

Figure C-2: Correlations between soil and vegetation parameters; "E" = evaporation parameter, "R" = rooting depth, "r" = stomatal resistance, "L" = LAI, and "H" = crop height. For soil layers parameters, depth increases in the downward and rightward directions.

Appendix D

Systematic Resampling Algorithm

The importance sampling scheme used in Chapter 2 produces unequal posterior weights for each prior parameter set to represent the data-conditioned parameter distribution. This distribution of parameter sets is then resampled to produce an ensemble of equally weighted sets; in other words, sets with high posterior weights after importance sampling are sampled multiple times while sets with negligible posterior weights are not chosen at all in the resampling. This is carried out using "systematic resampling," and the algorithm is provided in *Arulampalam et al.* [2002] for the SIR particle filter.

The idea behind systematic resampling is to uniformly sample the distribution; this can be critical for producing a representative draw when the sample size is small. In order to limit the computational load for the recharge predictions, a sample size of only 200 is drawn from the prior pool of over 30,000 samples, making the small sample size

misrepresentation problem a concern in our work. Systematic resampling is carried out via the following steps:

1) $\{X^i, w^i\}$, $i = 1, \ldots, N_{big}$ represents the posterior distribution after importance sampling, with unequal weights.

2) The cumulative distribution function $\{X^i, c^i\}$ is constructed by taking the cumulative sum of w^i.

3) A starting point u^1 on the CDF is selected by drawing from the uniform distribution over $[0, 1/N_{small}]$.

4) Starting at u^1, systematic samples of the CDF are taken at $1/N_{small}$ intervals; this gives $u^j = u^1 + (j-1)/N_{small}$, $j = 1, \ldots, N_{small}$.

5) For each u^j, the corresponding X^i value is found such that $c^{i-1} < u^j \leq c^i$. This X^i is assigned to X^j.

6) $\{X^j, w^j = 1/N_{small}\}$, $j = 1, \ldots, N_{small}$ is the resampled distribution.

References

Allison G. B., G. W. Gee, S. W. Tyler, Vadose zone techniques for estimating groundwater recharge in arid and semiarid regions, *Soil Sci. Soc. Am. J.*, 58, 6-14, 1994.

Allison, G. B. and M. W. Hughes, The use of natural tracers as indicators of soil-water movement in a temperate semi-arid region, *J. Hydrol.*, 60, 157-173, 1983.

Allen, M. R. and W. J. Ingram, Constraints on future changes in climate and the hydrological cycle, *Nature*, 419, 224-232, 2002.

Allen Jr., H. J., J. F. Baker, and K. J. Boote, The CO2 fertilization effect: higher carbohydrate production and retention as biomass and seed yield, In: Bazzaz F, Sombroek WG (eds), *Global climate change and agricultural production*, FAO and Wiley, Chichester, pp 65–100, 1996.

Arulampalam, M. S., S. Maskell, N. Gordon, and T. Clapp, A tutorial on particle filters for online nonlinear/non-Gaussian Bayesian tracking, *IEEE T. Signal Proces.*, 50(2), 174-188, 2002.

Askew, S. D. and J. W. Wilcut, Pale smartweed interference and achene production cotton, *Weed Science*, 50, 357-363, 2002.

Black, T. A., W. R. Gardner, and G. W. Thurtell, The prediction of evaporation, drainage, and soil water storage for a bare soil, *Soil Sci. Soc. Am. J.*, 33, 655-660.

Bland, W. L. and W. A. Dugas, Cotton root growth and soil water extraction, *Soil Sci. Soc. Am. J.*, 53, 1850-1855, 1989.

Brouyère, S., G. Carabin, and A. Dassargues, Climate change impacts on groundwater resources: modeled deficits in a chalky aquifer, Greer basin, Belgium, *Hydrogeol. J.,* 12, 123-134, 2004.

Chib, S. and E. Greenberg, Understanding the Metropolis-Hasting algorithm, *Am. Stat.*, 49(4), 327-335, 1995.

Climate Prediction Center, NOAA, http://www.cpc.ncep.noaa.gov/products/analysis_monitoring/ensostuff/ensoyears.shtml

Collins, D. B. G. and R. L. Bras, Plant rooting strategies in water-limited ecosystems, *Water Resour. Res.*, 43(6), W06407, doi:10.1029/2006WR005541.

Coupled Model Intercomparison Project phase 3 (CMIP3) multi-model dataset, World Climate Research Programme, http://www-pcmdi.llnl.gov/ipcc/about_ipcc.php

Cook, P. G., W. M. Edmunds, and C. B. Gaye, Estimating paleorecharge and paleoclimate from unsaturated zone profiles, *Water Resour. Res.*, 28(10), 2721-2731, 1992.

Cook, P. G., G. R. Walker, and I. D. Jolly, Spatial variability of groundwater recharge in a semiarid region, *J. Hydrol.*, 111, 195-212, 1989.

Croley II, T. E. and C. L. Luukkonen, Potential effects of climate change on ground water in Lansing, Michigan, *J. Am. Water Resour. As.*, 39(1), 149-163, 2003.

Daum, F. and J. Huang, Curse of dimensionality and particle filters, *IEEE Aerospace Conference Proceedings*, 4_1979- 4_1993, 2003.

Deng, Y., K. P. Bowman, and C. Jackson, Differences in rain rate intensities between TRMM observations and community atmosphere model simulations, *Geophys. Res. Lett.*, 34, L01808, doi:10.1029/2006GL027246, 2007.

de Vries, J. J., I. Simmers, Groundwater recharge: an overview of processes and challenges, *Hydrogeol. J.*, 10, 5-17, 2002.

Droogers, P., Estimating actual evapotranspiration using a detailed agro-hydrological model, *J. Hydrol.*, 229, 50-58, 2000.

Dunne, S. and D. Entekhabi, Land surface state and flux estimation using the ensemble Kalman smoother during the Southern Great Plains 1997 field experiment, *Water Resour. Res.*, 42, W01407, doi:10.1029/2005WR004334, 2006.

Easterling, D. R., G. A. Meehl, C. Parmesan, S. A. Changnon, T. R. Karl, and L. O. Mearns, Climate extremes: Observations, modeling, and impacts, *Science*, 289, 2068-2074, 2000.

Eckhardt, K. and U. Ulbrich, Potential impacts of climate change on groundwater recharge and streamflow in a central European low mountain range, *J. Hydrol.*, 284, 244-252, 2003.

Evensen, G., The Ensemble Kalman Filter: theoretical formulation and practical implementation, *Ocean Dynam.*, 53, 343-367, 2003.

Flint A. L., L. E. Flint, E. M. Kwicklis, J. T. Fabryka-Martin, and G. S. Bodvarsson, Estimating recharge at Yucca Mountain, Nevada, USA: comparison of methods, *Hydrogeol. J.*, 10, 180-204, 2002.

Foster, S. S. D. and P. J. Chilton, Groundwater: the processes and global significance of aquifer degradation, *Phil. Trans. R. Soc. Lond. B*, 358, 1957-1972, 2003.

Fowler, H. J., S. Blenkinsop, and C. Tebaldi, Linking climate change modelling to impact studies: recent advances in downscaling techniques for hydrological modelling, *Int. J, Climatol.*, 27, 1547-1578, 2007.

Gee G. W. and D. Hillel, Groundwater recharge in arid regions: review and critique of estimation methods, *Hydrol. Proc.*, 2, 255-266, 1988.

Gelb, A., *Applied Optimal Estimation*, The MIT Press, Cambridge, Massachusetts, 1974.

Ginn T. R. and E. M. Murphy, A transient flux model for convective infiltration: forward and inverse solutions for chloride mass balance studies, *Water Resour. Res.*, 33(9), 2065-2079, 1997.

Green T. R., B. C. Bates, S. P. Charles, and P. M. Fleming, Physically based simulation of potential effects of carbon dioxide-altered climates on groundwater recharge, *Vadose Zone J.*, 6, 597-609.

Gurdak, J. J., R. T. Hanson, P. B. McMahon, B. W. Bruce, J. E. McCray, G. D. Thyne, and R. C. Reedy, Climate variability controls on unsaturated water and chemical movement, High Plains Aquifer, USA, *Vadose Zone J.*, 6(2), 533-547, 2007.

Gutowski, W. J., K. A. Kozak, R. W. Arrit, J. H. Christensen, J. C. Patton, and E. S. Takle, A possible constraint on regional precipitation intensity changes under global warming, *J. Hydrometeorol.*, 8, 1382-1396, 2007.

Hanson, C. L., K. A. Cumming, D. A. Woolhiser, and C. W. Richardson, Microcomputer program for daily weather simulation, *Publ. ARS-114*, 38 pp., Agric. Res. Serv., U.S. Dep. Agric., Washington, D.C., 1994.

Herrera-Pantoja, M. and K. M. Hiscock, The effects of climate change on potential groundwater recharge in Great Britain, *Hydrol. Process.*, 22, 73-86, 2008.

Howell, T. A., S. R. Evett, J. A. Tolk, and A. D. Schneider, Evapotranspiration of full-, deficit-irrigated, and dryland cotton on the Northern Texas High Plains, *J. Irrig. Drain. E.-ASCE*, 130(4), 277-285, 2004.

Intergovernmental Panel on Climate Change (IPCC), *IPCC Fourth Assessment Report: Climate Change 2007 – The Physical Science Basis*, Cambridge University Press, Cambridge, UK, 2007.

Intergovernmental Panel on Climate Change (IPCC), *Special Report on Emissions Scenarios*, Cambridge University Press, Cambridge, UK, 2000.

Johnson, G. L., C. L. Hanson, S. P. Hardegree and E. B. Ballard, Stochastic weather simulation: Overview and analysis of two commonly used models, *J. Appl. Meteor.*, 35, 1878-1896.

Jolly, I. D., P. G. Cook, G. B. Allison, and M. W. Hugues, Simultaneous water and solute movement through an unsaturated soil following an increase in recharge, *J. Hydrol.*, 111, 391-396, 1989.

Jyrkama, M. I. and J. F. Sykes, The impact of climate change on spatially varying groundwater recharge in the grand river watershed (Ontario), *J. Hydrol.*, 338, 237-250, 2007.

Kailath T., A. H. Sayed, and B. Hassibi, *Linear Estimation*, Prentice Hall, Upper Saddle River, N.J., 2000.

Kalman R. E. and R. Bucy, New results in linear filtering and prediction, *J. Basic Eng.-T ASME*, 83D, 95-108, 1961.

Katz, R. W. and M. B. Parlange, Effects of an index of atmospheric circulation of stochastic properties of precipitation, *Water Resour. Res.*, 29(7), 2335-2344, 1993.

Kearns A. K. and J. M. H. Hendrickx, Temporal variability of diffuse groundwater recharge in New Mexico, *Tech. Rep. No. 309*, 43 pp., N.M. Water Resour. Res. Inst., Socorro, 1998.

Keese, K. E., B. R. Scanlon, R. C. Reedy, Assessing controls on diffuse groundwater recharge using unsaturated flow modeling, *Water Resour. Res.*, 41, W06010, doi:10.1029/2004WR003841, 2005.

Kharin, V. V. and F. W. Zwiers, Estimating extremes in transient climate change simulations, *J. Climate*, 18, 1156-1173, 2005.

Kirshen, P. H., Potential impacts of global warming on groundwater in eastern Massachusetts, *J. Water Res. Pl.-ASCE*, 128(3), 216-226, 2002.

Kitanidis, P. K., and R. L. Bras, Real-time forecasting with a conceptual hydrologic model: 1. Analysis of uncertainty, *Water Resour. Res.*, 16(6), 1025–1033, 1980.

Kroes, J. G. and J. C. van Dam (eds), *Reference Manual SWAP version 3.0.3*, Alterra-report 773, Alterra, Green World Research, Wageningen, The Netherlands, 2003.

Laio, F., P. D'Odorico, and L. Ridolfi, An analytical model to relate the vertical root distribution to climate and soil properties, *Geophys. Res. Lett.*, 33(18), L18401, doi:10.1029/2006GL027331, 2006.

Lascano, R. J., C. H. M. van Bavel, J. L. Hatfield, and D. R. Upchurch, Energy and water balance of a sparse crop, *Soil Sci. Soc. Am. J.*, 51, 1113-1121, 1987.

Leany, F. W., A. L. Herczeg, and G. R. Walker, Salinization of a fresh paleo-ground water resource by enhanced recharge, *Ground Water*, 41(1), 84-92, 2003.

Lewis, M. F. and G. R. Walker, Assessing the potential for significant and episodic recharge in southwestern Australia using rainfall data, *Hydrogeol. J.*, 10. 229-237, 2002.

Loáiciga, H. A., Climate change and ground water, *Ann. Assoc. Am. Geogr.*, 93(1), 30-41, 2003.

Margulis, S. A., D. McLaughlin, D. Entekhabi, and S. Dunne, Land data assimilation and estimation of soil moisture using measurements from the Southern Great Plains 1997 Field Experiment, *Water Resour. Res.*, 38, 1299, doi:10.1029/2001WR001114, 2002.

McLaughlin, D., L. B. Reid, S. G. Li, and J. Hyman, A stochastic method for characterizing groundwater contamination, *Ground Water*, 31(2), 237–249, 1993.

Monteith, J. L., Evaporation and surface temperature, *Quarterly J. Royal Soc.*, 107, 1-27, 1981.

Moradkhani, H., K.-L. Hsu, H. Gupta, and S. Sorooshian, Uncertainty assessment of hydrologic model states and parameters: Sequential data assimilation using the particle filter, *Water Resour. Res.*, 41, W05012, doi:10.1029/2004WR003604, 2005.

Murphy E. M., T. R. Ginn, and J. L. Phillips, Geochemical estimates of paleorecharge in the Pasco Basin: evaluation of the chloride mass balance technique, *Water Resour. Res.,* 32(9), 2853-2868, 1996.

National Renewable Energy Laboratory, *National Solar Radiation Database, 1991-2005 Update*, Tech. Rep. NREL/TP-581-41364, 2007.

National Climatic Data Center, Daily Surface Data, http://www.ncdc.noaa.gov/oa/ncdc.html, Accessed: August 2008.

Pan, M., E. F. Wood, R. Wójcik, and M. F. McCabeb, Estimation of regional terrestrial water cycle using multi-sensor remote sensing observations and data assimilation, *Remote Sens. Environ.*, 112(4), 1282-1294, 2008.

Priestly, M. B., *Spectral Analysis and Time Series*, Academic Press, San Diego, Calif., 1981.

Prudhomme, C., N. Reynard, and S. Crooks, Downscaling of global climate models for flood frequency analysis: where are we now? *Hydrol. Process.*, 16, 1137-1150, 2002.

Reichle R. H., D. Entekhabi, and D. B. McLaughlin, Downscaling of radio brightness measurements for soil moisture estimation: a four-dimensional variational data assimilation approach, *Water Resour. Res.*, 37(9), 2353-2364, 2001.

Reichle R. H., D. B. McLaughlin, and D. Entekhabi, Hydrologic data assimilation with the ensemble Kalman Filter, *Mon. Wea. Rev.*, 4, 130, 103-114.

Ritchie, G.L., C.W. Bednarz, P.H. Jost, and S.M. Brown, Cotton growth and development. [Online]. Available at http://pubs.caes.uga.edu/caespubs/pubs/PDF/B1252.pdf (accessed 15 Aug, 2008), University of Georgia College of Agricultural and Environmental Sciences, Cooperative Extension Service, Athens, GA, last revised 2007.

Ritchie, J. T., Model for predicting evaporation from a row crop with incomplete cover, *Water Resour. Res.*, 8(5), 1204-1213, 1972.

Robinson, R. A. and R. H. Stokes, *Electrolyte Solutions*, 2nd ed., Butterworth, London, 1965.

Rosenberg, N. J., D. J. Epstein, D. Wang, L. Vail, R. Srinivasan, and J. G. Arnold, Possible impacts of global warming on the hydrology of the Ogallala aquifer region, *Climatic Change*, 42, 677-692, 1999.

Rosenzweig, C., Crop response to climate change in the Southern Great Plains: a simulation study, *Prof. Geogr.*, 42(1), 20-37, 1990.

Sarwar, A. and R. A. Feddes, Evaluating drainage design parameters for the Fourth Drainage Project, Pakistan by using SWAP model: Part II – modeling results, *Irrig. Drain.*, 14, 281-299, 2000.

Schaap, M. G. and F. J. Leij, Improved prediction of unsaturated hydraulic conductivity with the Mualem-van Genuchten model, *Soil Sci. Soc. Am. J.*, 4, 843-851, 2000.

Schaap, M. G., F. J. Leij, and M. Th. van Genuchten, Rosetta: a computer program for estimating soil hydraulic parameters with hierarchical pedotransfer functions, *J. Hydrol.*, 251, 163-176, 2001.

Scanlon, B. R., Uncertainties in estimating water fluxes and residence times using environmental tracers in an arid unsaturated zone, *Water Resour. Res.*, 36(2), 395-409, 2000.

Scanlon, B.R. and R. S. Goldsmith, Field study of spatial variability in unsaturated flow beneath and adjacent to playas, *Water Resour. Res.*, 33(10), 2239-2252, 1997.

Scanlon B. R., K. Keese, R. C. Reedy, J. Simunek, and B. J. Andraski, Variations in flow and transport in thick desert vadose zones in response to paleoclimatic forcing (0-90 kyr): Field measurements, modeling, and uncertainties, *Water Resour. Res.*, 39(7), W1179, doi: 10.1029/2002WR001604, 2003

Scanlon B. R., R. W. Healy, and P. G. Cook, Choosing appropriate techniques for quantifying groundwater recharge, *Hydrogeol. J.*, 10, 18-39, 2002.

Scanlon B. R., R. C. Reedy, J. A. Tachovsky, Semiarid unsaturated zone chloride profiles: Archives of past land use change impacts on water resources in the southern High Plains, United States, *Water Resour. Res.*, 43(6), W06423, doi: 10.1029/2006WR005769, 2007.

Scibek J. and D. M. Allen, Modeled impacts of predicted climate change on recharge and groundwater levels, *Water Resour. Res.*, 42, W11405, doiL10.1029/2005WR004742, 2006.

Semenov, M. A., Development of high-resolution UKCIP02-based climate change scenarios in the UK, *Agr. Forest Meteorol.*, 144, 127-138, 2007.

Semenov, M. A., Simulation of extreme weather events by a stochastic weather generator, *Climate Res.*, 35, 203-212, 2008.

Semenov, M. A. and E. M. Barrow, Use of a stochastic weather generator in the development of climate change scenarios, *Climatic Change*, 35, 397-414, 1997.

Semenov, M. A., R. J. Brooks, E. M. Barrow, C. W. Richardson, Comparison of the WGEN and LARS-WG stochastic weather generators for diverse climates, *Climate Res.*, 10, 95-107, 1998.

Serrat-Capdevila, A., J. B. Valdés, J. González Pérez, K. Baird, L. J. Mata, and T. Maddock III, Modeling climate change impacts – and uncertainty – on the hydrology of a riparian system: the San Pedro Basin (Arizona/Sonora), *J. Hydrol.*, 347, 48-66, 2007.

Small E. E., Climatic controls on diffuse groundwater recharge in semiarid environments of the southwestern United States, *Water Resour. Res.*, 41, W04012, doi:10.1029/2004WR003193, 2005.

Smith, P. J., K. J. Beven, and J. A. Tawn, Detection of structural inadequacy in process-based hydrological models: A particle-filtering approach, *Water Resour. Res.*, 44, W01410, doi:10.1029/2006WR005205, 2008.

Sun, Y., S. Solomon, A. Dai, and R. W. Portmann, How often does it rain? *J. Climate*, 19, 916-934, 2006.

Sun, Y., S. Solomon, A. Dai, and R. W. Portmann, How often will it rain? *J. Climate*, 20, 4801-4818, 2007.

Trenberth, K. E., A. Dai, R. M. Rasmussen, and D. B. Parsons, The changing character of precipitation, *Bull. Amer. Meteor. Soc.*, 84, 1205-1217, 2003.

Tyler, S. W. and G. R. Walker, Root zone effects on tracer migration in arid zones, *Soil Sci. Soc. Am. J.*, 58, 25-31, 1994.

van Dam, J. C., P. Groenendijk, R. F. A. Hendriks, J. G. Kroes, Advances of modeling water flow in variably saturated soils with SWAP, *Vadose Zone J.*, 7(2), 640-653, 2008.

van Genuchten, M. Th., A closed form equation for predicting the hydraulic conductivity of unsaturated soils, *Soil Sci. Soc. Am. J.*, 44, 892-898, 1980.

Vörösmarty, C. J., P. Green, J. Salisbury, and R. B. Lammers, Global water resources: vulnerability from climate change and population growth, *Science*, 289, 284-288, 2000.

Vrugt, J. A., C. G. H. Diks, H. V. Gupta, W. Bouten, and J. M. Verstraten, Improved treatment of uncertainty in hydrologic modeling: Combining the strengths of global optimization and data assimilation, *Water Resour. Res.*, 41, W01017, doi:10.1029/2004WR003059, 2005.

Walker, G. R., I. D. Jolly, and P. G. Cook, A new chloride leaching approach to the estimation of diffuse recharge following a change in land use, *J. Hydrol.*, 128, 49-67, 1991.

Weerts, A. H. and G. Y. H. El Serafy, Particle filtering and ensemble Kalman filtering for state updating with hydrological conceptual rainfall-runoff models, *Water Resour. Res.*, 42, W09403, doi:10.1029/2005WR004093, 2006.

Wilks, D. S. and R. L. Wilby, The weather generation game: a review of stochastic weather models, *Prog. Phys. Geog.*, 23(3), 329-357, 1999.

Wood, W. W. and W. E. Sanford, Chemical and isotopic methods for quantifying ground-water recharge in a regional semiarid environment, *Ground Water*, 33, 458- 468, 1995.

Zhang, L., I. H. Hume, M. G. O'Connell, D. C. Mitchell, P. L. Milthorpe, M. Yee, W. R. Dawes, and T. J. Hatton, Estimating episodic recharge under difference crop/pasture rotations in the Mallee region. Part 1. Experiments and model calibration, *Agr. Water Manage.*, 42, 219-235, 1999a.

Zhang L., W. R. Dawes, T. J. Hatton, I. H. Hume, M. G. O'Connell, D. C. Mitchell, P. L. Milthorpe, and M. Yee, Estimating episodic recharge under different crop/pasture rotations in the Mallee region. Part 2. Recharge control by agronomic practices, *Agr. Water Manage.*, 42(2), 237-249, 1999b.

Zhou, Y. H., D. McLaughlin, D. Entekhabi, Assessing the performance of the ensemble Kalman filter for land surface data assimilation, *Mon. Weather Rev.*, 134(8), 2128-2142, 2006.